STREAM OF VARIATION AND SHAPE CONTROL FOR COMPOSITE FUSELAGE ASSEMBLY

A Dissertation
Presented to
The Academic Faculty

by

Yuchen Wen

In Partial Fulfillment
of the Requirements for the Degree
Doctor of Philosophy in the
School of Industrial and Systems Engineering

Georgia Institute of Technology

[May 2019]

STREAM OF VARIATION AND SHAPE CONTROL FOR COMPOSITE FUSELAGE ASSEMBLY

Approved by:

Dr. Jianjun (Jan) Shi, Advisor
School of Industrial and Systems Engineering
Georgia Institute of Technology

Dr. Jionghua (Judy) Jin
Department of Industrial and Operations Engineering
The University of Michigan

Dr. Kamran Paynabar
School of Industrial and Systems Engineering
Georgia Institute of Technology

Dr. Hsu-Pin (Ben) Wang
School of Industrial and Systems Engineering
Georgia Institute of Technology

Dr. Chun (Chuck) Zhang
School of Industrial and Systems Engineering
Georgia Institute of Technology

Date Approved: December 3, 2018

To my parents, and those who have supported me.

ACKNOWLEDGEMENTS

I would like to express my sincerest gratitude to my advisor, Professor Jianjun Shi, who has been supportive in the development of my career and research interests. He has trained my abilities to identify important research problems and further develop systematic ways to address them with data analytics integrated with engineering domain knowledge. When I met difficulties in exploring my research topics, his thought-provoking and insightful guidance helped me overcome many challenges. I am very fortunate and honored to have him as my advisor, and I shall benefit from his advice for the rest of my career and life. I would like to convey my special thanks to his wife, Mrs. Liping Luo, for her kindness and warm hospitality.

My gratitude also goes to my thesis committee members, including Professor Jionghua Jin, Professor Kamran Paynabar, Professor Ben Wang, and Professor Chuck Zhang. Their valuable suggestions and support not only helped me make significant improvements to the dissertation, but also greatly aided me during my Ph.D study.

I would like to thank Dr. Jeffrey Hunt at the Boeing Company. His kindness, passion for work and professionalism have made an important impact on the developments of my research and life. The weekly meetings with him in the past two years were productive and many of the ideas contributed to my dissertation. I would like to thank Dr. Alan Erera, Mrs. Amanda Ford, Dr. Nagi Gebraeel, Dr. Ran Jin, Dr. Kaibo Liu, Dr. Spiridon Reveliotis, and Dr. Hao Yan for their kind support and advice throughout my study.

I would like to express my special appreciation for Dr. Xiaowei Yue, my dear collaborator who has helped me and supported me. I have learned a lot from him on both aspects of research and a positive mentality. He has provided me with many constructive research advices and whenever I had a research problem, he would help me with great patience and carefulness. I would also like to express my gratitude to my friends and colleagues: Mrs. Juan Du, Dr. Xiaolei Fang, Dr. Li Hao, Mr. Mohammad Nabhan, Mr. Mostafa Reisi, Mrs. Xinran Shi, Mr. Andi Wang, Dr. Chen Zhang, Mr. Ruizhi Zhang, Dr. Tingyu Zhang and Mr. Zhen Zhong.

This journey would not have been possible without the support of my girlfriend, Xue Qin. Finally, I must thank my parents, for their unconditional love and continued support. I shall be able to overcome any challenge in the rest of my life with them standing by me.

TABLE OF CONTENTS

LIST OF TABLES

LIST OF FIGURES

SUMMARY

Composite parts have been increasingly used in aerospace industry because of their high strength-to-weight ratio and stiffness-to-weight ratio. Due to the diversity of suppliers and variation in the fabrication process of composite parts, dimensional variability of composite fuselages inevitably exists. One of the critical challenges to reduce the dimensional variability of the assembly process is the complex property of composite materials. The traditional physical models applied to metal materials cannot be directly applied here. It is of high importance to develop systematic methodologies to conduct dimensional analysis, variation reduction, and optimal shape adjustment for the composite fuselages' assembly process.

Based on these motivations, this dissertation focuses on developing systematic methodologies for effective system modeling, quality control and variability reduction in the composite fuselages assembly process. These advanced methodologies enable a better understanding of the composite fuselage structure with actuator applied, a more accurate handling of the fuselage shape control system, and a more precise way to analyze the residual stress during the fuselage assembly process.

This dissertation is organized as follows. Chapter 1 introduces a new shape control system with 10 actuators that is able to conduct dimensional shape adjustment before the airplane fuselage assembly process. In Chapter 2, a feasibility study is conducted to evaluate the proposed shape control concept. In the feasibility analysis, an accurate finite element model is developed to mimic the fabrication of composite fuselage, which includes the detailed materials setting, ply design, geometry and fixture structures. The finite

element model is validated and calibrated based on physical experimental data with a real fuselage on the production floor. The results show that the single-plane with ten actuators scheme is feasible for shape control, and that actuators do not damage the fuselage.

In Chapter 3, a surrogate model considering four types of uncertainties (actuator uncertainty, part uncertainty, modeling uncertainty, and unquantified uncertainty) has been developed for automatic optimal shape control of the system proposed in Chapter 2. A maximum likelihood estimation (MLE) algorithm is used for parameter estimation and response prediction. Afterwards, the surrogated model considering uncertainties is embedded into a feedforward control algorithm, which is achieved by conducting multivariate optimization to minimize the weighted summation of dimensional deviations of the response from the target. We show that the surrogate model considering uncertainties achieves satisfactory prediction performance and the automated optimal shape control system can significantly reduce the assembly cycle time with improved dimensional quality.

In Chapter 4, two active learning algorithms are proposed for Gaussian process considering uncertainties, which are the variance-based weighted active learning algorithm and D-optimal weighted active learning algorithm. These active learning algorithms effectively reduce the number of samples needed to get accurate statistical models for industrial systems that have numerous uncertainties, such as input uncertainties, measurement errors, modeling uncertainties, and uncertainties from system parameters. The proposed algorithms investigate stochastic Kriging model and surrogate model considering uncertainties, with information measure of variance-based information and Fisher information. The algorithms have been applied to improving the predictive

modeling for automatic shape control of composite fuselage. They can also be applied in other active learning scenarios for predictive models with multiple uncertainties.

From Chapter 2 to Chapter 4, we have focused on optimal shape control system for single fuselage. After the two fuselages are adjusted to the target shape, they will be assembled together, and the actuator forces are released afterwards. The release of actuator forces results in the springback of two fuselages and the occurrence of residual stresses. In Chapter 5, we investigate the process of fuselages assembly via the proposed control system and develop an FEA platform to simulate the dimensional change and stress change during and after the assembly process. Instead of reversing the actuator forces, we use dynamic forces to simulate the springback of the fuselages after releasing the actuators. The proposed approach is more accurate compared to the traditional simulation approach. The case studies show that the assembly process with our new shape control system is applicable and the residual stresses are lower than the failure threshold.

In Chapter 6, we discuss the potentials of future research. The automatic shape control system developed for single fuselage can be extended to variation reduction of multi-station fuselage assemblies. The surrogate modeling of residual stress is another area of interest, which could lead to fast stress prediction and optimization. Optimal fixture design is also of high importance due to the capability of stress reduction.

In summary, this thesis fuses the knowledge of statistics, mechanical engineering, and material science to obtain a better understanding and improvement of the composite fuselage assembly process. The methodologies and simulation platforms developed in this thesis have the potential to be applied to other advanced manufacturing systems.

CHAPTER 1. INTRODUCTION

1.1 Motivation

Composite materials have been increasingly used in aircraft industry due to their advantages like high strength-to-weight ratio, high stiffness-to-weight ratio, corrosion resistance, and high durability. Aircraft parts made from composite materials, such as fairings, spoilers, floor beams, and flight controls have been developed. These composite structures realize better weight savings over aluminum parts. New generation of large aircrafts are designed mostly with composite fuselages and wing structures. Dimensional control of the assembly process for these advanced composite parts requires an in-depth knowledge of composite structures, materials and their properties, which is very important for the quality management, high productivity of manufacturing process and running safety of assembled aircrafts. However, due to the diversity of suppliers and multiple manufacturing batches from each supplier, dimensional variability of composite fuselages inevitably exists. One of the critical challenges to reduce the dimensional variability of the assembly process is the complex property of composite materials. Traditional physical models applied to metal materials cannot be directly applied the dimensional variation of composite parts. There is a pressing need to develop systematic methodologies to realize dimensional analysis, variation reduction, and optimal shape adjustment for the composite fuselages assembly process. Based on these initiatives, this dissertation focuses on developing systematic methodologies for effective system modeling, quality control and variability reduction in composite fuselages assembly process.

1.2 Current Practice and Research Objectives

In order to reduce dimensional variability of the composite fuselage assembly process, a shape control system with multiple actuators is proposed to adjust dimension of a composite fuselage before its assembly. In the current practice, a “pogo” shape control system is used to reduce the dimensional deviations between the real composite part and the ideal shape. A photo and schematic diagram of the current “pogo” system are shown in Fig. 1 (a) and (b). The disadvantages of the current system include that (i) the capability of dimensional shape control is very limited, (ii) it takes a long time to adjust the actuators to get an acceptable dimensional shape, and (iii) highly skilled engineers are required to conduct the adjustment. Therefore, a new shape control system is designed to realize better dimensional quality control. As shown in Fig. 1 (c) and (d), ten actuators are installed across the edge of the lower semi-circle of the fuselage. These ten actuators will provide push and pull forces to change the in-plane shape of the fuselage.

Based on the current practice, the objectives of the research are to develop systematic methodologies for shape control and variability reduction of the composite fuselages assembly process. The proposed research focuses on the following topics:

(i) Build an accurate finite element model for the shape control system of the composite fuselage and validate the finite element model;

(ii) Evaluate the feasibility of the shape control system;

(iii) Develop a surrogate model and a control algorithm to determine the optimal actions of actuators for the adjustment of a single fuselage;

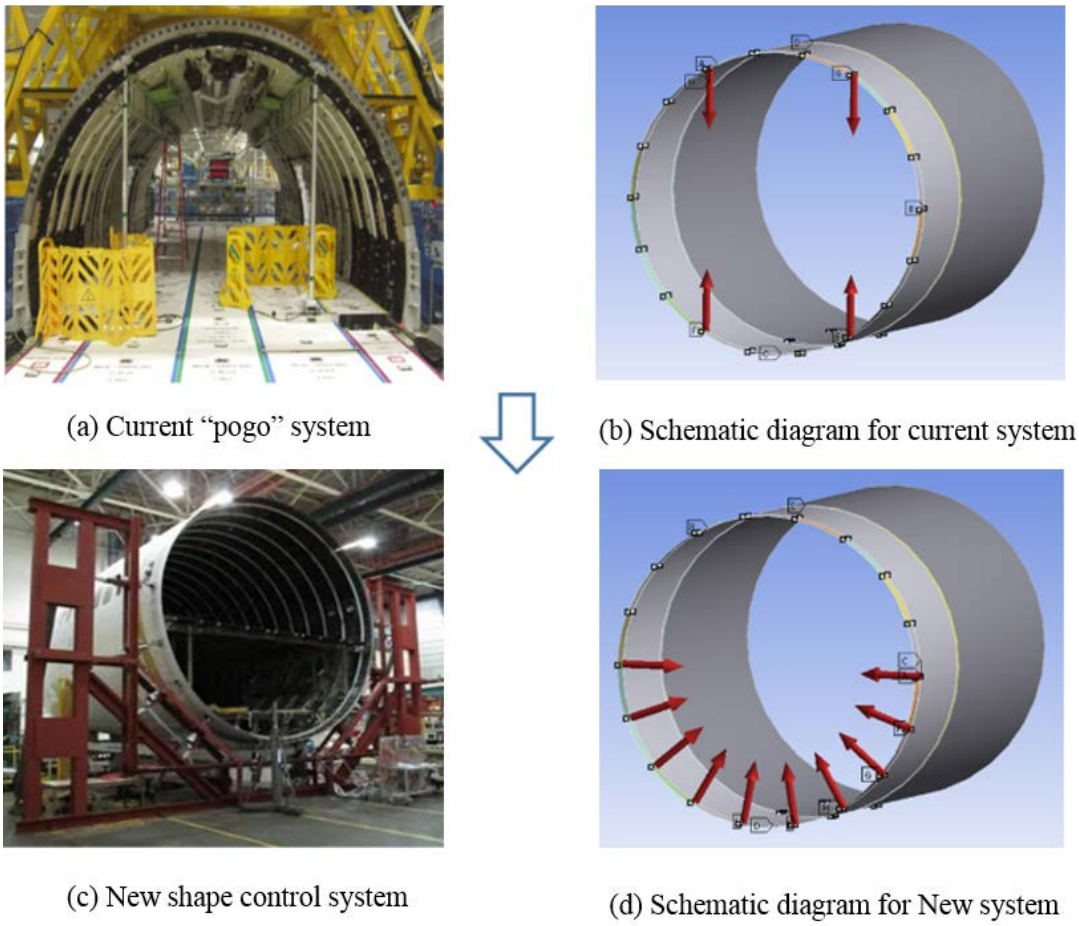

Fig. 1. Comparison between current system and new system

(iv) Propose an active learning algorithm to minimize the number of experiments while maintain the accuracy of the surrogate model;

(v) Construct an FEA platform that simulates the assembly process of two fuselages and shows the deformations and residual stresses during the assembly of two fuselages.

1.3 State-of-the-art

This section provides a literature review related to general frameworks of dimensional variation modeling of composite parts assembly process and conceptual

design of aircraft assembly line. Dong and Kang proposed an approach based on response surface method and analyzed the relationship between part variation and assembly variation/stress via virtual experiments and finite element model [1]. Zhang and Shi built a Stream of Variation (SoV) model for prediction and control of dimensional variations of composite part assembly in single-station [2] and multi-station process [3]. In their model, different sources of variabilities such as composite part manufacturing errors, fixture position errors, and relocation-induced errors were considered for the analysis of dimensional variation and its propagation. Gómez et al. proposed a supporting model and ad-hoc software for the decision-making process during the conceptual design of aircraft final assembly lines [4]. However, there is lack of papers related to the fuselage control system with actuators and a systematic study is in need.

There are numerous research topics have been conducted for modeling and analysis of dimensional variation reduction and control for the assembly of isotropic metal parts. Djurdjanovic and Ni proposed a linear state-space model by deriving explicit expressions for the influence of the errors in fixtures, locating datum features, and measurement datum features in the multistation machining process [5, 6]. A method of influence coefficient (MIC) was exploited to combine engineering structural mechanics with statistical methods to model the relationships between the incoming part deviations and the output assembly deviations in single-station [7] and multi-station assembly processes [8]. However, these models cannot be used directly in the composite fuselage shape control problem.

For model uncertainty in control theory [9, 10], uncertainty is illustrated via uncertain parameters or disturbances within a typically compact set. Robust or adaptive control algorithms are developed to deal with uncertainty explicitly. Decision support models

evaluate the extent of uncertainties and realize the balance between decision benefits and risk management [11]. Statistical models consider structural uncertainty via model selection as well as model validation, and consider parametric uncertainty by specified stochastic terms with random distributions [12]. More literature on uncertainty modeling can be found in [13].

1.4 Organization of the Thesis

This thesis is organized in a multiple manuscript format. Each of chapters 2, 3, 4, and 5 are written as a research paper. Among them, Chapters 2, 3, and 5 have been published [18, 50, 80] and chapter 4 is pending for sponsor's approval for submission [81]. Figure 2 presents the structure of the thesis and the relationships among the chapters.

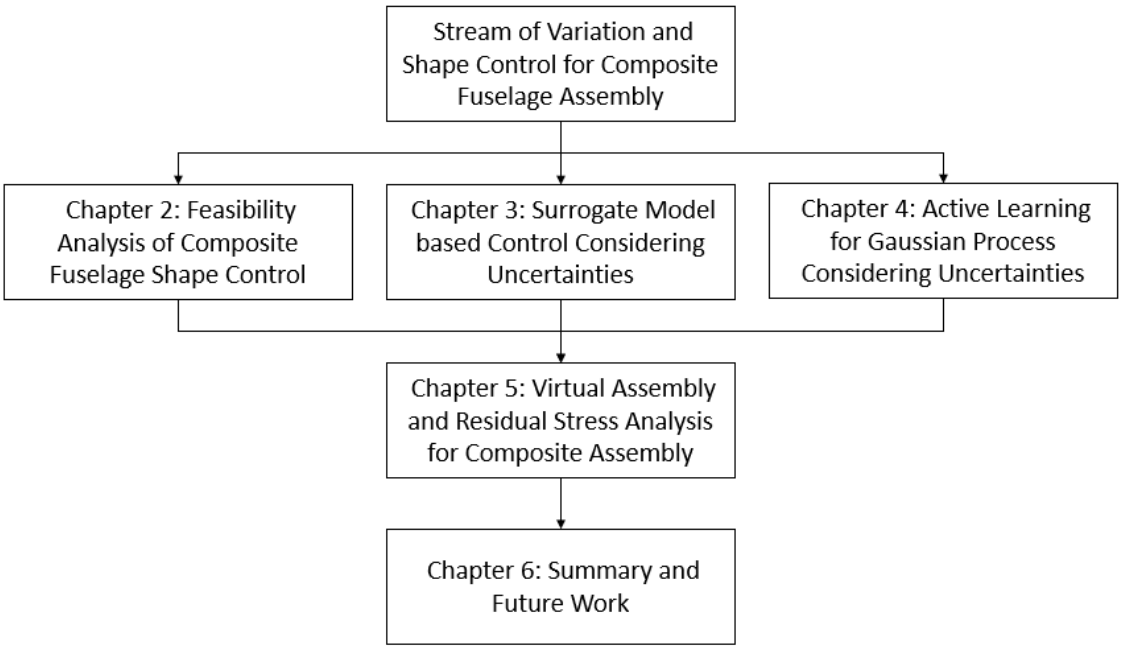

Figure 2. Outline of the thesis

In Chapter 2, the work is based on the new shape control system with 10 actuators that makes dimensional shape adjustment before the fuselage assembly. Our goal is to testify whether the actuators are capable of adjusting the fuselage and whether the adjustment will damage the fuselage. We develop a finite element model to mimic the fabrication of composite fuselage, including the detailed materials setting, ply design, geometry and fixture structures. The finite element model is then validated and calibrated based on physical experimental data with a real fuselage on the production floor.

In Chapter 3, the research focuses on the development of a systematic modeling method that is capable of the prediction of the fuselage adjustment. A surrogate model is developed to achieve automatic optimal shape control of the fuselage proposed in Chapter 2. An MLE estimation algorithm is used for parameter estimation and response prediction. A feedforward control algorithm that minimizes the weighted summation of dimensional deviations of the response to the target is developed to predict the optimal actuator forces that should be applied on the fuselage.

In Chapter 4, we proposed variance-based weighted active learning algorithm and D-optimal weighted active learning algorithm for Gaussian process considering various uncertainties. The main objective is to realize active learning for predictive analytics, which maximizes information acquisition with limited experimental samples. The proposed algorithms take information measures of variance-based information and Fisher information into consideration. The algorithms are applied to reduce the number of experiments while maintaining the accuracy of predictive modeling for automatic shape control of composite fuselage.

In Chapter 5, a new finite element simulation platform is developed to realize the virtual assembly of two composite fuselages with actuators' forces applied. We utilize the AOSC system to conduct the shape adjustment. For the assembly process, a new dynamic force curve approach is proposed to simulate the springback effect after the assembly. It is more accurate than the traditional three-step approach that uses a reversed force to simulate the springback. Our proposed simulation platform can estimate both deformations and stresses of the two fuselages during the entire assembly process, including the adjustments of two initial fuselages, the bond of the adjusted fuselages, and the release of actuators.

Chapter 6 summarizes the original contributions and the potential research topics to extend the single fuselage shape control to multi-station fuselage assemblies and the need of reducing residual stress after assembly.

CHAPTER 2. FEASIBILITY ANALYSIS OF COMPOSITE FUSELAGE SHAPE CONTROL VIA FINITE ELEMENT ANALYSIS

Composite parts have been increasingly used in aircraft industry because of their high strength-to-weight ratio and stiffness-to-weight ratio. Due to the diversity of suppliers and fabrication process variation of composite parts, dimensional variability of composite fuselages inevitably exists. In order to improve the dimensional quality and increase the productivity, a new shape control system has been proposed to conduct dimensional shape adjustment before the assembly process. By using finite element analysis, we conduct the feasibility analysis of this new shape control system. Firstly, we develop a finite element model with detailed material property, ply design, fixture structure, and actuators installation considered. The finite element model is then validated and calibrated by physical experimental data. Feasibility analysis via FEA includes single-plane dimensional control capability analysis, double-plane scheme analysis, stress/strain analysis, and failure test. We draw a conclusion that the single-plane with ten actuators scheme is feasible for the shape control, and the actuators do not damage the fuselage.

2.1 Introduction

Composite materials have been increasingly used in aircraft industry due to their advantages like high strength-to-weight ratio, high stiffness-to-weight ratio, corrosion resistance, and high durability [14]. Aircraft parts made from composite materials, such as

fairings, spoilers, floor beams, and flight controls have been developed. These composite structures realize better weight savings over aluminum parts [15]. New generation of large aircrafts are designed mostly with composite fuselage and wing structures. As an example, a commercial aircraft has major structural parts made from composite materials, and the composite parts represent more than 50% by weight [16]. Dimensional control of the assembly process for these advanced composite parts requires an in-depth knowledge of composite structures, materials and properties, which is very important for the quality management, high productivity of manufacturing process and running safety of assembled aircrafts. However, due to the diversity of suppliers and multiple manufacturing batches from each supplier, dimensional variability of composite fuselages inevitably exists. For instance, a report showed that a gap of 0.3 inch occurred when the nose-and-cockpit section lined up with the fuselage section [17].

An automatic shape control system will be developed that can effectively and efficiently adjust composite parts to an optimal configuration [18]. The new shape control system can (i) compute the optimal actuators' forces to minimize the dimensional deviations of current composite parts and the ideal shape; (ii) implement the adjustment automatically; (iii) release the workload of highly skilled engineers. Before the development of automatic shape control system, a feasibility analysis of the new shape control system for the composite parts should be conducted systematically.

In the literature, Pinkerton and Moses assessed the capabilities of a new out-of-plane displacement piezoelectric actuator called thin-layer composite-unimorph ferroelectric driver and sensor (THUNDER) to alter the upper surface geometry of a subscale airfoil to enhance the performance under aerodynamic loading [19], and the assessment was based

on physical experiments. Sofla et al. [20] reviewed the recent activity in conceptual design, prototype fabrication, and evaluation of shape morphing of aircraft wing, especially for smart materials including shape memory alloys, piezoelectric actuators, and shape memory polymers. Sodano et al. [21] presented the feasibility of using macro-fiber composites for vibration suppression and structural health monitoring. The aforementioned literature are focused on feasibility of variability monitoring and control during the design of composite fuselage and wings. For the assembly process of composite parts, Dong and Kang proposed an approach based on response surface method and analyzed the relationship between part variation and assembly variation/stress via virtual experiments and finite element model [1]. Zhang and Shi built a stream of variation (SoV) model for prediction and control of dimensional variations of composite part assembly in single-station [2], and multi-station process [3]. In their model, different sources of variabilities such as composite part manufacturing errors, fixture position errors, and relocation-induced errors were considered for analysis of dimensional variation and its propagation. Gómez et al. proposed a supporting model and ad-hoc software for the decision-making process during the conceptual design of aircraft final assembly lines [4]. The aforementioned literature give a general framework of dimensional variation modeling of composite parts assembly process and conceptual design of aircraft assembly line. However, there is no systematic analysis of the feasibility of the newly proposed automatic shape control system.

Feasibility analysis based on pure physical experiments is very expensive and time-consuming. Usually, before testing the real system with physical experiments, feasibility analysis based on computer simulation needs to be done. Finite element analysis (FEA) is a typical computer simulation method to analyze the complex properties of composite

materials for aerospace application [22]. The advantages of FEA include accurate representation of complex structures, inclusion of dissimilar material properties, capture of local effects, and accurate representation of the total solution. By using the commercial software like ANSYS or ABAQUS, it is viable to analyze the mechanical properties and predict dimensional, stress, and strain responses of the composite fuselage under different actuators' forces.

In order to implement the feasibility analysis of the new shape control system, an accurate finite element model is developed to mimic the fabrication process of a composite fuselage. The finite element model is calibrated and validated by physical experimental data, and the finite element model can accurately predict the dimensional shape change of the fuselage under different settings of actuators' forces. Then, feasibility analysis of the shape control system is conducted through dimensional control capability analysis, stress/strain analysis, and failure test.

The remainder of this paper is organized as follows. Section 2.2 introduces the detailed procedure of the finite element modeling of the composite fuselage and the actuator settings. Section 2.3 is the calibration and validation of the finite element model by comparing it with the physical experimental results. Section 2.4 consists of the feasibility analysis of the dimensional control capability, stress/strain analysis, and failure test. Section 2.5 provides the summary of the work.

2.2 Finite Element Modeling

In this section, we show the finite element modeling of the composite fuselage. With the commercial software ANSYS Composite PrepPost [23], we mimic the real fabrication

process of the composite fuselage, including material introduction with engineering properties, ply definition and design, material orientation, geometrical setting and so on. The engineering fixture constraints and actuators' forces are considered, and dimensional deformation, stress/strain responses, and advanced failure test are analyzed.

The developed finite element model by ANSYS Composite PrepPost (ACP) workbench is illustrated in Fig. 3. The ACP is an add-in to the workbench and is integrated with multiple functionalities for the analysis of layered composite structures. As shown in Fig. 3, the workflow for finite element modeling of the composite fuselage can be completed in three steps: (i) design and pre-processing, such as introducing composite materials and properties parameters in the engineering data module, designing the geometry of the composite fuselage, and setting up ply parameters and orientations; (ii) structural analysis including finite element meshing, assigning actuators' forces and engineering constraints, and response analysis; (iii) post-processing to evaluate the design performance and implement failure analysis.

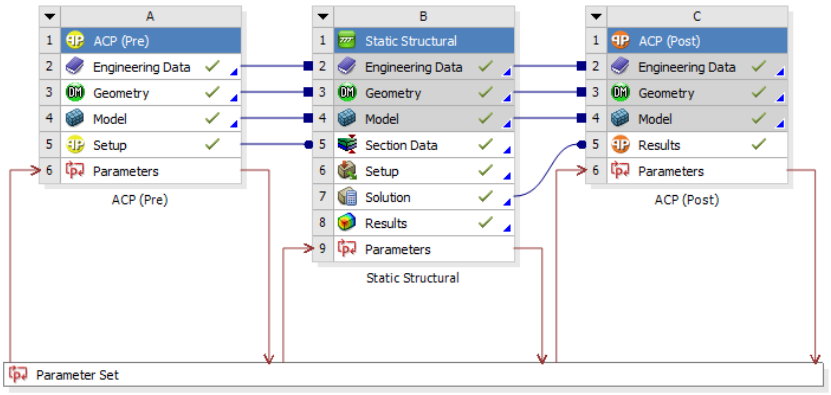

Fig. 3. The workbench of the finite element model

2.2.1 Key Material Properties

The materials used to build the composite fuselage are unidirectional carbon fiber and epoxy resin. Unidirectional carbon fiber has been the standard material within the aerospace industry, and the carbon fiber is typically pre-impregnated with a thermosetting epoxy resin system, which is called prepreg. The common fabrication process is to draw collimated raw carbon fibers into the impregnation machine where hot melted resins are combined with the strands using heat and pressure [15]. The structure of prepreg for aircraft composite fuselage can realize high strength by carbon fibers, high toughness by epoxy resin, and improvement of impact resistance by maintaining superior heat resistance of epoxy matrices. Other advantages include good part uniformity, good repeatability, less waste, less curing time, and so on. The highly toughened carbon fiber-reinforced epoxy prepreg is used in the finite element model. The key properties of the epoxy carbon prepreg [24] are listed in Table 1.

Table 1. Key properties of the Prepreg

Property Parameters	Magnitude
Density	93.02 lb./ft^3
Young's Modulus X direction	1.21×10^5 MPa
Young's Modulus Y/Z direction	8.60×10^3 MPa
Shear Modulus YZ direction	3.10×10^3 MPa
Shear Modulus XY/XZ direction	4.70×10^3 MPa
Poisson's Ratio YZ	0.4
Poisson's Ratio XY/XZ	0.27

2.2.2 Ply Design

The finite element model of composite fuselage mimics the real fabrication process. Specifically, the composite material introduced in section 2.2.1, such as carbon fiber prepreg, are used to form fabrics. From a production point of view, it is considered as one ply. The thickness of each ply is 0.008 inch and the properties of one ply including stretch stiffness parameters and shear stiffness parameter are shown in Fig. 4(a). The stretch stiffness and shear stiffness for one ply have orthogonal distribution pattern.

Fabrics are then stacked up depending on specified orientation that is ±45o. A stackup is a non-crimp fabric with a defined stacking sequence. The definition of the stackup can be given in both directions (Bottom-Up and Top-Down). In the Top-Down sequence, the first defined ply is placed first on the mold, which is on the bottom of the stackup and the other plies are placed over it. The sequence used for this study is Top-Down. The ply design and properties of one stackup are shown in Fig. 4(b). Next, fabrics and prepreg carbon fiber are used to manufacture sub-laminates with specified ply orientations and analysis of properties shown in Fig. 4(c). The layup sequence is Top-Down. Finally, the sub-laminates are integrated into the composite fuselage.

From Fig. 4, we can see that the properties change from fabrics, stackups, to sub-laminates. Besides, the 90o plies react to axial loads and ±45o plies react to shear loads and side loads. The strength design requirements are a function of the applied load direction, and ply orientation and ply sequence have to be correct [15]. To simplify the fabrication process and focus on the major factors, we do not consider the manufacturing defects such as delamination, resin starved areas, air bubbles, and wrinkles, etc. in the finite

element modeling process. Fig. 5(a) shows the total ply design of a sub-laminate and Fig. 5(b) shows the orientation of one ply in the finite element model.

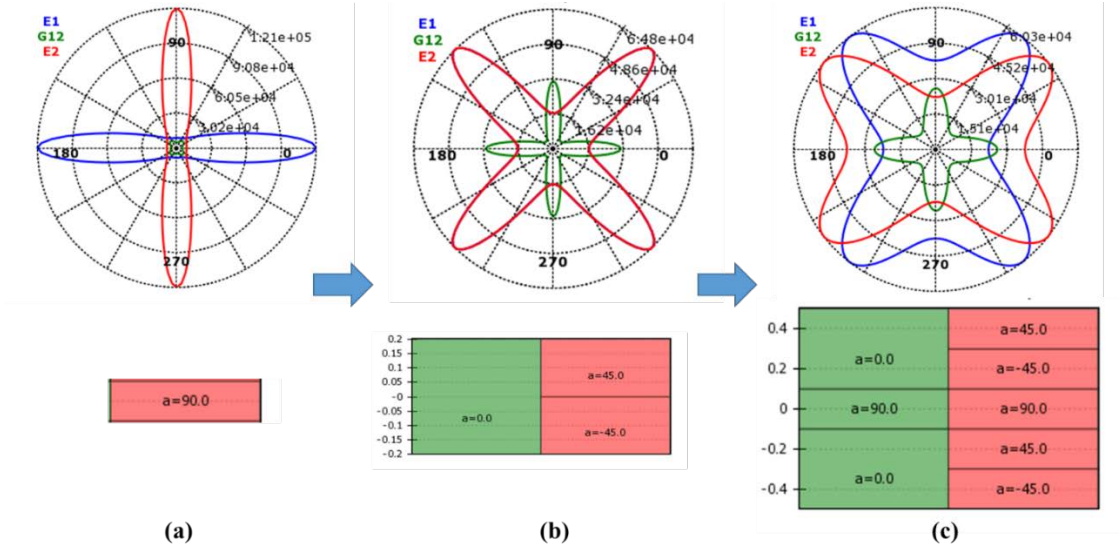

Fig. 4. Polar properties of (a) fabrics, (b) stackups, and (c) sub-laminates (Note: E1/E2: Young's modulus along different directions; G12: shear modulus)

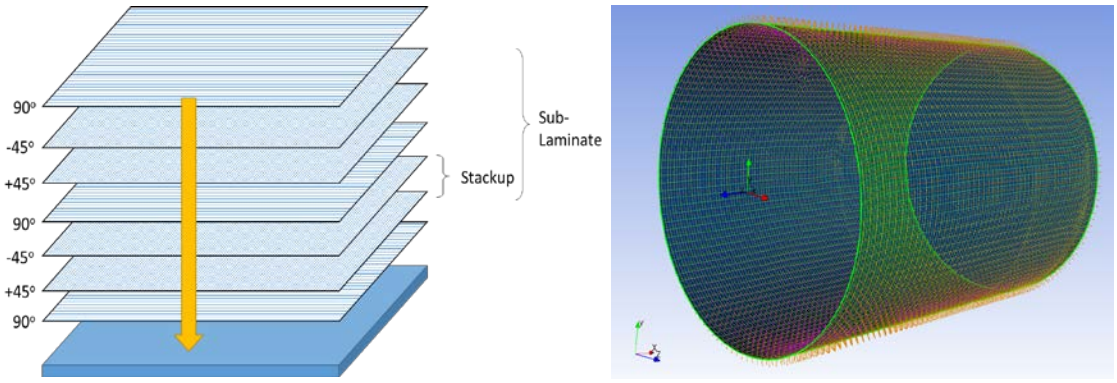

(a) **(b)**

Fig. 5. (a) Ply design, (b) the orientation of carbon fiber

2.2.3 Fuselage Geometry, Fixture Structure and Actuators

After introducing the key parameters and ply design, we illustrate the geometry of the fuselage, fixture setting, and actuators. The length of the fuselage in the finite element model is 24 feet and the diameter is 18 feet. The thickness of the fuselage is 0.295 inch. After the design of the geometry, material parameters, and ply structures are completed, the weight of the fuselage is then computed, which is 3100 pounds.

There are three fixture structures, two bottom supports and one strap fixture shown in Fig. 6. The bottom supports are 3.14 feet long and 1 foot wide. The distance between the support and the edge of the fuselage is 6 feet. The bottom supports are realized by constraining the z directional deformation of the supporting area of the fuselage. The 4-inch width strap support is a band that attaches the fuselage surface and the bottom support. It prevents the fuselage from shifting due to the applied actuator forces.

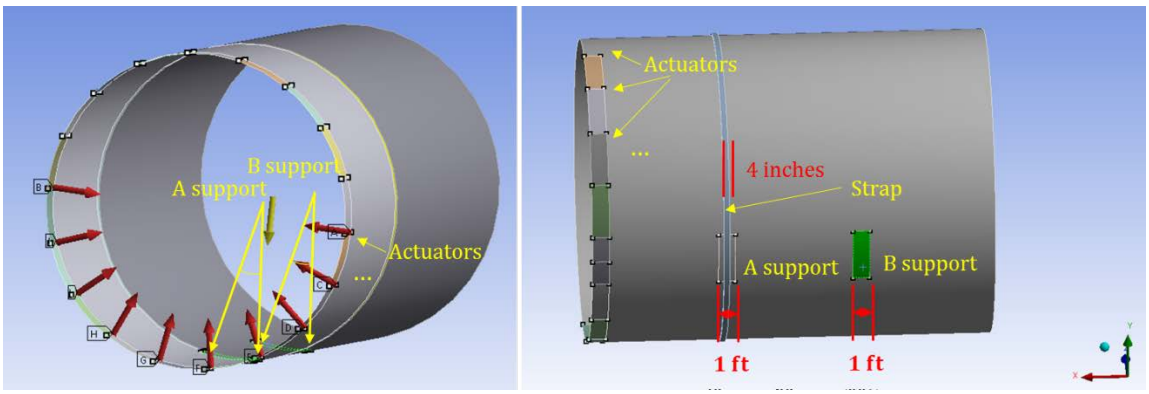

Fig. 6. Support structure of the fuselage in the FEA

The 10 actuators are realized by applying forces on the edge of the outer surface of the fuselage. The forces are equally distributed along the lower semi-fuselage. The distance between the actuator and the edge along x direction is 12 inches.

2.3 Model Validation

2.3.1 Set-Up of the Physical Experiment

A physical experiment with a real fuselage is conducted to validate the accuracy of the finite element model. The physical experiment set-up is shown in Fig. 7. Under the fuselage, mounting bar, force sensor, floor jack, and wood stand are installed successively. A three-dimensional laser metrology system is used to do deflection measurement along the side direction. The dimensional information of the fuselage is consistent with our simulation model parameters. Besides, contacting area between the fuselage and the actuator is a rectangle with the same size for both the finite element model and the physical experiment set-up. The physical experiment records the dimensional deformation of the fuselage under an actuator force changing from 100 pounds to 600 pounds.

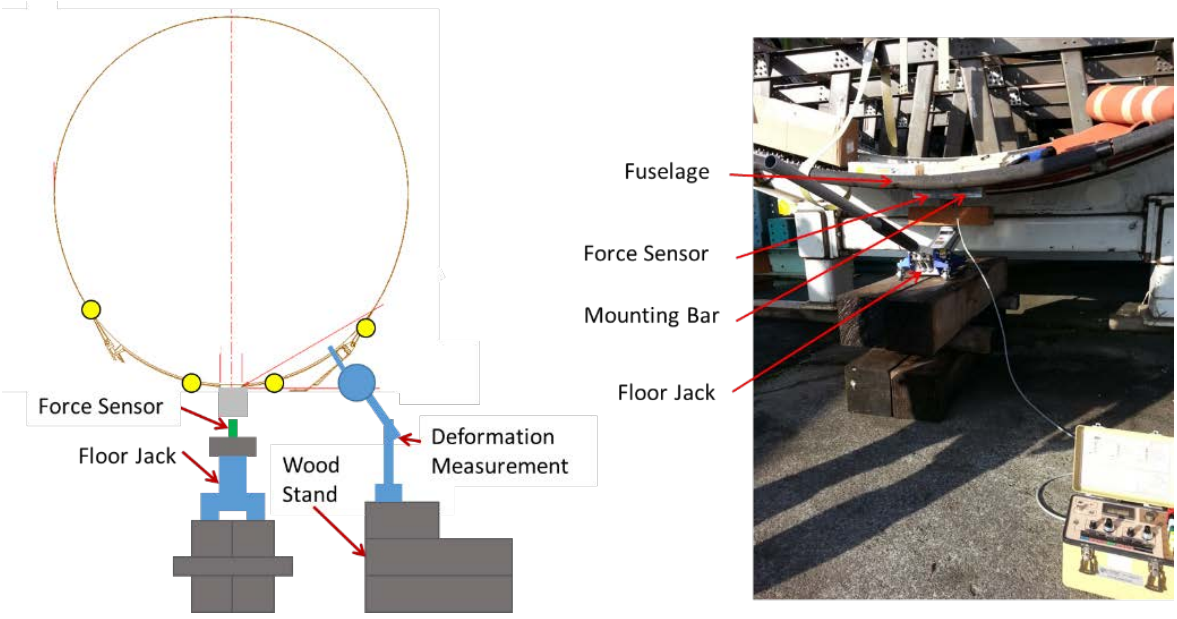

Fig. 7. The set-up of the physical experiment

2.3.2 Calibration of the Finite Element Model based on Physical Observations

After obtaining the physical experimental observations, we need to calibrate the finite element model to make it as accurate as possible. We apply an effective model calibration method via sensible variable identification and adjustment [25]. Calibration variables include thickness of fuselage, thickness ratio of carbon fiber and epoxy resin, temperature, ply orientation angle, support parameters and so on. In the calibration, the concept of sensible variables is introduced. Sensible variables are model parameters which are sensitive in the engineering modeling, and whose optimal values are different from the pre-specified design values. The effective calibration method to identify and adjust the sensible variables with limited physical experimental data is discussed in detail in [25]. We show the results under three actuator's force 200 pounds, 400 pounds and 600 pounds in Fig. 8a and 8b. The differences between FEA simulation data and physical experimental data before calibration are shown in Fig. 8a, and the ones after calibration are shown in Fig. 8b. By quantifying the difference between the FEA simulation data and physical experimental data, the calibration can improve the weighted summation of square error from 353.15 to 53.29 [25]. We can find that after calibration, the response of the finite element model matches the physical experimental data well. Model validation is also accomplished by comparing FEA simulation results and physical experimental data in Fig. 8b.

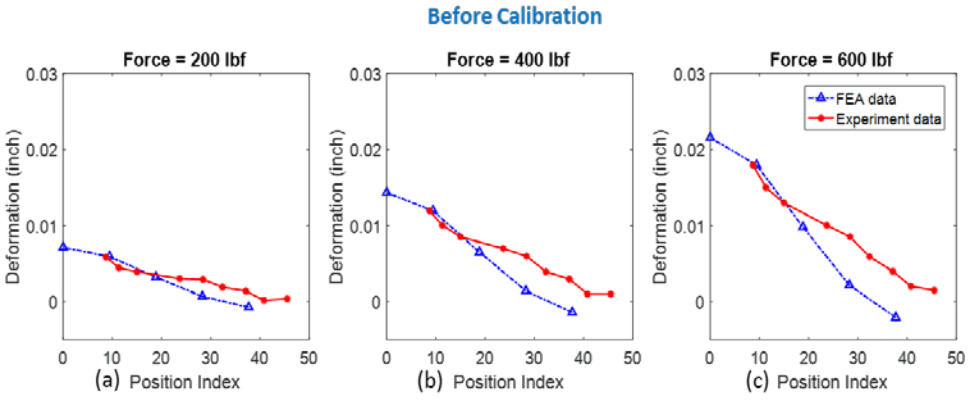

Fig. 8a. Comparison of FEA data and physical experimental data before calibration

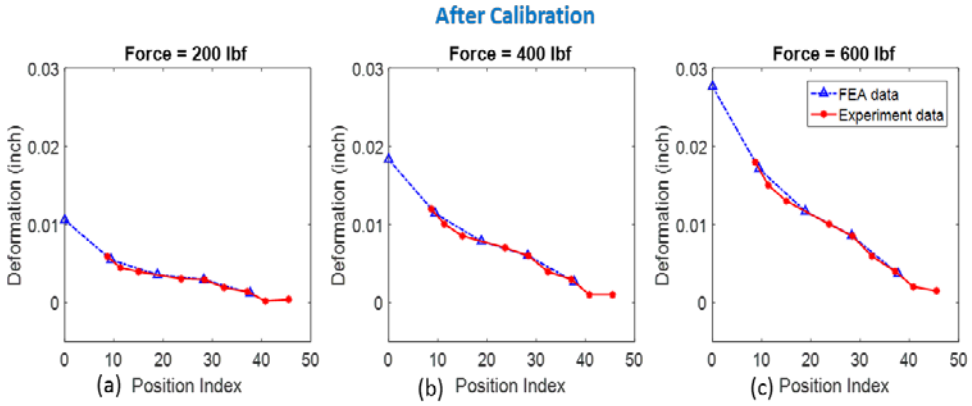

Fig. 8b. Comparison of FEA data and physical experimental data after calibration

2.4 Feasibility Evaluation and Analysis

The feasibility evaluation analyzes whether the actuators are capable of adjusting the shape of the composite fuselage to the desired shape without damage of the composite fuselage. The feasibility evaluation has two sections. First, the dimensional control feasibility evaluates if the actuator can adjust the fuselage within the actuator force limitation. Second, the stress analysis will show whether the fuselage is at the risk of being damaged during the shape control process.

2.4.1 Single-Plane Dimensional Control Feasibility

The dimensional control feasibility test aims to verify whether a fuselage with dimensional errors and natural deformation due to its weight can be compensated to the target shape under bounded actuators' forces. In order to test the deformation of the composite fuselage under different actuators' forces, we set up actuators scheme shown in Fig. 9 (a). All actuators are installed in a single plane with the same X-axis. To mimic the actuators' adjustments during the shape control process, the odd numbers of the actuators push outwards while the even numbers of the actuators push inwards. Each actuator's force has a range from 0 to 1000 pounds and we apply same magnitude of forces for all the actuators. The deformation result of the composite fuselage is shown in Fig. 9 (b). The dimensional deformation of the composite fuselage at the bottom half semi-circle is smaller than the top half due to the constraints of the fixtures. The patterns of the shape deformation are similar for different actuators' forces from 100 to 1000 pounds. We are particularly interested in the deformation at 1000 pounds because that it is the upper limit of forces specified for the actuators in design. The deformations at circumferential angle that is smaller than 45 degree and greater than 130 degree are larger than 1 inch, and the maximum deformation under 1000 pounds is about 5 inches. Thus, the shape control capability is beyond the general maximum manufacturing deviation of a real composite fuselage. Hence, it is feasible to adjust the composite fuselage deformation due to weight back to the ideal shape with less than 1000 pounds actuators' forces.

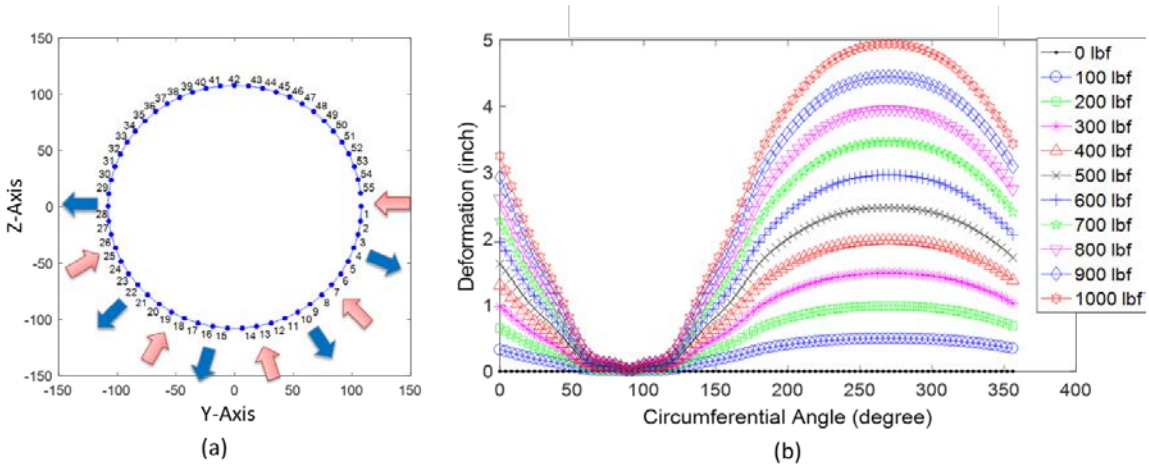

Fig. 9. (a) Scheme of actuators' forces, (b) deformation over circumferential angle under different actuators' forces

2.4.2 Double-Plane Dimensional Control Feasibility

In Section 2.4.1, the single-plane dimensional control feasibility has been studied. The necessity of using double-plane actuators to do shape control will be evaluated in this section. Shape control with more actuator planes has a potential to realize better shape control results. However, it will increase the complexity of the fixture system, and may also result in an over-constraints issue. In the FEA, we install actuators in two force planes. As shown in Fig. 10 (a), ten actuators are installed in the force plane I, with circumferential angles equal to [0^o, 20^o,…, 180^o]. As shown in Fig. 10 (b), nine actuators are installed in the force plane II, with circumferential angles equal to [10^o, 30^o,…, 170^o]. The distance between force plane I (or force plane II) and the edge is 6 inches (or 24 inches). We consider the dimensional response in the plane 1-7, shown in Fig. 10 (c). The distance between two neighboring response planes is 6 inches. The force plane I coincides with the response plane 2, and the force plane II coincides with the response plane 5.

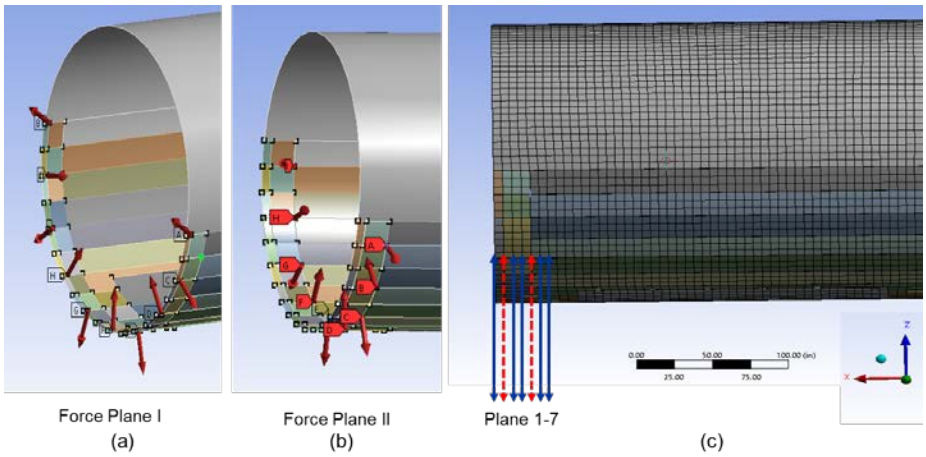

Fig. 10. (a) Actuators in the force plane I, (b) actuators in the force plane II, (c) response plane 1-7 (Note: the force plane I coincides with the response plane 2, and the force plane II coincides with the response plane 5)

Let F_{I} denote the equivalent actuators' forces in the force plane I, and F_{II} for the forces in the force plane II. The results under $F_{\mathrm{I}} = 100$ lbf and $F_{\mathrm{II}} = 0, 100, 200, \ldots, 600$ lbf are shown in Fig. 11. By adding extra nine actuators in the second force plane, the capability of the shape control becomes larger. Specifically, it can adjust about 0.3 inch more with $F_{\mathrm{II}} = 600$ lbf compared with $F_{\mathrm{II}} = 0$ lbf. In addition, with fixed actuators' forces in the force plane I, the deformation patterns under different forces in plane II over circumferential angles have nonlinear characteristics. When F_{II} is small, the shape deformation is relatively smooth. However, it tends to have more waves when F_{II} becomes larger. Furthermore, there exists twist effect in the lower semi-fuselage part, as shown in Fig. 11 (b). That means when the circumferential angle ranges from 40 degree to 120 degree, the angles correspond to the peak deformations becomes smaller from plane 1 to plane 7. Based on the study, our conclusion is as follows. (i) The double plane strategy has more dimensional control and compensation capabilities with less forces applied for each

individual actuator. This has merits to introduce less local stress or tension during the shape control process. With a well-designed control algorithm, double plane strategy can lead to better shape control results. (ii) The double plane strategy will lead to more complexity in the fixture design and maintenance. It also puts more demand in the design and optimization of the shape control algorithm. It should be pointed out that the double plane strategy studied here is to evaluate the shape control capability with multiple actuators installed in two different planes. In practice, further research needs to be done to study the optimal locations of the actuators on the fuselage. The locations of the actuators do not need to be constrained in two planes, but can be any locations on the fuselage with optimal decisions. This should be one of future research topics.

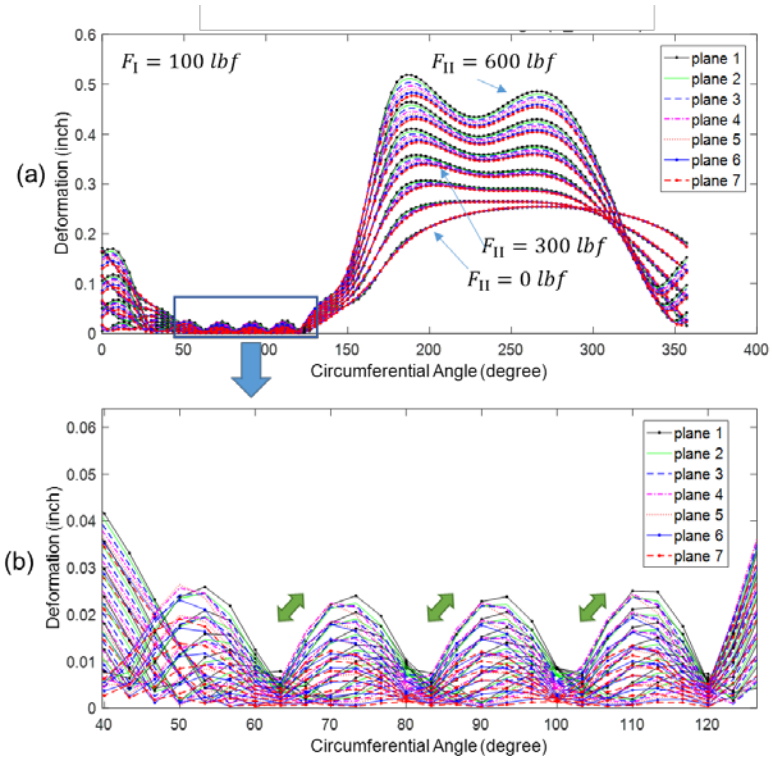

Fig. 11. (a) Deformation over circumferential angle under different actuators' forces ($F_{\mathrm{I}} = 100\ lbf$, and $F_{\mathrm{II}} = 0{\sim}600\ lbf$), (b) enlarged local deformation pattern

2.4.3 Stress/Strain Analysis and Failure Test

In order to make sure the actuators do not damage the composite fuselage, a stress/strain analysis needs to be conducted. Since the maximum force can be applied to the actuator is 1000 pounds by engineering knowledge, we analyze the stress/strain response when actuators' forces range from 100 to 1000 pounds. The results of stress/strain analysis are shown in Fig. 12. We explore the equivalent (von Mises) stress, maximum principal stress, middle principle stress, minimum principal stress, and maximum shear stress in Fig. 12 (a). Even for the situation of 1000 pounds, the maximum principal stress is 35.33 MPa, which is lower than the threshold 100 MPa. The maximum shear stress is 18.9 MPa, which is within the threshold 32 MPa. The strain is the response of a system to an applied stress. We are also interested in whether the strain of the composite fuselage under the bounded actuators' forces, and make sure it will not exceed the strain limit. As shown in Fig. 12 (b), the maximum equivalent elastic strain under 1000 pounds is 0.0011, which is lower than the limit 0.0032. The maximum shear elastic strain is 0.0012, which is lower than the shear strain limit 0.011. From the result, we can conclude that there is no plastic strain that results in unwanted failure of material, such as cracking.

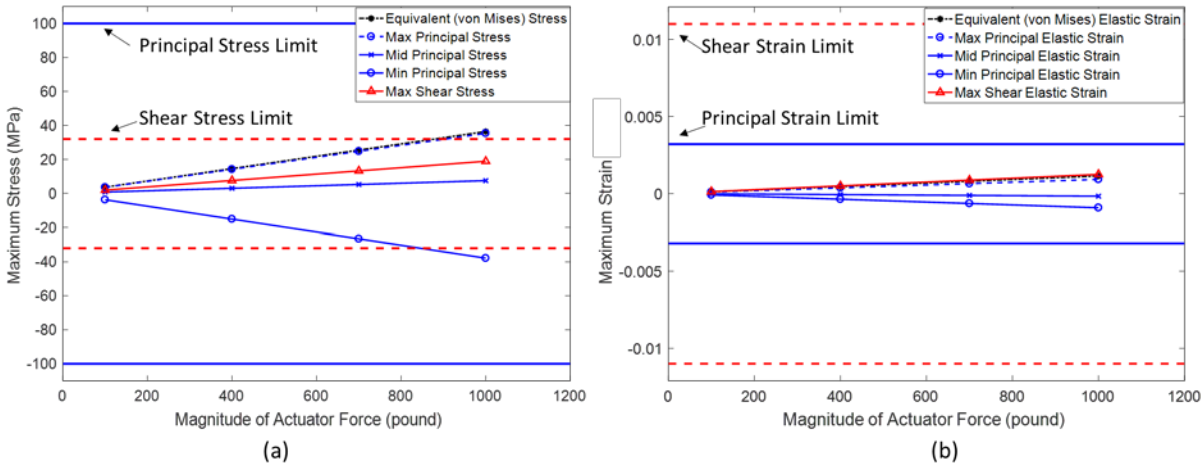

Fig. 12. Maximum (a) stress, (b) strain, under different magnitude of actuators' forces

We also explore the stress distribution in each plies. Fig. 13 (a) shows the setup of actuators with magnitude of forces equal to 1000 pounds. The corresponding equivalent stress map and equivalent elastic shear stress map are shown in Fig. 13 (b, c). For the stress distribution in each kind of interior plies, stress maps in a bottom ply of carbon fabrics, a core ply of epoxy resin, and a top ply of carbon fabrics, are shown in Fig. 13 (d-f). The majority of stress resulted from the actuators is located at the bottom plies of carbon fabrics, while the stress from the bottom fixture supports is located at the top plies of carbon fabrics.

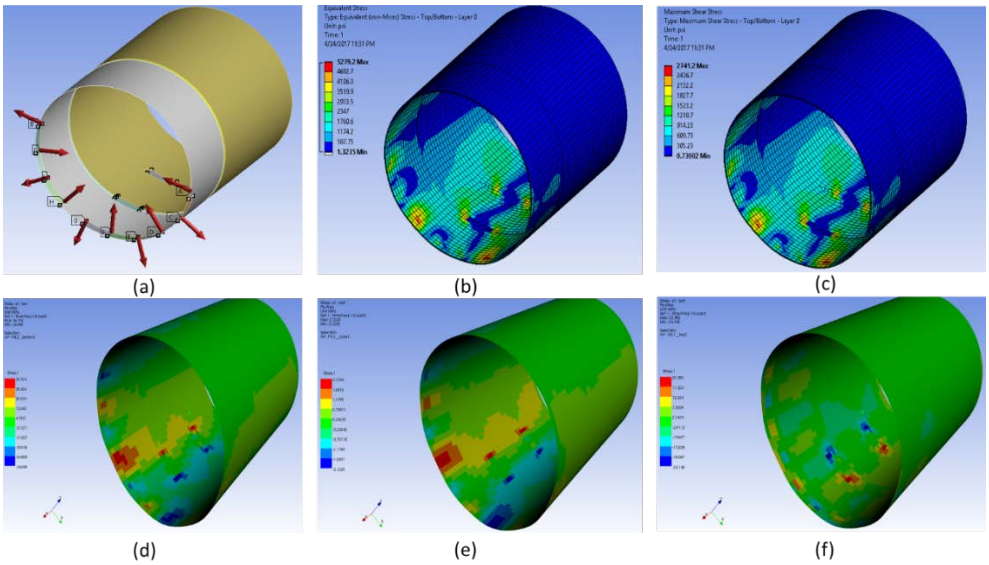

Fig. 13. (a) Setup of actuators, (b) equivalent stress map, (c) equivalent elastic strain map, (d) stress in a bottom ply of carbon fabrics, (e) stress in a core ply of epoxy resin, (f) stress in a top ply of carbon fabrics

Furthermore, failure test has been conducted based on multiple popular criteria including maximum strain/stress, Tsai-Wu, Tsai-Hill, Hoffman, Hashin criteria [16]. The results show that the inverse reserve factor, which defines the inverse margin to failure, is 0.27, which is lower than the failure threshold 1.00. Therefore, the actuators will not damage the composite fuselage when the maximum actuators' force is 1000 pounds

2.5 Summary

Composite parts have been widely used in aircraft industry due to their superior mechanical properties. Dimensional variability reduction and shape control of composite fuselages are bottleneck problems for the massive production of high quality aircrafts. In order to address the dimensional control problem, a new concept of shape control system is proposed and it can (i) compute the optimal actuators' forces to minimize the dimensional

deviations of current composite parts and the ideal shape, (ii) implement the adjustment automatically, (iii) release the workload of highly skilled engineers.

In this paper, a feasibility study is conducted to evaluate the proposed shape control concepts. In order to do the feasibility analysis, an accurate finite element model is developed to mimic the fabrication of composite fuselage, including the detailed materials setting, ply design, geometry and fixture structures. The finite element model is validated and calibrated based on physical experimental data with a real fuselage on the production floor. Based on the validated FEA model, the feasibility analysis has been conducted, which confirms that

(i) Single-plane shape control system has the capability to adjust the deformed composite fuselage back to the ideal shape with less than 1000 pounds actuators' forces.

(ii) Double-plane scheme has a better capability of dimensional shape control, but it increases the complexity of the fixture design and shape control algorithm.

(iii) The distribution map of stress for each typical ply is investigated. The stress/strain analysis and failure test indicate that the actuators do not damage composite fuselages under the single-plane with ten actuators' scheme.

In summary, the proposed shape control of fuselage dimension is feasible and worthy of further investigation. The future R&D efforts should address the following issues: (i) optimal number of actuators and their locations on the fuselage, (ii) optimal control algorithms for the shape control, (iii) uncertainty quantification and dimensional control accuracy assessment, and (iv) physical testing and validation of the fuselage control system.

CHAPTER 3. SURROGATE MODEL BASED CONTROL CONSIDERING UNCERTAINTIES FOR COMPOSITE FUSELAGE ASSEMBLY

Shape control of composite parts is vital for large-scale production and integration of composite materials in the aerospace industry. The current industry practice of shape control uses passive manual metrology. This has three major limitations: (i) low efficiency: it requires multiple trials to achieve the desired shape during the assembly leading to longer assembly times; (ii) non-optimal: it makes it challenging to reach optimal deviation reduction; and (iii) experience-dependent: highly skilled engineers are required during the assembly process. This paper describes an automated shape control system that can adjust composite parts to an optimal configuration in a manner that is highly effective and efficient. The objective is accomplished by (i) building a finite element analysis platform, validated by experimental data; (ii) developing a surrogate model with consideration of actuator uncertainty, part uncertainty, modeling uncertainty, and unquantified uncertainty to achieve predictive performance and embedding the model into a feed-forward control algorithm; (iii) conducting multivariable optimization to determine the optimal actions of actuators. We show that the surrogate model considering uncertainties achieves satisfactory prediction performance and that the automated optimal shape control system can significantly reduce the assembly time with improved dimensional quality.

3.1 Introduction

Composite parts have been widely used in industry due to their unique characteristics, such as high strength-to-weight ratio, high stiffness-to-weight ratio, potentially long life and low life-cycle cost. Over the past decades, aircraft manufacturers have been gradually increasing the application of composite parts in the design of aircrafts. Assembly of composite parts is a manufacturing process of joining two or more composite parts together using various joining techniques. Due to multiple suppliers and multiple manufacturing batches, dimensional variability of composite parts inevitably exists when the composite parts are assembled. Therefore, effective methodologies are needed for dimensional analysis, variation reduction, and optimal shape adjustment for composites parts assembly to achieve satisfactory dimensional accuracy.

In order to achieve dimensional (or shape) adjustment of a fuselage section, a number of adjustable actuators, as shown in Fig. 14 (a, b), may be used in practice to provide push or pull forces to reduce dimensional deviations and generate the required shape of the parts. In Fig. 14 (b), the center of the fuselage edge circle without the actuators is defined as the original point of the coordinate system. The horizontal intermediate cross plane is defined as the X-Y plane of the coordinate system. Z-axis is vertical upwards with the X-Y plane. The responses are the total dimensional deviations under the impact of actuators' forces, (Here we focus on multiple key points in fuselage edge plane near the actuators, as shown in Fig. 14 (c)). Currently, the adjustment of each actuator is conducted by a trial-and-error method based on in-situ measurements of the section until reaching a

desired acceptable shape. The current practice has three limitations: (i) low efficiency: it may take long time and multiple trials to adjust actuators to achieve a desired shape during the assembly process; (ii) non-optimality: it may reach an acceptable dimensional quality rather than the optimal deviation reduction; (iii) highly skilled engineers requirement: the quality and efficiency of assembly depend on the skills of engineers, which increases the uncertainties of the time and quality of the fuselage assembly task. In order to reduce the cycle time, increase the productivity, as well as decrease the dimensional variation of the composite assembly, an automatic optimal shape control (AOSC) system will be developed to realize composites modeling and control for optimal adjustment of all actuators simultaneously.

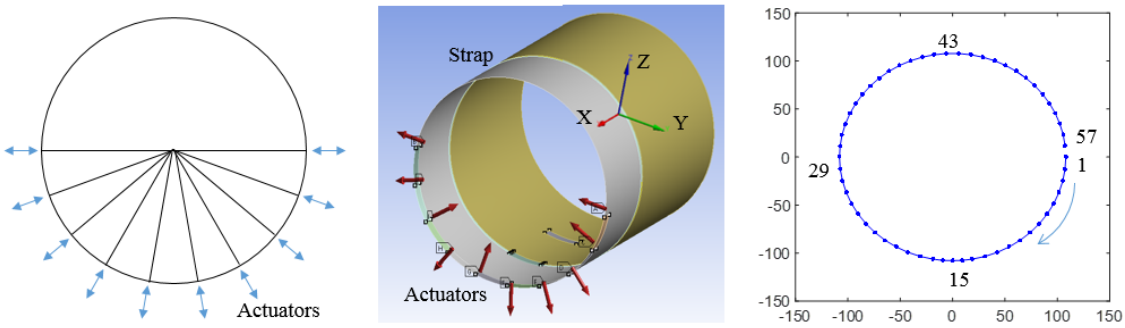

(a) Layout of ten actuators, (b) Sketch map of the shape adjustment, (c) Key points

Fig. 14 Schematic diagram for shape adjustment

In the literature, there are numerous research topics have been conducted for modeling and analysis of dimensional variation reduction and control for the assembly of isotropic metal parts. Jin and Shi introduced a state-space modeling methodology for

dimensional control of sheet metal assembly [26], and later extended to the Stream of Variation (SoV) methodology that has been developed and implemented in various multistage manufacturing processes [27]. Djurdjanovic and Ni proposed a linear state-space SoV modeling by deriving explicit expressions for the influence of the errors in fixtures, locating datum features and measurement datum features in the multistation machining process [5, 6]. A method of influence coefficient (MIC) was exploited to combine engineering structural mechanics with statistical methods to model the relationships between the incoming part deviations and the output assembly deviations in single-station [7] and multi-station assembly processes [8]. A detailed literature review of modeling and variation analysis of compliant assembly of metal parts can be found in the papers [2, 3]. It is a more challenging task to model the dimensional variation of compliant composite parts with anisotropic characteristics. Zhang and Shi built a stream of variation (SoV) model for compliant composite part assembly in single-station [2] and multi-station processes [3]. In their model, part manufacturing errors, fixture position errors, and relocation induced errors were considered for the analysis of dimensional variation and its propagation in a multistage process. However, this SoV modeling method cannot be directly used in the AOSC system of composite fuselage assembly because that the SoV model in [2] and [3] is based on engineering physical mechanics, and material property parameters such as equivalent stiffness matrix and compliance matrix about the composite parts are required. It is difficult to obtain an accurate estimation of those parameters, especially for large composite parts with complex structures. Other than the SoV type of models, other types of models have been used to improve the quality control of assembly

process, such as robust pattern-matching technique for variation source identification [28], adaptive product, process and tooling design strategy for optimal dimensional quality [29], modeling of operator effects on process quality [30], and variation analysis using component geometric covariance [31] et al. However, these models cannot be used directly in the composite fuselage shape control problem.

In the literature about control strategies, Zhong et al. [32] proposed a feed-forward control strategy that explicitly took the uncertainties of model coefficients into account. However, the model with uncertainties was developed for rigid metal parts and the parameters depended on the geometrical transformation of rigid parts, which was not suitable for composite parts with highly nonlinear anisotropic properties. Djurdjanovic and Ni [33] proposed a novel SoV model based stochastic control of dimensional quality to minimize the least square of difference between the dimensions at the end of the line and the nominal dimensions. In their model the measurement and process noise, as well as the accuracy of actuation of flexible tooling elements are considered. As this control strategy is built upon a SoV model with the state space structure [5, 6], which is not suitable for the fuselage shape control where a different model structure is adopted. For other control strategies considering model uncertainties, adaptive control [34], H-Infinity optimal control [35], and Fuzzy control [36] were proposed and applied in the dynamic systems. However, these methods cannot be directly used in the shape control of composite fuselage assembly process because of the difference between dynamic model and static dimensional model for variation reduction [32]. Thus, an effective modeling and control methodology needs to be developed for the AOSC system of composite fuselage assembly.

Next we review the literature about model uncertainty. Since the model uncertainty is an important and widely encountered problem, which is associated with control theory, automation, mechanical engineering, manufacturing, statistics and applied mathematics [9-13], it is a challenging task to illustrate all different techniques of treating model uncertainty in all those domains. For model uncertainty in control theory [9, 10], uncertainty is illustrated via uncertain parameters or disturbances within a typically compact set, and robust or adaptive control is developed to deal with uncertainty explicitly. Decision support models evaluate the extent of uncertainties and realize the balance between decision benefits and risk management [11]. Statistical models consider structural uncertainty via model selection as well as model validation, and consider parametric uncertainty by specified stochastic terms with random distributions [12]. More literature on uncertainty modeling can be found in [13]. In this paper, we are mainly focused on the review of the model uncertainty corresponding to statistical models, which is closely related to the topic of this paper. In Section 2.2.1, the authors review the conventional methods including the multivariate Regression model, the Universal Kriging model, and the Stochastic Kriging model, where uncertainties are illustrated by different stochastic terms.

In the paper, we propose a methodology to develop a surrogate model considering various uncertainties and applying this model to achieve automatic optimal shape control. An overview of the proposed methodology is given in Fig. 15. According to the tooling parameters (e.g. number, positions, and maximum forces of actuators), material parameters, and dimensional parameters of the composite part, we build a finite element

analysis (FEA) platform for the methodology development and validation. The FEA platform is validated by a set of real experiments with industrial set-ups. Based on the validated FEA platform, a scheme of computer experiment is generated by design of experiment and then conducted to collect input variables and output responses. A surrogate model considering part uncertainty, actuator uncertainty, and model uncertainty is developed to link the relationship between inputted actuators' forces and outputted dimensional deviations. The surrogate model is validated by the testing experiments. After that, the surrogate model considering uncertainties is embedded into an automatic optimal shape control algorithm. A feed-forward control law is obtained by solving the optimization problem that minimizes the weighted sum of square of dimensional deviations between the real dimensional positions and the designed positions of the part. The main contribution of this paper is to study the composite fuselage shape control problem. In conventional control papers, most of the models are differential or difference equations, e.g. dynamic equations, which cannot be adequately used to describe the dimensional control problem for composite fuselage. In this paper, we use a surrogate model with Gaussian process term and other random terms, which is able to model the relationships among the fuselage dimension and actuators' forces, as well as address actuator uncertainty, part uncertainty, modeling uncertainty and unquantified uncertainty. With this new type of model, we propose a feedforward control strategy and apply it to a composite fuselage shape control problem.

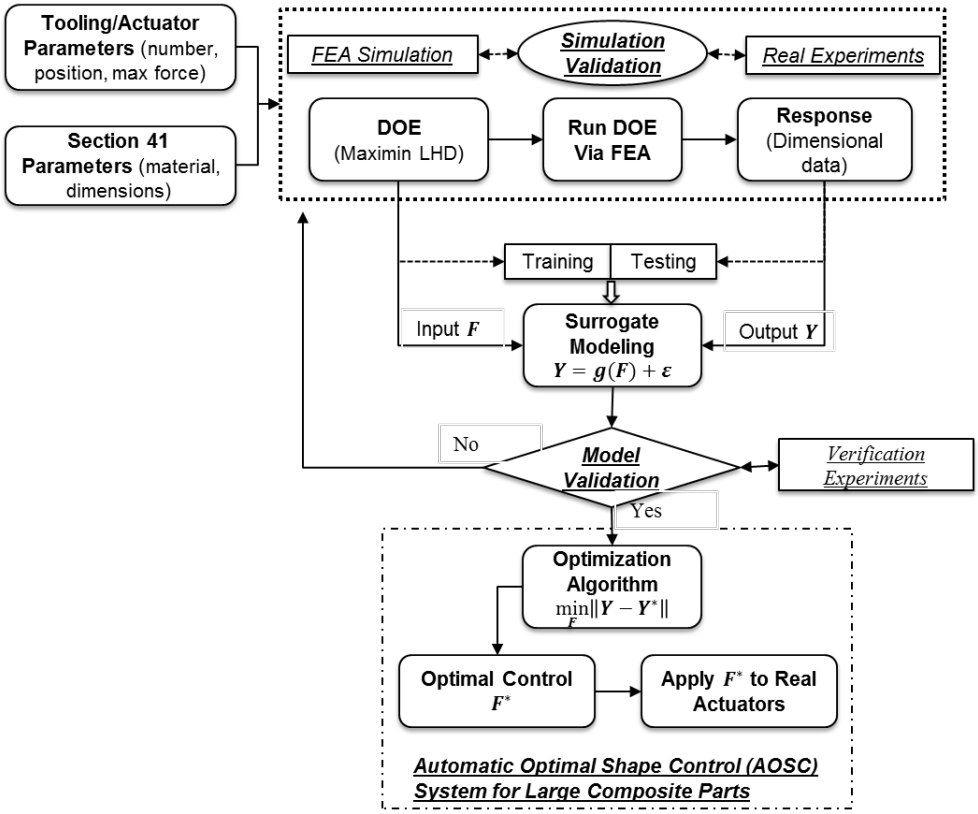

Fig. 15 Overview of the proposed methodology

The remainder of this paper is organized as follows. Section 3.2 illustrates the surrogate modeling process considering various uncertainties. A maximum likelihood estimation (MLE) algorithm is developed to realize the parameter estimation and the response prediction for incoming inputs. Section 3.3 describes a feed-forward automatic control algorithm for shape control of composite assembly process. Section 3.4 presents the process of building the finite element analysis platform and its validation by real experimental data. In addition, a case study is conducted to demonstrate the implementation procedures, including design of experiment, prediction results, control

results, sensitivity analysis, and stress analysis. Finally, a brief summary is provided in Section 3.5.

3.2 Surrogate Model Considering Uncertainties

In this section, we are interested in building a model to link the response variables (dimensional deviations) with control variables (actuators' forces). The model should have sufficient prediction capability and precision with consideration of various uncertainties. We will first review the conventional multivariate regression model, the Universal Kriging Model (UKM), and the Stochastic Kriging Model (SKM). Then, a novel Surrogate Model considering Uncertainties (SMU) will be proposed. After that, a maximum likelihood estimation (MLE) algorithm is developed to estimate the parameters of the SMU.

3.2.1 Review of Conventional Models

3.2.1.1 Multivariate Regression Model

According to the mechanics of composite materials and classical lamination theory, a linear relationship between dimensional deviations and actuators' forces is expected within the elastic zone [37]. Assuming that there is a noise term to describe the unquantified errors, such as error from modeling nonlinear property by linear approximation, error from part uncertainty et al., we can use a linear regression model [38] to describe how the actuators' forces impact on the part deviations,

$$\boldsymbol{Y}_{i\cdot}(\boldsymbol{F}) = \boldsymbol{FS} + \boldsymbol{\varepsilon}_{i\cdot} \tag{1}$$

where $\boldsymbol{F}_{1\times q}$ is the actuator force vector with dimension of $1 \times$ q; $\boldsymbol{Y}_{i\cdot}(\boldsymbol{F})$, with dimension $1 \times$ p , is the output dimensional variable under the i^{th} replication at $\boldsymbol{F}$; $\boldsymbol{S}$ is the sensitivity matrix that quantifies the relationship between actuators' forces and fuselage deviations; $\boldsymbol{\varepsilon}_{i\cdot}$ is assumed to follow a multivariate normal distribution $\boldsymbol{\varepsilon}_{i\cdot}\sim\mathbb{N}(\mathbf{0},\ \boldsymbol{\Sigma}_{\boldsymbol{\varepsilon}})$, that represents the unquantified errors.

3.2.1.2 Universal Kriging Model

Now consider an ideal simulation experiment where the response could be observed without noise. The Universal Kriging Model (UKM) could be developed to show the deterministic relationship in a statistical framework [39]:

$$Y_j(\boldsymbol{F}) = \boldsymbol{F}\boldsymbol{S}_j + z_j(\boldsymbol{F}) \tag{2}$$

where $Y_j(\boldsymbol{F})$ denotes the j^{th} dimensional variable of fuselage at the actuators' forces $\boldsymbol{F}$; $\boldsymbol{S}_j$ represents the sensitivity matrix corresponding to the j^{th} response, $j = 1,2,\dots,\text{p}$; $z_j(\boldsymbol{F})$ is a stochastic process with mean 0. Usually, we consider z_j $(\boldsymbol{F})$ as a Gaussian process $z_j\sim\boldsymbol{GP}(\mathbf{0},\ \boldsymbol{\Sigma}_{zj})$, where $\boldsymbol{\Sigma}_{zj}$ is a covariance matrix of stochastic process. Similar to the notation in the reference [39], the covariance between vector $\boldsymbol{a}$ and vector $\boldsymbol{b}$ satisfies $\boldsymbol{\Sigma}_{zj}(\tau_j^2,\boldsymbol{\theta},\boldsymbol{a},\boldsymbol{b}) = \tau_j^2 R_{zj}(\boldsymbol{\theta},\boldsymbol{a}-\boldsymbol{b})$, where $R_{zj}(\boldsymbol{\theta},\boldsymbol{a}-\boldsymbol{b})$ is one of the correlation functions. With spatial correlation, $z_j(\boldsymbol{F}_{\text{m}})$ and $z_j(\boldsymbol{F}_{\text{n}})$ tend to be similar (e.g. $R_{zj,\text{mn}} = R_{zj}(\boldsymbol{\theta},\boldsymbol{F}_{\text{m}},\boldsymbol{F}_{\text{n}})$ tends to be large) if $\boldsymbol{F}_{\text{m}}$ and $\boldsymbol{F}_{\text{n}}$ are close. Note that, since the response of simulation could be observed without noise, there is no replication needed.

3.2.1.3 Stochastic Kriging Model

Considering both a noise term $\boldsymbol{\varepsilon}_{i\cdot}$ and a stochastic process term $z_j(\boldsymbol{F})$ that are regarded as intrinsic uncertainty and extrinsic uncertainty respectively, the Stochastic Kriging model can be developed [28] as

$$Y_{ij}(\boldsymbol{F}) = \boldsymbol{F}\boldsymbol{S}_j + z_j(\boldsymbol{F}) + \varepsilon_{ij}\,, \tag{3}$$

where $Y_{ij}(\boldsymbol{F})$ denotes the j^{th} dimensional variable of the fuselage under the i^{th} replication at the actuators' forces $\boldsymbol{F}$; $\boldsymbol{S}_j$ represents the sensitivity matrix corresponding to the j^{th} response, $j = 1,2,\dots,\text{p}$; $z_j(\boldsymbol{F})$ is a stochastic process with mean 0, which represents the extrinsic uncertainty from randomly sampling from functional mapping during surrogate modelling; The intrinsic noise ε_{ij} is assumed to be independent and identically distributed with a normal distribution $\varepsilon_{ij} \sim \mathbb{N}(0,\ \sigma_{\boldsymbol{\varepsilon j}})$.

For experiment setting, pairs $(\boldsymbol{F}_t, \text{n}_t)$, $t = 1,2,\dots,k$, where n_t is the number of simulation replications taken at the design setting $\boldsymbol{F}_t$, are implemented to collect the simulation data. The stochastic process $z_j(\boldsymbol{F})$ is usually assumed to be a Gaussian process $\boldsymbol{GP}(\boldsymbol{0},\ \boldsymbol{\Sigma}_{zj})$ with covariance matrix $\boldsymbol{\Sigma}_{zj}$ with dimension $k \times k$. For any two vectors of the actuators' forces, the covariance is $\boldsymbol{\Sigma}_{zj}(\boldsymbol{F}_{\text{m}}, \boldsymbol{F}_{\text{n}}) = cov[z_j(\boldsymbol{F}_{\text{m}}), z_j(\boldsymbol{F}_{\text{n}})]$. Let $\boldsymbol{\Sigma}_{zj}(\boldsymbol{F}_0, \cdot) = (cov\left[z_j(\boldsymbol{F}_0), z_j(\boldsymbol{F}_1)\right], \dots,\ cov\left[z_j(\boldsymbol{F}_0), z_j(\boldsymbol{F}_{\text{k}})\right]$ as the covariance between z_j's at design points and new actuators' forces $\boldsymbol{F}_0$.

We know the sample mean at $\boldsymbol{F}_t$ as $\bar{\boldsymbol{Y}}_j(\boldsymbol{F}_t) = \sum_{\boldsymbol{i=1}}^{\mathrm{n}_t} Y_{ij}(\boldsymbol{F}_t)\,/\mathrm{n}_t$. Let $\bar{\boldsymbol{Y}}_j = (\bar{\boldsymbol{Y}}_j(\boldsymbol{F}_1), \dots, \bar{\boldsymbol{Y}}_j(\boldsymbol{F}_k))^{\boldsymbol{T}}$, and the noise covariance matrix is $\boldsymbol{\Sigma}_{\varepsilon j}$, a $k \times k$ covariance matrix with (a, b) element is $\mathrm{Cov}\left[\sum_{i=1}^{n_a} \varepsilon_{ij}(\boldsymbol{F}_a)/n_a\,, \sum_{i=1}^{n_b} \varepsilon_{ij}(\boldsymbol{F}_b)/n_b\right]$. Let $\boldsymbol{F}_{DOE} = (\boldsymbol{F}_1; \dots; \boldsymbol{F}_k)$ denote all the design points of the actuators' forces. Let $\boldsymbol{R}_j(\boldsymbol{F}_0,\cdot) = \left(\mathrm{Cov}\left[Y_j(\boldsymbol{F}_0), \bar{Y}_j(\boldsymbol{F}_1)\right]; \dots; \mathrm{Cov}\left[Y_j(\boldsymbol{F}_0), \bar{Y}_j(\boldsymbol{F}_k)\right]\right)$.

We can get the MSE-optimal linear predictor as

$$\widehat{\boldsymbol{Y}}_j(\boldsymbol{F}_0) = \boldsymbol{F}_0\boldsymbol{S}_j + \boldsymbol{R}_j(\boldsymbol{F}_0,\cdot)^{\boldsymbol{T}}\left[\boldsymbol{\Sigma}_{zj} + \boldsymbol{\Sigma}_{\varepsilon j}\right]^{-\mathbf{1}}(\bar{\boldsymbol{Y}}_j - \boldsymbol{F}_{DOE}\boldsymbol{S}_j).$$

3.2.2 Surrogate Model Considering Uncertainties

The conventional models discussed in Section 3.2.1 cannot handle all the uncertainties in our application, such as uncertainties from actuators variability and part-to-part variability (uncertainties sources will be explained further in Section 3.2.4. We propose a novel surrogate model considering various uncertainties. Experiment design pairs $(\boldsymbol{F}_t\,, \mathrm{n}_t)$, $t = 1,2, \dots, k$, are implemented to collect the response, which is the dimensional deviations $Y_{ij}(\boldsymbol{F}_t)$. Afterwards, a surrogate model considering uncertainties is proposed as

$$Y_{ij}(\boldsymbol{F}_t) = \boldsymbol{F}_t\boldsymbol{S}_j + \boldsymbol{F}_t\tilde{\boldsymbol{S}}_j + \widetilde{\boldsymbol{F}}_t\boldsymbol{S}_j + z_j(\boldsymbol{F}_t) + \varepsilon_{ij}(\boldsymbol{F}_t), \tag{4}$$

where $i = 1,2, \dots, n_t$; $j = 1,2, \dots, p$; p is the number of output responses (key dimensional features). $\boldsymbol{F}_t$ is the target actuators' forces vector (row vector) to be implemented; $\widetilde{\boldsymbol{F}}_t$ is an

additional random deviations of actuators' forces that results from the actuators' uncertainty, whose distribution $\mathbb{N}(\mathbf{0},\ \boldsymbol{\Sigma_F})$, can be obtained from the tolerance of actuators instructions; $\boldsymbol{F}_t + \widetilde{\boldsymbol{F}}_{\boldsymbol{t}}$ is a true actuators' force vector at the i^{th} replication of $\boldsymbol{F}_t$. $\boldsymbol{S}_j$ is an ideal sensitivity vector (column vector) and $\tilde{\boldsymbol{S}}_j$ represents the random sensitivity vector variability from the part uncertainty, which is assumed to follow $\mathbb{N}(\mathbf{0},\ \boldsymbol{\Sigma_S})$. Both $\boldsymbol{S}_j$ and $\boldsymbol{\Sigma_S}$ are unknown. $\boldsymbol{z}_j(\boldsymbol{F}_t)$ is a zero mean stochastic process, which is assumed to be a stationary Gaussian process $z_j \sim \boldsymbol{GP}(\mathbf{0},\ \boldsymbol{\Sigma}_{zj})$. $\varepsilon_{ij}(\boldsymbol{F}_t)$ is assumed to follow an independent normal distribution $\varepsilon_{ij}(\boldsymbol{F}_t) \sim \mathbb{N}(0,\ \sigma^2_{\varepsilon j}(\boldsymbol{F}_t))$, that represents the inherent simulation variability in a stochastic simulation. ε_{ij}, $\widetilde{\boldsymbol{F}}_t$, $\tilde{\boldsymbol{S}}_j$, and z_j are assumed to be mutually independent, and their higher order interaction terms $\widetilde{\boldsymbol{F}}_{\boldsymbol{t}} \cdot \tilde{\boldsymbol{S}}_j$ is assumed to be zero. The model can be interpreted as a decomposition of the response $Y_{ij}(\boldsymbol{F}_t)$ into three parts: a regression term $\boldsymbol{F}_t\boldsymbol{S}_j + \boldsymbol{F}_t\tilde{\boldsymbol{S}}_j + \widetilde{\boldsymbol{F}}_t\boldsymbol{S}_j$, a Gaussian process term $z_j(\boldsymbol{F}_t)$**,** and a noise term $\varepsilon_{ij}(\boldsymbol{F}_t)$.

Let $\bar{Y}_j(\boldsymbol{F}_t)$ be the sample mean at $\boldsymbol{F}_t$, that denotes $\bar{Y}_j(\boldsymbol{F}_t) = \sum_{i=1}^{n_t} Y_{ij}(\boldsymbol{F}_t)\,/n_t$. Let $\boldsymbol{F}_{DOE} = (\boldsymbol{F}_1; \ldots; \boldsymbol{F}_k)$ denote the design matrix of actuators' forces. Let $Y_j(\boldsymbol{F}_0)$ be the true response at $\boldsymbol{F}_0$. The purpose of building a surrogate model is to realize accurate prediction on $Y_j(\boldsymbol{F}_0)$. Let $\boldsymbol{\Sigma}_{\varepsilon j}$ represent the covariance matrix associated with the noise term with (a, b) element $\mathrm{Cov}\left[\sum_{i=1}^{n_a} \varepsilon_{ij}(\boldsymbol{F}_a)/n_a\,, \sum_{i=1}^{n_b} \varepsilon_{ij}(\boldsymbol{F}_b)/n_b\right]$**,** and $\boldsymbol{\Sigma}_{\varepsilon j}$ is assumed to be diagonal, which indicates that the correlations among the noise terms under different design points are zeros.

In our method, we model the actuators' uncertainty, part uncertainty, and unquantified uncertainty by using random vectors with Gaussian distributions and describe the modeling uncertainty with a Gaussian process term. The reason to use this technique is that the proposed surrogate model considering uncertainties can decompose the dimensional deviations into multiple components. These components are associated with different physical sources of uncertainties. In addition, the assumption of Gaussian distribution for actuators' forces and sensitivity vector is reasonable because of engineering tolerance of specific variables. The Gaussian process can extract the complex material properties information from the training samples and realize good prediction performance.

Firstly, we derive the joint distribution shown in Proposition 1.

Proposition 1. The model (4) implies that $Y_j(\boldsymbol{F}_0)$ and a sample mean vector $\overline{\boldsymbol{Y}}_j = \left[(\overline{Y}_j(\boldsymbol{F}_1), \overline{Y}_j(\boldsymbol{F}_2), \dots, \overline{Y}_j(\boldsymbol{F}_k)\right]^T$ follows a multivariate normal distribution

$$\begin{pmatrix} Y_j(\boldsymbol{F}_0) \\ \overline{\boldsymbol{Y}}_j \end{pmatrix} \sim \mathbb{N}_{1+k}\left(\begin{pmatrix} \boldsymbol{F}_0\boldsymbol{S}_j \\ \boldsymbol{F}_{DOE}\boldsymbol{S}_j \end{pmatrix}, \begin{pmatrix} \tau_j^2 & \boldsymbol{R}^T(\boldsymbol{F}_0,\cdot) \\ \boldsymbol{R}(\boldsymbol{F}_0,\cdot) & \boldsymbol{R} \end{pmatrix}\right),$$

where $\boldsymbol{R}_j(\boldsymbol{F}_0,\cdot) = \left(\mathrm{Cov}\left[Y_j(\boldsymbol{F}_0), \overline{Y}_j(\boldsymbol{F}_1)\right]; \dots; \mathrm{Cov}\left[Y_j(\boldsymbol{F}_0), \overline{Y}_j(\boldsymbol{F}_k)\right]\right) = \left(\boldsymbol{F}_0\boldsymbol{\Sigma}_{\boldsymbol{S}}\boldsymbol{F}_1^T + \tau_j^2 R_{zj}(\boldsymbol{\theta}, \boldsymbol{F}_0 - \boldsymbol{F}_1); \dots; \boldsymbol{F}_0\boldsymbol{\Sigma}_{\boldsymbol{S}}\boldsymbol{F}_k^T + \tau_j^2 R_{zj}(\boldsymbol{\theta}, \boldsymbol{F}_0 - \boldsymbol{F}_k)\right)$, and $\boldsymbol{R}_j = \boldsymbol{F}_{DOE}\boldsymbol{\Sigma}_{\boldsymbol{S}}\boldsymbol{F}_{DOE}^T + \boldsymbol{\Sigma}_{zj} + \boldsymbol{S}_j^T\boldsymbol{\Sigma}_{\boldsymbol{F}}\boldsymbol{S}_j \cdot \boldsymbol{I} + \boldsymbol{\Sigma}_{\varepsilon j}$.

Proof:

According to the model (4) and its assumptions,

$$\mathrm{Cov}\left[Y_{mj}(\boldsymbol{F}_a), Y_{hj}(\boldsymbol{F}_b)\right]$$

$$= \mathrm{Cov}\left[\boldsymbol{F}_a\tilde{\boldsymbol{S}}_j + \widetilde{\boldsymbol{F}}_a\boldsymbol{S}_j + z_j(\boldsymbol{F}_a) + \varepsilon_{mj}, \boldsymbol{F}_b\tilde{\boldsymbol{S}}_j + \widetilde{\boldsymbol{F}}_b\boldsymbol{S}_j + z_j(\boldsymbol{F}_b) + \varepsilon_{hj}\right]$$

$$= \boldsymbol{F}_a\boldsymbol{\Sigma}_{\boldsymbol{S}}\boldsymbol{F}_b^T + \boldsymbol{S}_j^T\mathrm{Cov}\left[\widetilde{\boldsymbol{F}}_a, \widetilde{\boldsymbol{F}}_b\right]\boldsymbol{S}_j + \tau_j^2 R_{zj}(\boldsymbol{\theta}, \boldsymbol{F}_a - \boldsymbol{F}_b) + \mathrm{Cov}\left[\varepsilon_{mj}, \varepsilon_{hj}\right]$$

$$= \begin{cases} \boldsymbol{F}_a\boldsymbol{\Sigma}_{\boldsymbol{S}}\boldsymbol{F}_a^T + \boldsymbol{S}_j^T\boldsymbol{\Sigma}_{\boldsymbol{F}}\boldsymbol{S}_j + \tau_j^2 + \sigma_{\varepsilon j}^2(\boldsymbol{F}_a) & a = b, m = h \\ \boldsymbol{F}_a\boldsymbol{\Sigma}_{\boldsymbol{S}}\boldsymbol{F}_a^T + \boldsymbol{S}_j^T\boldsymbol{\Sigma}_{\boldsymbol{F}}\boldsymbol{S}_j + \tau_j^2 & a = b, m \neq h \\ \boldsymbol{F}_a\boldsymbol{\Sigma}_{\boldsymbol{S}}\boldsymbol{F}_b^T + \tau_j^2 R_{zj}(\boldsymbol{\theta}, \boldsymbol{F}_a - \boldsymbol{F}_b) & a \neq b \end{cases},$$

Moreover, similarly, we can derive that

$$\mathrm{Cov}\left[Y_j(\boldsymbol{F}_0), Y_{mj}(\boldsymbol{F}_a)\right] = \boldsymbol{F}_0\boldsymbol{\Sigma}_{\boldsymbol{S}}\boldsymbol{F}_a^T + \tau_j^2 R_{zj}(\boldsymbol{\theta}, \boldsymbol{F}_0 - \boldsymbol{F}_a).$$

The noise item ε_{ij} is independent among simulation replications and actuator force vectors, thus obtaining the sample mean of replications at actuator force vector $\boldsymbol{F}_a$ only affects

$$\mathrm{Cov}\left[\bar{Y}_j(\boldsymbol{F}_a), \bar{Y}_j(\boldsymbol{F}_a)\right] = \boldsymbol{F}_a\boldsymbol{\Sigma}_{\boldsymbol{S}}\boldsymbol{F}_a^T + \boldsymbol{S}_j^T\boldsymbol{\Sigma}_{\boldsymbol{F}}\boldsymbol{S}_j + \tau_j^2 + \sigma_{\varepsilon j}^2(\boldsymbol{F}_a)/n_a.$$

Let $\boldsymbol{R}_j(\boldsymbol{F}_0, \cdot)$ be the k × 1 vector $\left(\mathrm{Cov}\left[Y_j(\boldsymbol{F}_0), \bar{Y}_j(\boldsymbol{F}_1)\right]; \ldots; \mathrm{Cov}\left[Y_j(\boldsymbol{F}_0), \bar{Y}_j(\boldsymbol{F}_k)\right]\right) = \left(\boldsymbol{F}_0\boldsymbol{\Sigma}_{\boldsymbol{S}}\boldsymbol{F}_1^T + \tau_j^2 R_{zj}(\boldsymbol{\theta}, \boldsymbol{F}_0 - \boldsymbol{F}_1); \ldots; \boldsymbol{F}_0\boldsymbol{\Sigma}_{\boldsymbol{S}}\boldsymbol{F}_k^T + \tau_j^2 R_{zj}(\boldsymbol{\theta}, \boldsymbol{F}_0 - \boldsymbol{F}_k)\right)$. Let $\boldsymbol{R}_j = \boldsymbol{F}_{DOE}\boldsymbol{\Sigma}_{\boldsymbol{S}}\boldsymbol{F}_{DOE}^T + \boldsymbol{\Sigma}_{zj} + \boldsymbol{S}_j^T\boldsymbol{\Sigma}_{\boldsymbol{F}}\boldsymbol{S}_j \cdot \boldsymbol{I} + \boldsymbol{\Sigma}_{\varepsilon j}$, where $\boldsymbol{F}_{DOE} = (\boldsymbol{F}_1; \ldots; \boldsymbol{F}_k)$, and $\boldsymbol{I}$ denotes identity matrix.

Therefore, we can get the multivariate normal distribution as

$$\begin{pmatrix} Y_j(\boldsymbol{F}_0) \\ \overline{\boldsymbol{Y}}_j \end{pmatrix} \sim \mathbb{N}_{1+k}\left(\begin{pmatrix} \boldsymbol{F}_0\boldsymbol{S}_j \\ \boldsymbol{F}_{DOE}\boldsymbol{S}_j \end{pmatrix}, \begin{pmatrix} \tau_j^2 & \boldsymbol{R}_j^T(\boldsymbol{F}_0,\cdot) \\ \boldsymbol{R}_j(\boldsymbol{F}_0,\cdot) & \boldsymbol{R}_j \end{pmatrix} \right). \quad \square$$

Proposition 2. Assume that $\boldsymbol{S}_j$, $\boldsymbol{\Sigma}_{zj}$, $\boldsymbol{\Sigma}_{\boldsymbol{F}}$, $\boldsymbol{\Sigma}_{\varepsilon}$, and $\boldsymbol{\Sigma}_{\boldsymbol{S}}$ are known, the best MSPE (mean square prediction error) linear unbiased predictor is

$$\widehat{\boldsymbol{Y}}_j(\boldsymbol{F}_0) = \boldsymbol{F}_0\boldsymbol{S}_j + \boldsymbol{R}_j^T(\boldsymbol{F}_0,\cdot)\boldsymbol{R}_j^{-1}(\overline{\boldsymbol{Y}}_j - \boldsymbol{F}_{DOE}\boldsymbol{S}_j),$$

where $\boldsymbol{R}_j = \boldsymbol{F}_{DOE}\boldsymbol{\Sigma}_{\boldsymbol{S}}\boldsymbol{F}_{DOE}^T + \boldsymbol{\Sigma}_{zj} + \boldsymbol{S}_j^T\boldsymbol{\Sigma}_{\boldsymbol{F}}\boldsymbol{S}_j \cdot \boldsymbol{I} + \boldsymbol{\Sigma}_{\varepsilon j}$, and $\boldsymbol{R}_j(\boldsymbol{F}_0,\cdot) = \Big(\boldsymbol{F}_0\boldsymbol{\Sigma}_{\boldsymbol{S}}\boldsymbol{F}_1^T + \tau_j^2 R_{zj}(\boldsymbol{\theta}, \boldsymbol{F}_0 - \boldsymbol{F}_1);\ \ldots; \boldsymbol{F}_0\boldsymbol{\Sigma}_{\boldsymbol{S}}\boldsymbol{F}_k^T + \tau_j^2 R_{zj}(\boldsymbol{\theta}, \boldsymbol{F}_0 - \boldsymbol{F}_k)\Big)$.

The mean square error (MSE) of the predictor $\widehat{\boldsymbol{Y}}_j(\boldsymbol{F}_0)$ is $\text{MSE}^* = \tau_j^2 - \boldsymbol{R}_j^T(\boldsymbol{F}_0,\cdot)\boldsymbol{R}_j^{-1}\boldsymbol{R}_j(\boldsymbol{F}_0,\cdot)$. The best MSPE linear unbiased predictor is also called simply a best linear unbiased predictor (BLUP).

Proof:

From Proposition 1, we get that the $\left(Y_j(\boldsymbol{F}_0); \overline{\boldsymbol{Y}}_j\right)$ follows a multivariate normal distribution. According to the standard conclusions for the multivariate normal distribution [29], we can get the distribution of $Y_j(\boldsymbol{F}_0)$ given $\overline{\boldsymbol{Y}}_j$ as

$$Y_j(\boldsymbol{F}_0)\big|\overline{\boldsymbol{Y}}_j \sim \mathbb{N}(\bar{\mu}, \bar{\Sigma}),$$

where $\bar{\mu} = \boldsymbol{F}_0\boldsymbol{S}_j + \boldsymbol{R}_j^T(\boldsymbol{F}_0,\cdot)\boldsymbol{R}_j^{-1}(\overline{\boldsymbol{Y}}_j - \boldsymbol{F}\boldsymbol{S}_j)$, $\bar{\Sigma} = \tau_j^2 - \boldsymbol{R}_j^T(\boldsymbol{F}_0,\cdot)\boldsymbol{R}_j^{-1}\boldsymbol{R}_j(\boldsymbol{F}_0,\cdot)$.

According to the theorem 3.2.1 [39], the best MSPE predictor of $Y_j(\boldsymbol{F}_0)$ is

$$\hat{Y}_j(\boldsymbol{F}_0) = \boldsymbol{E}\left[Y_j(\boldsymbol{F}_0)\middle|\overline{\boldsymbol{Y}}_j\right] = \boldsymbol{F}_0\boldsymbol{S}_j + \boldsymbol{R}_j^T(\boldsymbol{F}_0,\cdot)\boldsymbol{R}_j^{-1}(\overline{\boldsymbol{Y}}_j - \boldsymbol{F}_{DOE}\boldsymbol{S}_j).$$

It is obvious that the MSE of the predictor $\hat{Y}_j(\boldsymbol{F}_0)$ is $\boldsymbol{E}\left[\left(\hat{Y}_j(\boldsymbol{F}_0) - Y_j(\boldsymbol{F}_0)\right)^2\right] = \bar{\Sigma} = \tau_j^2 - \boldsymbol{R}_j^T(\boldsymbol{F}_0,\cdot)\boldsymbol{R}_j^{-1}\boldsymbol{R}_j(\boldsymbol{F}_0,\cdot)$. □

Following similar procedures in [40], we can prove that $\boldsymbol{\Sigma}_{\varepsilon j}$ and $\boldsymbol{S}_j^T\boldsymbol{\Sigma}_{\boldsymbol{F}}\boldsymbol{S}_j$ inflate the MSE. However, we cannot mathematically prove if $\boldsymbol{\Sigma}_{\boldsymbol{S}}$ inflates or deflates the MSE.

3.2.3 Maximum Likelihood Estimation

In this section, we will derive the maximum likelihood estimation of $(\boldsymbol{S}_j, \tau_j^2, \boldsymbol{\theta}_j, \boldsymbol{\Sigma}_{\boldsymbol{S}})$ with the assumption that $(\boldsymbol{\Sigma}_{\boldsymbol{F}}, \boldsymbol{\Sigma}_{\varepsilon})$ is known**.** $\boldsymbol{\Sigma}_{\boldsymbol{F}}$ can be obtained from the tolerance of the actuators' forces, and $\boldsymbol{\Sigma}_{\varepsilon}$ can be estimated from the samples.

Under the multivariate normal distribution, the log-likelihood function of $(\boldsymbol{S}_j, \tau_j^2, \boldsymbol{\theta}, \boldsymbol{\Sigma}_{\boldsymbol{S}})$ is

$$\ell\left(\boldsymbol{S}_j, \tau_j^2, \boldsymbol{\theta}_j, \boldsymbol{\Sigma}_{\boldsymbol{S}}\right) = -\frac{1}{2}\ln[(2\pi)^k] - \frac{1}{2}\ln\left[\det\left(\boldsymbol{R}_j\right)\right] - \frac{1}{2}(\overline{\boldsymbol{Y}}_j - \boldsymbol{F}_{DOE}\boldsymbol{S}_j)^T\boldsymbol{R}_j^{-1}(\overline{\boldsymbol{Y}}_j - \boldsymbol{F}_{DOE}\boldsymbol{S}_j), \quad (5)$$

where $\boldsymbol{R}_j = \boldsymbol{F}_{DOE}\boldsymbol{\Sigma}_{\boldsymbol{S}}\boldsymbol{F}_{DOE}^T + \boldsymbol{\Sigma}_{zj} + \boldsymbol{S}_j^T\boldsymbol{\Sigma}_{\boldsymbol{F}}\boldsymbol{S}_j \cdot \boldsymbol{I} + \boldsymbol{\Sigma}_{\varepsilon j}$.

To estimate the $\boldsymbol{\Sigma}_{\varepsilon j}$ from the samples, we can use the sample variance

$$\hat{\boldsymbol{\Sigma}}_{\varepsilon j} = \mathrm{diag}[\frac{1}{n_1-1}\sum_{i=1}^{n_1}\left(Y_{ij}(\boldsymbol{F}_1) - \bar{Y}_j(\boldsymbol{F}_1)\right)^{\mathbf{2}}, \ldots, \frac{1}{n_k-1}\sum_{i=1}^{n_k}\left(Y_{ij}(\boldsymbol{F}_k) - \bar{Y}_j(\boldsymbol{F}_k)\right)^{\mathbf{2}}], \quad (6)$$

which is strongly consistent for $\boldsymbol{\Sigma}_{\varepsilon j}$. Recalling Equation (5), $\boldsymbol{R}_j = \boldsymbol{F}_{DOE}\boldsymbol{\Sigma}_{\boldsymbol{S}}\boldsymbol{F}_{DOE}^T + \boldsymbol{\Sigma}_{zj} + \boldsymbol{S}_j^T\boldsymbol{\Sigma}_{\boldsymbol{F}}\boldsymbol{S}_j \cdot \boldsymbol{I} + \boldsymbol{\Sigma}_{\varepsilon j}$. When we consider the impact of estimating $\boldsymbol{\Sigma}_{\varepsilon j}$, we can regard $\boldsymbol{F}_{DOE}\boldsymbol{\Sigma}_{\boldsymbol{S}}\boldsymbol{F}_{DOE}^T + \boldsymbol{\Sigma}_{zj} + \boldsymbol{S}_j^T\boldsymbol{\Sigma}_{\boldsymbol{F}}\boldsymbol{S}_j \cdot \boldsymbol{I}$ in Equation (5) as one term. Then, it is similar to $\boldsymbol{R}_j = \boldsymbol{\Sigma}_M + \boldsymbol{\Sigma}_\varepsilon$ in the Stochastic Kriging [40]. According to similar proof procedure of Theorem 1 in the Stochastic Kriging [40], we can show that estimating $\boldsymbol{\Sigma}_{\varepsilon j}$ in this way introduces no *prediction bias.*

The MLE-based estimation procedure can be summarized as Algorithm 1.

Algorithm 1: MLE based algorithm for the surrogate model considering uncertainties

---

While $\boldsymbol{j = 1:p}$

Initialization:

(i) estimate the $\widehat{\boldsymbol{\Sigma}}_{\boldsymbol{\varepsilon j}}$ from equation (6);

(ii) set the $\boldsymbol{\Sigma}_{\boldsymbol{F}}$ according to the tolerance of actuators' forces;

End

Estimation:

(i) set the starting points $\boldsymbol{S_{j0} = (F_{DOE}^T * F_{DOE})^{-1}F_{DOE}^T Y_j(F_{DOE})}$, $\boldsymbol{\tau_{j0}^2 = \mathbf{var}(Y_j(F_{DOE}) - F_{DOE}S_{j0})}$, $\boldsymbol{\theta_{j0} = 1/2}$, $\boldsymbol{\Sigma_{S0} = 0}$;

(ii) Use $\widehat{\boldsymbol{\Sigma}}_{\boldsymbol{\varepsilon j}}$ to replace $\boldsymbol{\Sigma}_{\boldsymbol{\varepsilon j}}$ and then maximize the log-likelihood function (5) over $\widehat{\boldsymbol{S}}_{\boldsymbol{j}}, \widehat{\boldsymbol{\tau}}_{\boldsymbol{j}}^{\boldsymbol{2}}, \widehat{\boldsymbol{\theta}}_{\boldsymbol{j}}, \widehat{\boldsymbol{\Sigma}}_{\boldsymbol{S}}$.

End

Prediction:

(i) predict $\widehat{\boldsymbol{Y}}_{\boldsymbol{j}}(\boldsymbol{F_0})$ by the equation

$$\widehat{\boldsymbol{Y}}_{\boldsymbol{j}}(\boldsymbol{F_0}) = \boldsymbol{F_0}\widehat{\boldsymbol{S}}_{\boldsymbol{j}} + \widehat{\boldsymbol{R}}_{\boldsymbol{j}}^{\boldsymbol{T}}(\boldsymbol{F_0}, \cdot)\widehat{\boldsymbol{R}}_{\boldsymbol{j}}^{-\mathbf{1}}(\overline{\boldsymbol{Y}}_{\boldsymbol{j}} - \boldsymbol{F_{DOE}}\widehat{\boldsymbol{S}}_{\boldsymbol{j}})$$

where $\boldsymbol{R_j = F_{DOE}\widehat{\Sigma}_S F_{DOE}^T + \widehat{\Sigma}_{zj} + \widehat{S}_j^T \Sigma_F \widehat{S}_j \cdot I + \widehat{\Sigma}_{\varepsilon j}}$.

(ii) calculate the MSE of the estimator by

$$\mathbf{MSE}_j = \hat{\tau}_j^2 - \widehat{R}_j^T(F_0,\cdot)\widehat{R}_j^{-1}\widehat{R}_j(F_0,\cdot)$$

where $\widehat{R}_j(F_0,\cdot) = \left(F_0\widehat{\Sigma}_S F_1^T + \hat{\tau}_j^2 R_{zj}\left(\widehat{\theta}, F_0 - F_1\right); \ldots; F_0\widehat{\Sigma}_S F_k^T + \hat{\tau}_j^2 R_{zj}\left(\widehat{\theta}, F_0 - F_k\right)\right)$.

End

End

3.2.4 Uncertainty Analysis

In Sections 3.2.2 and 3.2.3, we have investigated the theoretical impact of different uncertainties. In this section, we analyze the uncertainty sources based on the engineering knowledge during the composite part assembly process. Four kinds of uncertainties are considered in the equation (4). Those uncertainties are actuator uncertainty ($\widetilde{F}$), part uncertainty ($\tilde{S}_j$), modeling uncertainty ($z_j(F)$), and unquantified uncertainty (ε_{ij}), respectively. We analyze sources of each uncertainty as follows.

(i) $\widetilde{F}$: Actuator uncertainty. When a force is implemented by an actuator, it may not be exactly the ideal magnitude and direction. The magnitude and direction of the forces may vary naturally due to the fabrication device tolerances of the hydraulic or electromechanical system of actuators. Part of directional variability is due to the deviations of contact geometry of actuators and their installations.

(ii) $\tilde{\boldsymbol{S}}_j$: Part uncertainty. A large composite part is usually manufactured by multiple batches and steps. The part uncertainty is originated in variability of raw materials (e.g. thickness variability of carbon fiber fabrics and organic impurities in epoxy resin) and the fabrication process (e.g. uncertainty of carbon fiber orientation, existence of delamination, resin rich/starved areas, air bubbles or blisters et al.) [42]. The part uncertainty will impact the mechanical properties and quantitative values of the sensitivity matrix.

(iii) $\boldsymbol{z}_j(\boldsymbol{F})$: Modeling uncertainty. The surrogate modeling can be regarded as a process to build the link between control variables and responses. $\boldsymbol{z}_j$ ($\boldsymbol{F}$) is a realization of a mean 0 stochastic process which indicates the values being randomly sampled from a space of functional mappings. This stochastic property contributes to the modeling uncertainty.

(iv) $\boldsymbol{\varepsilon}_{ij}$: Unquantified uncertainty. When we measure a part in practice, measurement errors inevitably exist in the sensor readings. Moreover, if we use finite element analysis (FEA) to mimic real experiments, there are errors between the FEA model and the real system. Computational accuracy, relevant to the meshing resolution, will also impact the precision of the FEA model. These errors, together with other random noise or unquantified errors, will be classified into the unquantified uncertainty.

To emphasize the motivation of introducing this novel methodology, we want to compare the Stochastic Kriging with our method. In the Stochastic Kriging, the model covers all the uncertainties by extrinsic uncertainty and intrinsic uncertainty. It is a generic decomposition without considering physical sources and characteristics of different uncertainties. In the proposed surrogate model, we bring in two more stochastic terms to separate the actuators' variability and part-to-part variability. There are two advantages: (i) We can make full use of corresponding engineering knowledge to enhance the prediction accuracy of the model. For example, we can get actuators' force tolerance from engineering knowledge, and then we integrate this information into the model to achieve better prediction. (ii) A more detailed decomposition helps us understand the impacts of different uncertainties with physical interpretations. Potentially, it lays a foundation for further exploration of optimal uncertainty control to improve the quality of the composite assembly process.

3.3 Feed-Forward Automatic Optimal Shape Control

After a surrogate model considering uncertainties is built and validated, the surrogate model will be embedded into the AOSC system. A feedforward control strategy will be applied as [43]. Control actions will be implemented by ten actuators for the shape control.

We develop the following feed-forward automatic optimal control algorithm to realize the shape adjustment of a fuselage, as shown in Fig. 16. For an incoming fuselage, its dimensional information Y will be measured with an in-line 3D laser metrology system.

Given any virtual tooling adjustment with actuators' forces $\boldsymbol{F}$, we can use the surrogate model to predict the fuselage dimensions $\widehat{\boldsymbol{Y}}(\boldsymbol{F})$ when force F is applied to the fuselage. Next, the predicted shape deviations from the target can be derived by subtracting designed dimensions $\boldsymbol{Y}^*$ from the predicted dimensions $\widehat{\boldsymbol{Y}}(\boldsymbol{F}) + \boldsymbol{Y_c}$. Then a weighted multivariable optimization criterion can be used to determine optimal control actions among iterative runs of virtual shape adjustment. After the optimal actuators' forces $\boldsymbol{F}^*$ is obtained, a true shape adjustment can be implemented. We will introduce details about the objective function for the optimization as follows.

The objective of feed-forward automatic optimal shape control algorithm is to minimize the deviations between the current dimensions and the designed dimensions by iteratively virtual shape adjustment. Besides, the optimization should also take the magnitude constraints of actuators' forces into consideration. Therefore, the objective function is

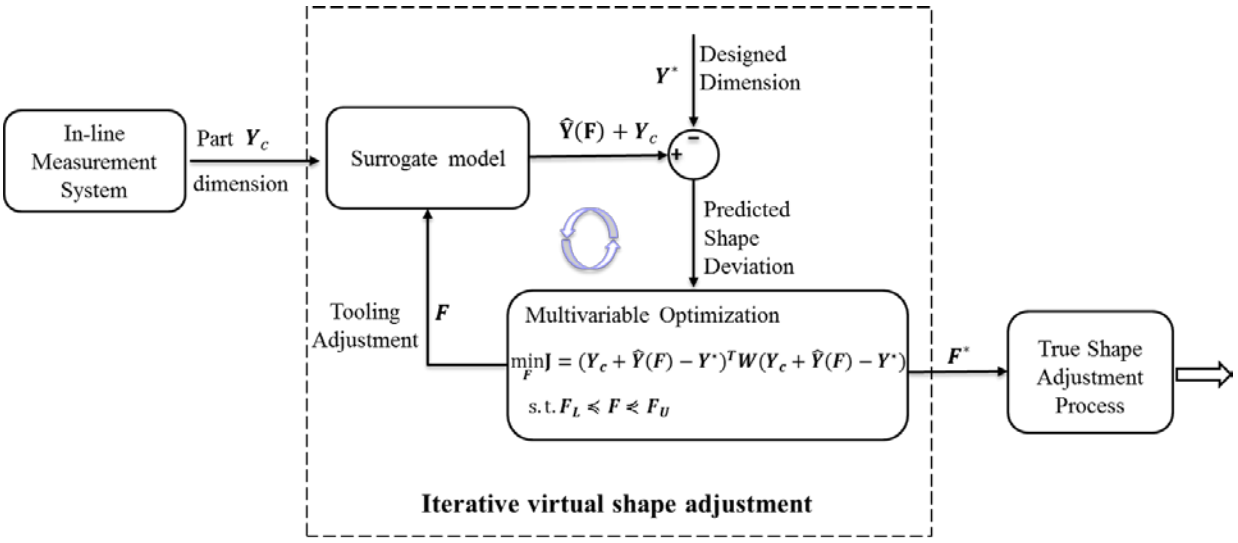

Fig. 16 Feed-forward automatic optimal shape control algorithm

$$\min_{\boldsymbol{F}} \boldsymbol{J} = (\boldsymbol{Y_c} + \hat{\boldsymbol{Y}}(\boldsymbol{F}) - \boldsymbol{Y}^*)^{\boldsymbol{T}} \boldsymbol{W} (\boldsymbol{Y_c} + \hat{\boldsymbol{Y}}(\boldsymbol{F}) - \boldsymbol{Y}^*)$$

$$s.t. \qquad \boldsymbol{F_L} \preccurlyeq \boldsymbol{F} \preccurlyeq \boldsymbol{F_U} \tag{7}$$

where $\boldsymbol{Y_c}$ is an in-line measured dimensional vector of current fuselage. $\hat{\boldsymbol{Y}}(\boldsymbol{F})$ is the predicted dimensional deviation vector, $\hat{Y}_j(\boldsymbol{F}) = \boldsymbol{F}\boldsymbol{S}_j + \boldsymbol{R}_j^T(\boldsymbol{F},\cdot)\boldsymbol{R}_j^{-1}(\overline{\boldsymbol{Y}}_j - \boldsymbol{F}_{DOE}\boldsymbol{S}_j)$; $\boldsymbol{Y}^*$ is the designed target dimensional vector; $\boldsymbol{W}$ is the weighting coefficients matrix, whose diagonal elements reflect the relative importance of corresponding dimensional variables; Non-diagonal elements of $\boldsymbol{W}$ are assumed to be zeros; $\preccurlyeq$ denotes component-wise inequality; $\boldsymbol{F_L}$ and $\boldsymbol{F_U}$ are the lower bound and the upper bound of actuators force vector $\boldsymbol{F}$. Thus, we can write the objective function as

$$\min_{\boldsymbol{F}} \boldsymbol{J} = \sum_{j=1}^{p} w_j \cdot \left[\boldsymbol{F}\boldsymbol{S}_j + \boldsymbol{R}_j^T(\boldsymbol{F},\cdot)\boldsymbol{R}_j^{-1}\left(\overline{\boldsymbol{Y}}_j - \boldsymbol{F}_{DOE}\boldsymbol{S}_j\right) + Y_{cj} - Y_j^*\right]^2$$
$$s.t. \qquad \boldsymbol{F_L} \preccurlyeq \boldsymbol{F} \preccurlyeq \boldsymbol{F_U} \tag{8}$$

where w_j is a weighting coefficient, which is the j^{th} diagonal entry of $\boldsymbol{W}$. $\boldsymbol{R}_j = \boldsymbol{F}_{DOE}\boldsymbol{\Sigma_S}\boldsymbol{F}_{DOE}^T + \boldsymbol{\Sigma}_{zj} + \boldsymbol{S}_j^T\boldsymbol{\Sigma_F}\boldsymbol{S}_j \cdot \boldsymbol{I} + \boldsymbol{\Sigma}_{\varepsilon j}$, $\boldsymbol{R}_j(\boldsymbol{F},\cdot) = \left(\boldsymbol{F}\boldsymbol{\Sigma_S}\boldsymbol{F}_1^T + \tau_j^2 R_{zj}(\boldsymbol{\theta}, \boldsymbol{F} - \boldsymbol{F}_1);\ \ldots;\ \boldsymbol{F}\boldsymbol{\Sigma_S}\boldsymbol{F}_k^T + \tau_j^2 R_{zj}(\boldsymbol{\theta}, \boldsymbol{F} - \boldsymbol{F}_k)\right)$. Y_{cj} and Y_j^* are the j^{th} entry of $\boldsymbol{Y_c}$ and $\boldsymbol{Y}^*$ respectively.

The control method takes weighted summation of square of dimensional deviations as an objective function with a bounded constraint of actuators' forces. Some general control methods in the literature usually calculate the optimum control actions via minimization of both the response deviations $\boldsymbol{J}$ and control efforts (e.g. a weighted $\boldsymbol{L_2}$ norm loss $\boldsymbol{F}\boldsymbol{W_F}\boldsymbol{F^T}$ with a weight matrix $\boldsymbol{W_F}$). In this way, they can realize acceptable control performance as well as reserve control energy. However, in the shape control problem of the composite fuselage, the objective is to achieve minimized dimensional deviations of the fuselage to the target dimensions. The adjusting actuators' forces is very easy with no constraints in energy consumption. Thus, there is no need to include a weighted loss $\boldsymbol{F}\boldsymbol{W_F}\boldsymbol{F^T}$ in the objective function, which will dilute the performance of dimensional quality control. Instead, we consider that the actuators' forces are bounded by the actuators' capability and engineering specifications of their maximum forces. Thus, the control

function in our method considers minimizing dimensional deviations and limiting the bounds of actuators' forces. After we get the control objective function, we can find that this is a quadratic programming problem with box constraints, which can be solved by the interior point method [44].

3.4 Case Study

3.4.1 FEA modeling and validation

The finite element analysis (FEA) is an effective numerical technique for composite part analysis. During the development of the AOSC system, a set of testing experiments need to be implemented for providing training data and testing data. If we can build a finite element model that is consistent with a real composite fuselage, it will increase the flexibility and efficiency of system development.

ANSYS Composite PrepPost is an add-in module to the ANSYS Workbench and is integrated with standard analysis functions for composite parts [45]. By Composite PrepPost, two kind of materials, carbon fiber and epoxy resin, are used to generate multiple fabrics with different geometric parameters. Fabrics can be stacked up depending on specific sequence and orientations. Moreover, then, stack-ups are used to generate sub-laminates and further integrated into a composite part. Furthermore, the boundary conditions and composite meshing are applied to the structure in the pre-processing stage. A post-processing is used to evaluate the design performance or material failure. In another word, the FEA model can be used to predict the finished product under simulated real-

world fabrication conditions. Both stress and deviations in addition to a range of failure criteria can be analyzed by using the FEA model.

After a composite fuselage is built in the ANSYS Workbench, two support areas and one 4-inch width strap are used to fix the fuselage. Ten actuators are applied to adjust the shape of the composite fuselage. The dimension between actuators and edge of the fuselage is 12 inches. The FEA model, as shown in Fig. 17 (a), is used to mimic the fuselage and assembly fixture set-up during assembly.

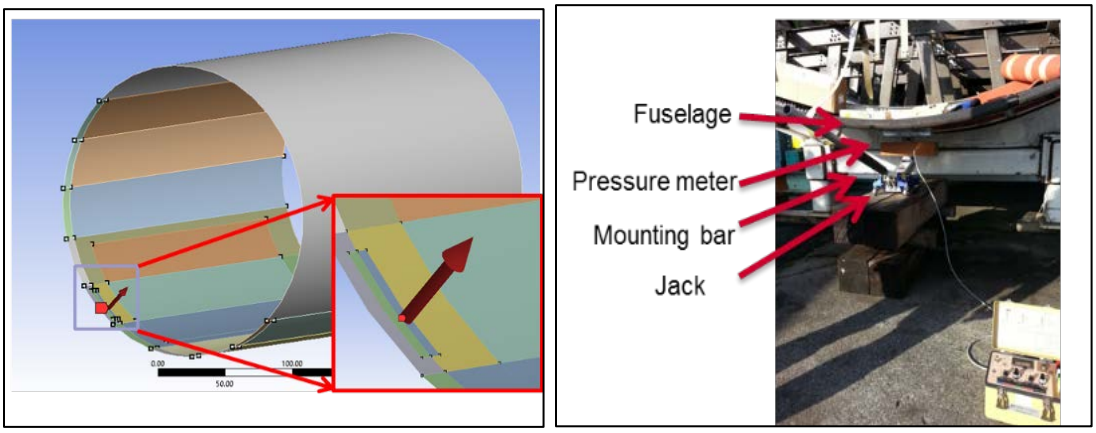

(a) FEA simulation model, (b) Real testing experiment set-up

Fig. 17 Comparison between FEA simulation model and real testing experiment set-up

In order to validate whether the FEA model is consistent with the real composite part, a physical testing experiment is set up to measure the deviations of the fuselage under different actuators' forces. We ensure that the key parameters including length, width, thickness, weight, and maximum deviation under gravity are consistent between the FEA simulated part and the real fuselage. In the validation test, the actuators' forces are changed

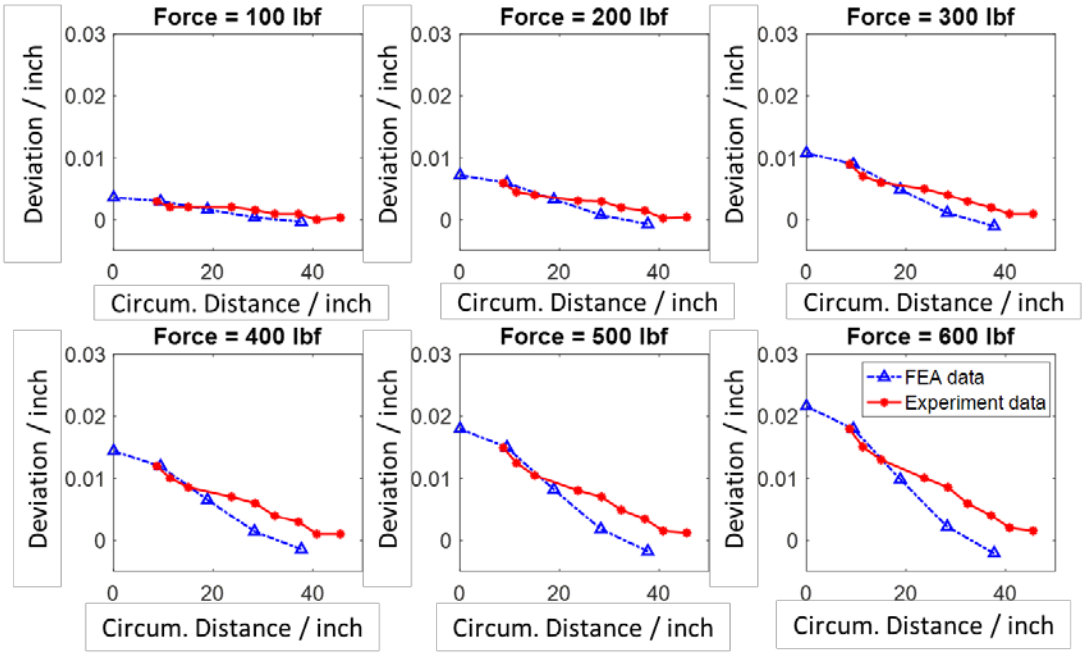

Fig. 18 The dimensional deviations under different actuator' forces in the FEA simulation and the physical experiment

from 100 pounds to 600 pounds. The differences of the dimensional deviations of outputs between the FEA simulated part and the real fuselage under different actuators' forces are shown in Fig. 18. The horizontal axis is the circumferential distance from the center, and the vertical axis is the dimensional deviation under the actuator' force. We can find that the dimensional outputs from the FEA model are relatively consistent with the dimensional measurements of the real fuselage testing. As the actuator force increases, the difference between FEA simulated part and the real fuselage has a slight increase. However, the maximum difference is about five mils (Note: 1 mil is a thousandth of an inch) even with 600 pounds of actuator forces.

We can find that there is a systematic error between the FEA simulation and the physical experiment. In order to calibrate the model, physical experimental observations are collected. However, there is a challenge to calibrate a bunch of system parameters with very limited physical experimental observations. We have investigated this particular problem and proposed an effective calibration method with sensible variables identification and adjustment [25]. Because this paper is focused on the shape control problem for a composite fuselage, we take the FEA model and model calibration as a given in this paper. In the rest of this paper, we use this FEA model to generate data, do the modeling and control, and validate the methodology we proposed. It is worth pointing out that the physical experimental data is only used in the validation of the FEA simulation platform. Then all the prediction results and control results shown in Section 3.4.3-3.4.6 are based on the simulated data by using the validated FEA simulation platform.

3.4.2 Design of Experiment Considering Uncertainties

In practice, the shapes of fuselages are not exactly same between different fuselages due to the part uncertainty discussed in Section 3.2.4. Thus, we may need several fuselages to collect training dataset by experiments. In this case study, two fuselages with a different thickness ratio of carbon fiber and epoxy resin are generated to mimic the part uncertainty. When generating those fuselages with different dimensions/shapes, we fix the thickness of carbon fiber fabrics and change the thickness ratio of carbon fiber and epoxy resin by revising the thickness of epoxy resin. Four groups of fuselages are built considering the different degree of part uncertainty, which is shown in Table 2.

Taking group 1 with uncertainty 1% as an example, epoxy resin thicknesses of fuselages 1 and 2 are 0.826×(101%) inch and 0.826× (99%) inch. The uncertainty degree for groups 1 to 4 is 1%, 2%, 4% 7%, respectively. It needs to be pointed out that the tolerance of thickness of regular carbon fiber/epoxy resin fabrics is 2%. Thus, we have covered a larger range of part uncertainties than the tolerance of parts in the design. After we generate these four groups of fuselages, we also validate them by maximum deviation under gravity. Their maximum deviations under gravity are within the range of 7.573 to 9.444 inches, which are consistent with the range of real fuselages in the production floor.

Table. 2 Design of experiment considering different degree of part uncertainty

Fuselage		**Group 1 / inch**	**Group 2 / inch**	**Group 3 / inch**	**Group 4 / inch**
Fuselage 1	Epoxy resin thickness	0.826×(101%)	0.826× (102%)	0.826× (104%)	0.826× (107%)
	Max deviation under gravity	8.295	8.167	7.921	7.573
Fuselage 2	Epoxy resin thickness	0.826× (99%)	0.826× (98%)	0.826× (96%)	0.826× (93%)
	Max deviation under gravity	8.561	8.698	8.985	9.444

For each fuselage, 30 training samples are generated by a Latin hypercube design [47]. Therefore, for each group of training dataset, there are 60 training samples from different fuselages will be used. These samples are generated from the FEA model. The

FEA model described early has been calibrated separately in Section 3.4.1. Thus the output of the FEA model is reflected as a calibrated one.

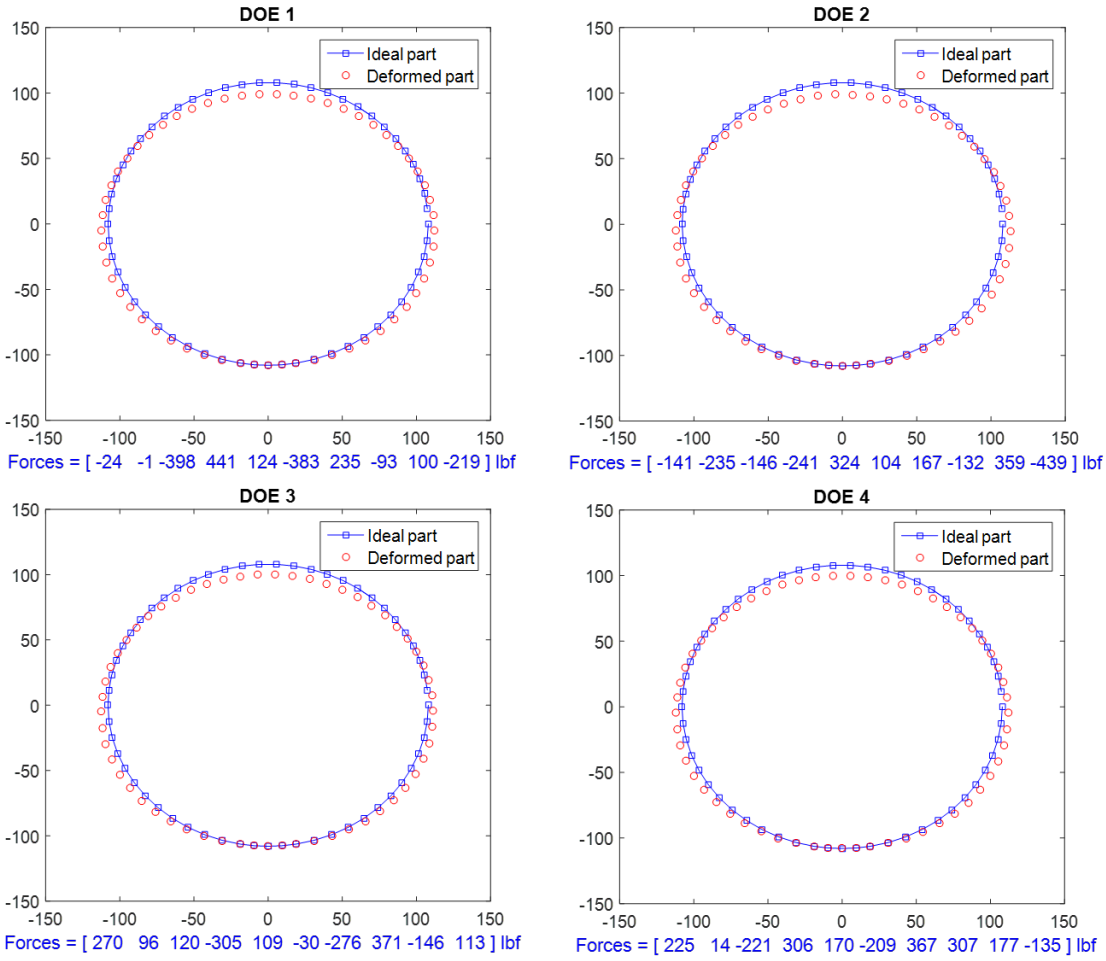

Fig. 19 Examples of datasets generated with a designed experiment

After we obtained those fuselages, designed experiments are conducted to generate the datasets of actuators' forces and their corresponding fuselage shape changes. In the design of experiment, the input variables are ten actuators' forces with a range of $\pm$ 1000

pounds. The responses are dimensional deviations of the fuselage. The design of experiment will mimic the real experiments to collect training dataset and testing dataset for calibration of the AOSC system. The responses under different actuators' forces are able to provide training dataset for determining the parameters in the model. And then testing dataset is used to mimic the real application of the AOSC system and test the performance. Examples of datasets generated with a designed experiment are shown in Fig. 6.

When we use the AOSC system, incoming new fuselages to be assembled are different from the fuselages used to calibrate the AOSC system. To mimic this real production situation, 20 fuselages with different dimensions are generated to mimic incoming new fuselages to be assembled, which provide the testing dataset. After the parameter estimation based on the training dataset, a surrogate model considering uncertainties is built and validated by the testing dataset. Hereafter, a multivariable optimization is conducted to obtain the optimal control for best dimensional quality. Twenty testing fuselages with different dimensions are used to validate the effectiveness and efficiency of the AOSC system.

3.4.3 Surrogate Modeling and Prediction Results

After we implement the design of experiment in the FEA simulation platform, the training dataset and testing dataset are collected. This training dataset is used to develop the surrogate model discussed in Section 3.2. A parameter estimation is conducted by using the training dataset. The simulation is conducted in a computer with Intel Core i7-4500U CPU with 8.00GB memory. In order to evaluate the obtained surrogate model, a prediction performance is evaluated for both the training dataset and the testing dataset. The concept of the prediction evaluation is shown in Fig. 14 (c). Predicted dimensional deviations are compared with the FEA outputted deviations, and the prediction errors are calculated.

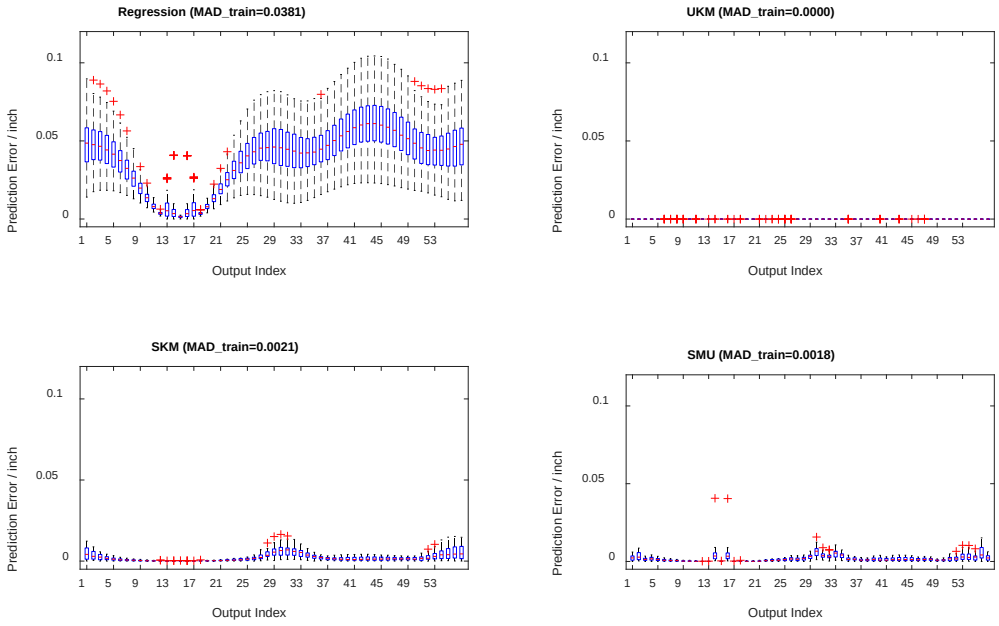

Fig. 20 Prediction errors of the four methods based on the training dataset

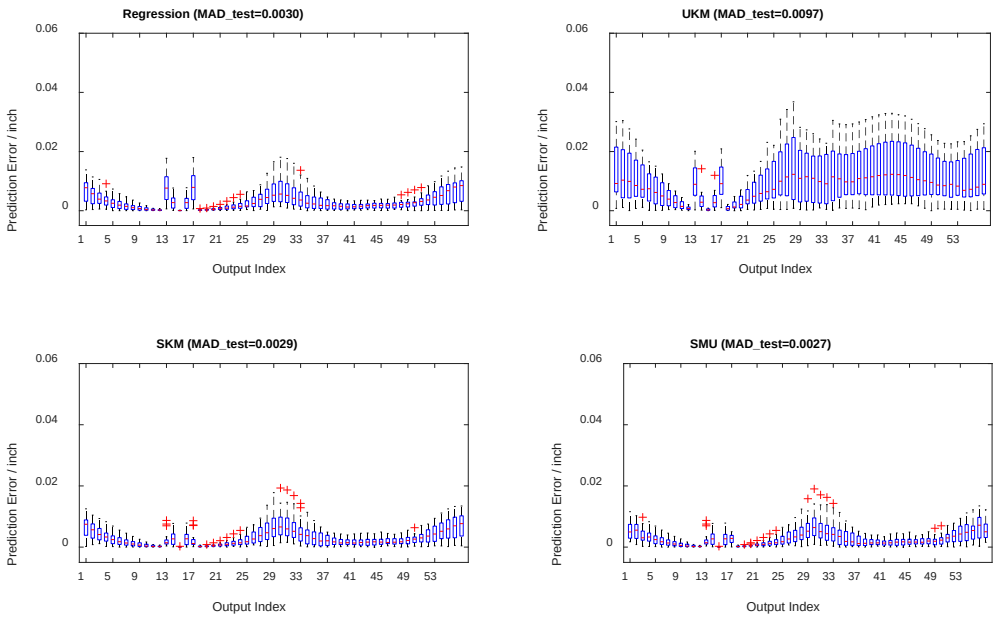

Fig. 21 Prediction errors of the four methods based on the testing dataset

The comparison of prediction errors among four methods is shown in Fig. 20 and Fig. 21. Fig. 20 is the boxplot based on the training dataset and Fig. 21 is the boxplot based on the testing dataset. The X axis denotes the output index associated with different quality features on the fuselage. The Y axis represents dimensional prediction errors with a unit inch. Mean absolute deviation is calculated for each method in order to show the quantitative performance. Meanwhile, the run time per sample is collected. All these results are summarized in Table 3. We can see that the Universal Kriging model (UKM) has the least training prediction error, which is reasonable because of the properties of Kriging. While the prediction error of the UKM based on the testing dataset is the worst, which can be explained by overfitting. Quantitatively, the mean absolute deviations of training samples for the regression model, the UKM, the SKM, and the proposed SMU are 0.0381,

2.59×e-16, 0.0021 and 0.0018, respectively. The mean absolute deviations of the testing samples for the regression model, the UKM, the SKM, and the proposed SMU are 0.0030, 20.0097, 0.0029 and 0.0027, respectively. Therefore, the proposed SMU performs better than the regression model and the SKM in both the training samples and testing samples. Thus, the proposed SMU can realize the best prediction capability than the other three benchmark methods. Even though the run time per sample for the SMU is the largest, 0.3140 second is acceptable for the feedforward control of shape adjustment of the composite fuselage.

Table. 3 Mean absolute deviations (MAD) and run time for the four methods

	Regression	UKM	SKM	Proposed SMU
MAD Training / inch	0.0381	2.59e-16	0.0021	0.0018
MAD Testing / inch	0.0030	0.0097	0.0029	0.0027
Run Time Per Sample / second	0.0483	0.0538	0.0706	0.3140

It is worth noting that the prediction errors of the four methods follow a specific pattern for different output indices. For example, the prediction errors for the output index 1-28 (corresponding to the lower half of the composite fuselage) tend to be smaller than the ones for the output index 29-57 (corresponding to the upper half of the composite

fuselage). The reason is that the adjustable actuators are installed in the lower half of the fuselage. Thus, the sampling data can capture more information for the lower half and realize better prediction. The prediction errors for output index 13-17 are relatively larger than the neighboring key points because of the impact of supporting fixture constraints. In addition, this pattern can be changed if we adjust the positions of the actuators. Where and how to distribute the actuators are future topics to be investigated.

3.4.4 Automatic Shape Control Results

A case study is conducted to illustrate the effectiveness and efficiency of the feed-forward control strategy developed in the paper. The case study is motivated by the real application of the AOSC system. We summarize the procedure of the proposed AOSC system as following steps:

(i) The initial incoming fuselage dimensions are measured by in-situ 3D metrology.

(ii) The obtained dimensional measurements will be fed into the control algorithm.

(iii) The control algorithm will do an iterative optimization to find the optimal forces to be used in the dimensional control. The convergence of virtual shape adjustment can be guaranteed because the optimization problem is convex. The algorithm can get a global optimal solution.

(iv) A feedforward control strategy is applied for the shape control by using the obtained optical forces. The shape adjustment is achieved by adjusting the physical actuators once in practice. There are no iterations in this step.

For verification, twenty new incoming testing fuselages with different dimensions are used to test the system. The control results are shown in Fig. 22 and Table 4. We can see that the AOSC system based on the surrogate model considering uncertainties can achieve the best control performance, which indicates the smallest deviations after control. Quantitatively, the mean of the absolute deviations after control is 1.26×e-04 inch, which is lower than the control requirement. The run time per sample for the control system based on the SMU is a little larger than other methods. However, 2.9738 seconds is acceptable for the shape adjustment of the composite fuselage according to engineering knowledge.

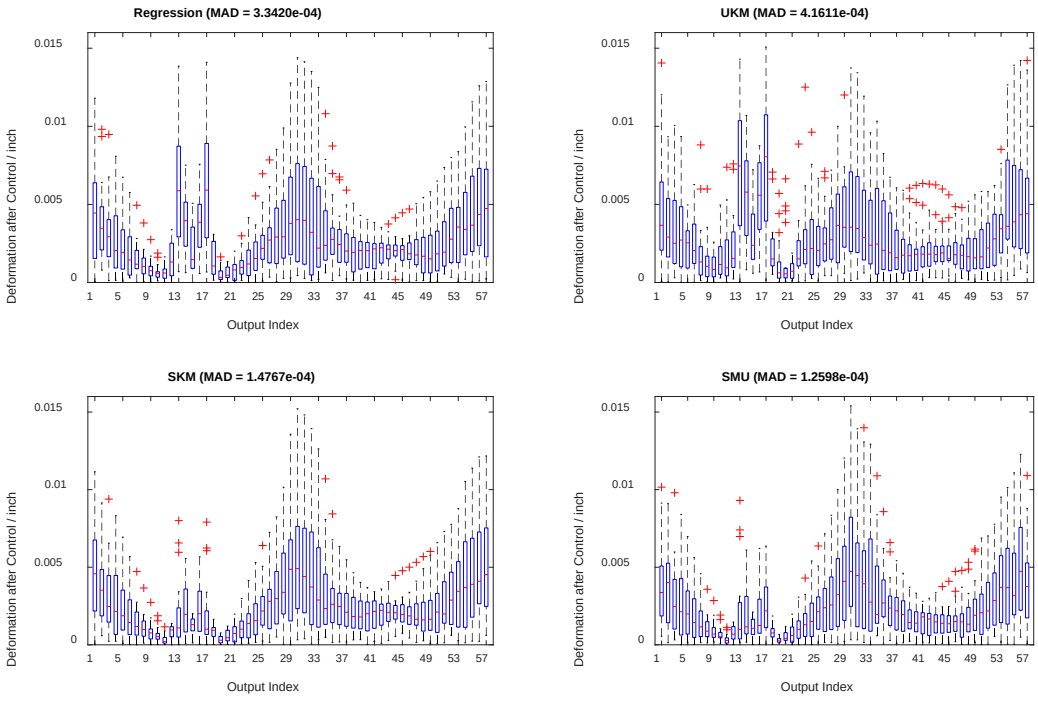

Fig. 22 Deviations after control based on the four models.

Table. 4 Design of experiment considering different degree of part uncertainty

	Regression	UKM	SKM	SMU
MAD After Control / inch	3.34×e-04	4.16×e-04	1.48×e-04	1.26×e-04
Run Time Per Sample / second	0.1727	2.9516	2.0641	2.9738

We can find that the deviations after control also follow a specific pattern similar to the pattern of prediction errors in Section 3.4.3. This control performance is mainly determined by the prediction errors in Section 3.4.3. However, this control performance of each dimensional variable can be changed by adjusting the weight matrix $\boldsymbol{W}$ in Equation (7). Usually, the weight matrix $\boldsymbol{W}$ is adjusted by the relative importance of corresponding dimensional variables according to engineering knowledge.

3.4.5 Sensitivity Analysis

We also conduct the sensitivity analysis of the control performance. For one thing, we explore how the magnitude of fuselage variability impacts the control performance; for another, we make a thorough inquiry about the maximum actuator force should be used in the AOSC system. The maximum actuator force determines the bounds $\boldsymbol{F_L}, \boldsymbol{F_U}$ in the control system.

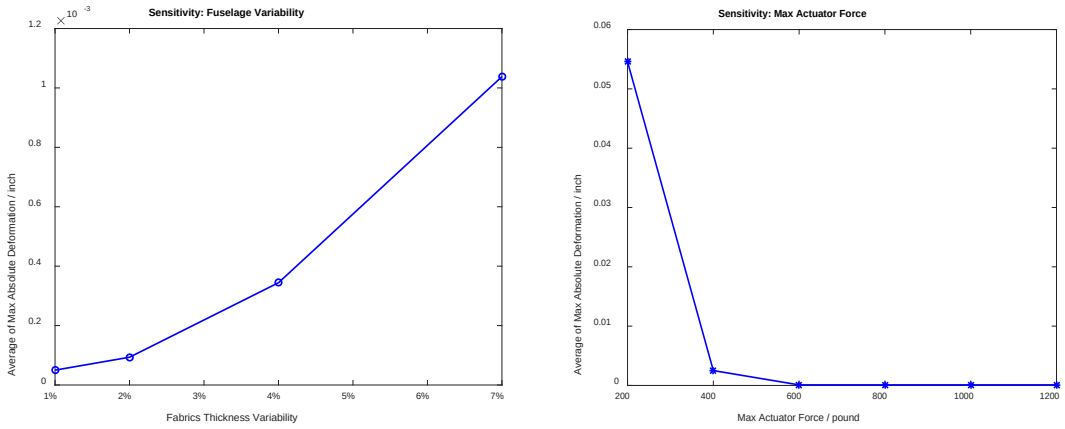

Fig. 23 Sensitivity analysis for fuselage variability and maximum actuators' forces in the AOSC system

The results of sensitivity analysis are shown in Fig. 23. It shows that as fabrics thickness variability increases from 1% to 7%, the average of maximum absolute deviations also becomes larger. However, even for fabrics thickness variability with 7%, the average of maximum absolute deviations is still $1.2 \times$ e-3, which is within the engineering specifications of the assembly requirement. For the sensitivity analysis of the maximum actuators' forces, we assume that the fuselage variability is 2%. In this case, when the maximum actuator force is lower than 600 pounds, the increase of maximum actuator force will improve the control performance dramatically. Also, no further improvements can be observed if the maximum actuator force is increased more than 600 pounds. Thus, 600 pounds is the upper limit that can provide sufficient control capability for the fuselage variability with 2%.

3.4.6 Stress Analysis and Failure Test

Engineers may worry about whether large actuators' forces may damage the composite fuselage. In order to address this concern, we conducted the stress analysis and failure test. The result of stress analysis is shown in Fig. 24. We can see that the maximum/middle/minimum principal stress, the maximum shear stress and equivalent (von Mises) stress all become larger as the magnitude of actuators' forces increases from 100 to 1000 pounds. Even for the 1000 pounds, the maximum stresses are within the limit of stress. We also implement failure test based on multiple popular criteria including Max strain/stress, Tsai-Wu, Tsai-Hill, Hoffman, Hashin criteria [37]. The result of failure test shows that Inverse Reserve Factor (IRF), which defines the inverse margin to failure, is 0.27 and is lower than the failure threshold 1.00.

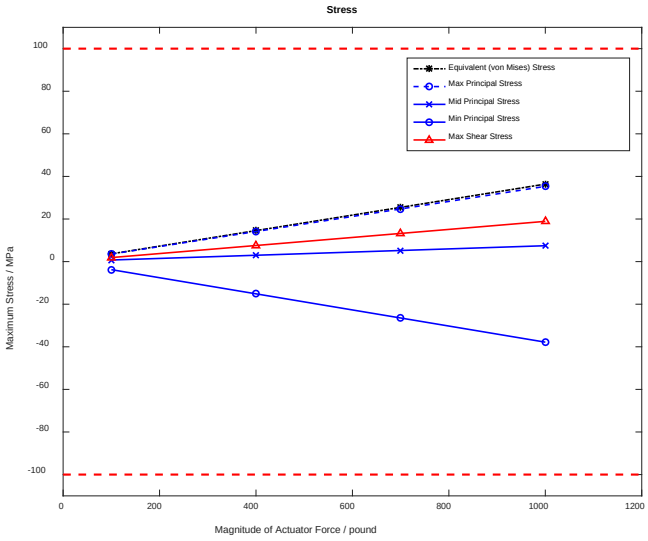

(Note: the upper and lower dashed line represents the limit of stress)

Fig. 24 Maximum stress under different magnitude of actuators' forces

3.5 Summary

Composite parts have been widely used in the airplanes due to its numerous superior material properties. However, dimensional control and variation reduction of composite parts are not as well understood as comparing with the conventional metal parts such as aluminum and titanium.

Motivated by reducing dimensional errors when joining two composite parts, an automatic optimal shape control system has been developed in this paper. Firstly, a finite element analysis (FEA) platform is built to mimic the composite part fabrication process and simulate the dimensional changes of a composite part under various external forces. The FEA platform is validated with experimental data obtained from a real part set-up in a production floor. The validated FEA model is to generate the dimensional response data under different set of actuators' forces designated by designed experiments. Based on those datasets, a surrogate model considering four types of uncertainties (actuator uncertainty, part uncertainty, modeling uncertainty, and unquantified uncertainty) has been developed to achieve good prediction performance. An MLE estimation algorithm has been used for parameter estimation and response prediction. Afterward, the surrogated model considering uncertainties is embedded into a feedforward control algorithm, which is achieved by conducting multivariable optimization to minimize the weighted summation of dimensional deviations of the response to the target.

A case study reveals that the surrogate model considering uncertainties achieves better prediction performance than three other benchmark methods (e.g. the regression

model, the Universal Kriging model, and the Stochastic Kriging model). The automatic optimal shape control system can significantly improve the dimensional product quality and reduce the cycle time in the assembly process of composite parts. Furthermore, a sensitivity analysis has been conducted to explore the control performance for different fuselage variability and different bounds in the AOSC system. Stress analysis and failure test show that the actuators force 1000 pounds will not damage the composite parts.

CHAPTER 4. ACTIVE LEARNING FOR GAUSSIAN PROCESS CONSIDERING UNCERTAINTIES WITH APPLICATION TO SHAPE CONTROL OF COMPOSITE FUSELAGE

In the machine learning domain, active learning is an iterative data selection algorithm for maximizing information acquisition and improving model performance with limited training samples. It is very useful especially for the industrial applications where training samples are expensive, time-consuming, or difficult to obtain. Existing methods mainly focus on active learning for classification, and a few methods are designed for regression such as linear regression or Gaussian process. Uncertainties from measurement errors and intrinsic input noise inevitably exist in the experimental data, which further affect the modeling performance. The existing active learning methods do not incorporate these uncertainties for Gaussian process. In this paper, we propose two new active learning algorithms for the Gaussian process with uncertainties, which are variance-based weighted active learning algorithm and D-optimal weighted active learning algorithm. Through numerical study, we show that the proposed approach can incorporate the impact from uncertainties and realize better prediction performance. This approach has been applied to improving the predictive modeling for automatic shape control of composite fuselage.

4.1 Introduction

Active learning is a type of iterative supervised learning which focuses on maximizing information acquisition with limited samples. In statistics literature, this process is also called optimal experimental design, or sequential design. The main idea of active learning is to iteratively pose "query" or "design" to explore the most informative new experimental samples according to the information obtained from the current samples.

In many machine learning applications, especially in some industrial systems, the explanatory data X are rich and easy to get, but the response data Y are very expensive, time-consuming, or difficult to obtain. For example, when training autonomous driving algorithms, a lot of media (e.g., images, videos) require that oracle users mark them with particular labels, such as "vehicle", "street sign" or "road lines". It can be tedious, redundant and time-consuming to annotate lots of these instances. In composite fuselage shape control problem, it is very expensive, and time-consuming to collect the dimensional shape under specific actuators' forces. Other examples such as speech recognition, factual information extraction, computational biology etc. can be found [46]. In these scenarios, active learning is well-motivated because it can reduce the samples needed as well as obtain sufficient information for parameter inference of predictive modeling.

Different sampling strategies have been proposed to realize active learning. In machine learning literature, these strategies are classified into query synthesis, stream-based selective sampling, and pool-based sampling [46]. In statistics literature, space-filling designs, criterion-based designs, and expected improvement (EI) algorithm have

been proposed for sequential design. For comparison between active learning and sequential design, they have several common characteristics. For example, (i) they both iteratively pose "query" or "design" to explore the most informative new samples according to the information obtained from the current samples; (ii) some criteria are similar for active learning and sequential design. The uncertainty sampling in active learning and sequential designs are based on certain optimality criteria (e.g., mean squared prediction error and maximum entropy) that are mathematically equivalent [46, 47].

However, there exist some differences between active learning and sequential design, in particular, (i) sequential design literature is mainly for regression and prediction problems, while active learning literature mainly focuses on classification problems in machine learning, and a few papers focus on regression; (ii) In sequential design, usually the experiment will be conducted at the selected points from an input space; while in active learning, the experiment sampling may be from a large pool of existent unlabeled data, and the learner can conduct the experiment at a selected point or discard it. In Section 3.2, we will review the literature from two perspectives: machine learning (computational learning) and statistics (sequential design), in detail. Other than Section 3.2, we use active learning as a consistent terminology.

In this paper, we develop two active learning algorithms for Gaussian process model with uncertainties. Uncertainties inevitably exist in the input and output data of any system. Ankenman et al. separated the uncertainties into intrinsic uncertainty inherent to stochastic simulation, and extrinsic uncertainty about unknown response surface [40]. They proposed

the stochastic Kriging model for stochastic computer experiments. Cervone and Pillai investigated Gaussian process regression with input uncertainty from measurement errors and showed that approximate methods for incorporating location measurement error are essential to valid parameter inference [48]. Wang et al. compared the best linear unbiased predictor and stochastic Kriging predictor, and proved their asymptotic properties [49]. The existing active learning methods cannot be straightforwardly extended to Gaussian process with uncertainties. To propose an active learning algorithm for Gaussian process regression considering both intrinsic and extrinsic uncertainties is our main focus in this paper.

The proposed active learning approach is applied to improving the predictive modeling for the automatic shape control system of composite fuselage. The automatic shape control system is essential to reducing the dimensional deviations of composite fuselage as well as the flow time of the aircraft assembly process. Ten actuators are installed cross the edge of the composite fuselage. These actuators are able to provide push and pull forces to change the in-plane shape of the composite fuselage. The automatic shape control system effectively and efficiently adjusts composite fuselages to the optimal configuration [50]. Precise prediction of the dimensional shape of composite fuselage is essential for the shape control, while it is challenging to develop predictive modeling because of multiple uncertainties. A surrogate model considering part uncertainty, actuator uncertainty, and model uncertainty was developed to link the relationship between actuators' forces and dimensional deviations [51]. This approach assumes that the training samples are sufficiently large, and it does not consider the efficient experimental sampling and effective information acquisition. However, obtaining the experimental samples in the

composite fuselage assembly process is time-consuming and expensive. To find an approach to minimize the sample size and improve predictive modeling in a sequential way would be beneficial. In this paper, we propose active learning algorithms for maximizing information extractions for Gaussian process model considering uncertainties. We firstly derive the log-likelihood for general Gaussian process model considering uncertainties, including stochastic model and surrogate model considering uncertainties. Then we take two kinds of information measure into consideration: variance-based information measure, and Fisher information measure. Based on the information measure, we proposed the variance-based weighted active learning algorithm and D-optimal weighted active learning algorithm. The initial design and stopping criterion have also been explored. The proposed active learning strategies have been applied to improving the predictive modeling of composite fuselage shape control.

The remainder of this paper is organized as follows: Section 4.2 illustrates the literature review about active learning and sequential design from machine learning perspective and statistics perspective. Section 4.3 describes the predictive modeling based on Gaussian process, and then proposes the active learning approach for Gaussian process model considering uncertainties. Section 4.4 presents the case study, including an introduction for automatic shape control of composite fuselage, validation procedure, evaluation criteria, and comparison between the performance of our proposed method and benchmark methods. Finally, a brief summary is provided in Section 4.5.

4.2 Literature Review

In this section, we review the existing active learning and sequential design methodologies from machine learning (computational learning) and statistics (sequential design) perspectives.

4.2.1 Literature from Machine Learning Domain

In computational learning theory literature, active learning is sometimes called "query learning". There are three kinds of scenarios: query synthesis, stream-based selective sampling, and pool-based sampling [46]. In query synthesis, the learner may request any unlabelled data instance in the input space. While in stream-based selective sampling, each unlabelled instance is typically drawn one at a time from the input space and then the learner decides whether to query or discard it. For pool-based sampling, there are a set of labelled data and a large pool of unlabelled data available, and queries are selected from the pool. Detailed descriptions about these three scenarios can be found in [46].

Settles and Olsson provided a very detailed literature review on active learning for classification problems [46, 51]. While in this paper, we mainly focus on the literature review on active learning for regression problems.

Lewis and Catlett proposed one active learning strategy called uncertainty sampling [52]. In this strategy, the learner regards the unlabelled samples with the largest uncertainty as the most informative samples. Therefore, the learner queries these unlabelled samples in

order to generalize information from the current samples. In regression, the learner can query the unlabelled samples for which the model has the highest prediction variance. Under the Gaussian assumption, this variance-based uncertainty sampling approach is equivalent to the entropy-based uncertainty sampling because the entropy is a monotonic function of its variance [46]. Cohn Ghahramani and Jordan proposed an active learning strategy which selects design points by minimizing the integrated average variance of the learner [53]. Sugiyama proposed a new active learning method called ALICE (Active Learning using the Importance-weighted least-squares learning based on Conditional Expectation of the generalization error) [54]. This method predicts conditional expectation of the generalization error given training input points, while most of existing methods predict the full expectation of the generalization error. Burbidge et al. investigated an active learning strategy for regression based on Query by Committee [55], which considers choosing sequential points according to the average expected variance over the reference points. Sugiyama and Rubens developed a new ensemble active learning approach for solving active learning and model selection in linear regression simultaneously [56]. However, this approach is mainly designed for linear regression, and not easy to extend to other models like the Gaussian process. Pasolli and Melgani proposed two active learning strategies for Gaussian Process (GP) regression [57]. One is based on adding samples that have large kernel distance from the current training samples, which considers space filling properties. The other exploits an intrinsic GP regression outcome to pick up the samples with the largest variance. Cai et al. proposed a new active learning framework for regression called Expected Model Change Maximization (EMCM) [58], which aims to

choose the examples that lead to the largest change to the current model. However, the EMCM is sensitive to outliers, which may result in non-stationary parameter estimations. Schreiter et al. proposed a safe exploration for active learning with Gaussian processes [59]. A differential entropy criterion was used to explore the relevant data regions. These existing active learning methods do not straightforwardly extend to incorporate uncertainties in the automatic shape control system of composite fuselages.

4.2.2 Literature from Statistics Domain

In statistics domain, the sequential design is to propose experiment designs at a limited number of times, and inputs/responses from the previous design may impact the following design. The basic idea behind the sequential design is to select input points that will allow us to model and minimize the discrepancy between the output from the computer model and predictions from the surrogate model.

For experimental designs relevant to computer experiments, there are two categories: space-filling designs and criterion-based designs. Space-filling designs (e.g. Latin hypercube designs, maximin designs, Sobol's sequence [60]) assume that samples provide information equally across the entire input space, which encourages the exploration among the whole input space. However, these designs are not adaptive to the information from the response surface. Designs based on certain optimality criteria, such as mean squared prediction error [61] and entropy [62], make full use of information from both inputs and outputs. However, they do not consider the shape of the response surface.

Expected improvement (EI) algorithm is a global optimization algorithm proposed by Mockus [63] and then brought to the field of computer experiments [64]. The main idea of EI algorithm is to identify the nature of input-output relationships, and then subsequently choose design points one at a time, or in groups, to maximize the expected improvement on the objective. Williams et al. modified the EI algorithm by considering both control and environmental variables [65], which computed the posterior expected improvement over the current optimum for each untested point, and then selected the next point to maximize modified EI. They further extended the EI algorithm to bivariate modified expected improvement algorithm, which realizes sequential design for computer experiments where there is a bivariate response [66]. Vazquez and Bect investigated the convergence properties of the EI algorithm [67]. Provided that the objective function belongs to the reproducing kernel Hilbert space, the EI algorithm produces a dense sequence of evaluation points in the search domain.

In addition, Lam proposed a modified integrated mean squared prediction error (IMSPE) criterion by imposing a penalty to prevent the additional design points from clustering together [47]. This method can realize the trade-off between exploration and exploitation. Deng et al. pointed out that there were two kinds of approaches to generate sequential designs: stochastic approximation and optimal design [68]. The optimal design approach has better performance when the assumed model is the true model, but it is not robust to model assumption. They used a combination of stochastic approximation and D-optimal designs to judiciously select the design points [68]. By maximizing the estimated variance of the hyperplane, they placed the next point at the location of the greatest

uncertain. The proposed method improved the process of money laundering detection. Crombecq et al. proposed a hybrid sequential design strategy which used a Monte-Carlo-based approximation of a Voronoi tessellation for exploration and local linear approximations of the simulator for exploitation [69]. The advantage of this method is that it is independent of the model type, and can be used in heterogeneous modeling environments.

From an engineering perspective, there are several literature presenting the sequential strategies for other objectives, such as measurement and detection. Jin et al. proposed a sequential measurement strategy for efficient wafer geometric profile estimation [70]. This strategy reduced the number of samples measured in wafers as well as provided an adequate accuracy for quality feature estimation. The sequential samples are chosen based on the gradient and error of profile prediction. Hao proposed a sequential sampling strategy called Adaptive Kernelized Maximum-Minimum Distance (AKM2D) to speed up inspection and anomaly detection process [71]. The proposed method realized the trade-off between space filling sampling (exploration) and focused sampling near the anomalous region (exploitation). However, this method is mainly focused on efficient detection, not for predictive modeling.

4.3 Active Learning for Gaussian Process Considering Uncertainties

Gaussian process models have been widely used as surrogate models of expensive deterministic computer simulations. It has many advantages, such as good prediction performance, good flexibility from multiple correlation choices, complete mathematical

properties in both Bayesian and frequentist statistical framework, and capability of uncertainty quantification. In Section 4.2, several active learning strategies relevant to the Gaussian process models have been reviewed, including uncertainty sampling [52, 57], entropy-based active learning [59], and EI algorithms [64-66]. These strategies work well for the data acquisition of the deterministic computer simulations, while in some other cases, there exist multiple input or output uncertainties in the datasets. To the best of our knowledge, there lacks a tailored active learning strategy for Gaussian process considering uncertainties. In this paper, we first review two Gaussian process models considering uncertainties for automatic shape control of composite fuselage. One is the stochastic Kriging, and the other is the surrogate model considering uncertainties. These models can provide very accurate prediction for composite fuselage shape control. Then, we proposed new active learning strategies for Gaussian process considering uncertainties.

4.3.1 Gaussian Process with Nugget Effects: Stochastic Kriging

Cressie represented measurement error or uncertainties as a nugget effect for Gaussian process [72]. Ankenman et al. integrated the intrinsic uncertainty and extrinsic uncertainty with their stochastic Kriging model [40]. Cervone and Pillai investigated Gaussian process regression with input uncertainty from measurement errors and showed that approximate methods for incorporating location measurement error are essential to valid parameter inference [48]. In this section, we summarize the Gaussian process model with nugget effects for composite fuselage shape control.

Consider a set of design setting $\mathcal{X}$, which includes pairs $\{\boldsymbol{F}_t, \mathrm{n}_t\}$, $t = 1,2,\dots,k$, where $\boldsymbol{F}_t$ is the input vector (actuators' forces) with dimension of $1 \times \mathrm{q}$, n_t is the number of replications for the design point $\boldsymbol{F}_t$. Consider that the p-dimension output (dimensional deviations) for the design point $\boldsymbol{F}_t$ is $\boldsymbol{Y}(\boldsymbol{F}_t)$, where each element $Y_{ij}(\boldsymbol{F}_t)$ denotes the j^{th} variable of the output vector under the i^{th} replication at the input $\boldsymbol{F}_t$. We use the set $\mathcal{D}$ to represent the input/output pairs $\{\boldsymbol{F}_t, \boldsymbol{Y}(\boldsymbol{F}_t)\}$. Considering both a noise term $\boldsymbol{\varepsilon}_i$. and a stochastic process term $z_j(\boldsymbol{F})$ that are regarded as intrinsic uncertainty (measurement error) and extrinsic uncertainty respectively, the Gaussian process with nuggets effects (or called the stochastic Kriging) model can be developed as

$$Y_{ij}(\boldsymbol{F}) = \boldsymbol{F}\boldsymbol{S}_j + z_j(\boldsymbol{F}) + \varepsilon_{ij}\,, \tag{9}$$

where $\boldsymbol{S}_j$ represents the sensitivity matrix corresponding to the j^{th} response, $j = 1,2,\dots,\mathrm{p}$. $z_j(\boldsymbol{F})$ is a stochastic process that represents the extrinsic uncertainty relevant to functional mapping. Specifically, the stochastic process $z_j(\boldsymbol{F})$ is assumed to be a Gaussian process $\boldsymbol{GP}(\boldsymbol{0},\ \boldsymbol{\Sigma}_{zj})$ with covariance matrix $\boldsymbol{\Sigma}_{zj}$ with dimension $k \times k$. For any two vectors of the actuators' forces, the covariance is $\boldsymbol{\Sigma}_{zj}(\boldsymbol{F}_{\mathrm{m}}, \boldsymbol{F}_{\mathrm{n}}) = cov[z_j(\boldsymbol{F}_{\mathrm{m}}), z_j(\boldsymbol{F}_{\mathrm{n}})]$. Let $\boldsymbol{\Sigma}_{zj}(\boldsymbol{F}_0,\cdot) = (cov\big[z_j(\boldsymbol{F}_0), z_j(\boldsymbol{F}_1)\big], \dots,\ cov\big[z_j(\boldsymbol{F}_0), z_j(\boldsymbol{F}_{\mathrm{k}})\big]$ as the covariance between z_j's at design points and new actuators' forces $\boldsymbol{F}_0$. The intrinsic noise ε_{ij} is assumed to be independent and identically distributed with a normal distribution $\varepsilon_{ij} \sim \mathbb{N}(0,\ \sigma_{\boldsymbol{\varepsilon j}})$. the noise covariance matrix is $\boldsymbol{\Sigma}_{\varepsilon j}$, a $k \times k$ covariance matrix with (a, b) element is $\mathrm{Cov}\big[\sum_{i=1}^{n_a} \varepsilon_{ij}(\boldsymbol{F}_a)/\ n_a\,, \sum_{i=1}^{n_b} \varepsilon_{ij}(\boldsymbol{F}_b)/n_b\big]$. The sample mean at $\boldsymbol{F}_t$ as $\overline{\boldsymbol{Y}}_j(\boldsymbol{F}_t) = \sum_{\boldsymbol{i=1}}^{\mathrm{n}_t} Y_{ij}(\boldsymbol{F}_t)\ /\mathrm{n}_t$. Let $\overline{\boldsymbol{Y}}_j =$

$(\bar{\boldsymbol{Y}}_j(\boldsymbol{F}_1), \ldots, \bar{\boldsymbol{Y}}_j(\boldsymbol{F}_k))^{\boldsymbol{T}}$, and Let $\boldsymbol{F}_{DOE} = (\boldsymbol{F}_1; \ldots; \boldsymbol{F}_k)$ denote all the design points of the actuators' forces. Let $\boldsymbol{R}_j(\boldsymbol{F}_0, \cdot) = \left(\mathrm{Cov}\left[Y_j(\boldsymbol{F}_0), \bar{Y}_j(\boldsymbol{F}_1)\right]; \ldots; \mathrm{Cov}\left[Y_j(\boldsymbol{F}_0), \bar{Y}_j(\boldsymbol{F}_k)\right]\right)$. The covariance between vector $\boldsymbol{a}$ and vector $\boldsymbol{b}$ satisfies $\boldsymbol{\Sigma}_{zj}(\tau_j^2, \boldsymbol{\theta}, \boldsymbol{a}, \boldsymbol{b}) = \tau_j^2 R_{zj}(\boldsymbol{\theta}, \boldsymbol{a} - \boldsymbol{b})$, where $R_{zj}(\boldsymbol{\theta}, \boldsymbol{a} - \boldsymbol{b})$ is one of the correlation functions. With spatial correlation, $z_j(\boldsymbol{F}_{\mathrm{m}})$ and $z_j(\boldsymbol{F}_{\mathrm{n}})$ tend to be similar (e.g. $R_{zj,\mathrm{mn}} = R_{zj}(\boldsymbol{\theta}, \boldsymbol{F}_{\mathrm{m}}, \boldsymbol{F}_{\mathrm{n}})$ tends to be large) if $\boldsymbol{F}_{\mathrm{m}}$ and $\boldsymbol{F}_{\mathrm{n}}$ are close.

According to the literature [40, 48, 18], we know the best MSPE (mean square prediction error) linear unbiased predictor as

$$\widehat{\boldsymbol{Y}}_{\boldsymbol{j}}(\boldsymbol{F_0} \mid \boldsymbol{\mathcal{D}}) = \boldsymbol{F_0 S_j} + \boldsymbol{R_j}(\boldsymbol{F_0}, \cdot)^{\boldsymbol{T}}\left[\boldsymbol{\Sigma_{zj}} + \boldsymbol{\Sigma_{\varepsilon j}}\right]^{-\mathbf{1}}(\bar{\boldsymbol{Y}}_{\boldsymbol{j}} - \boldsymbol{F_{DOE} S_j}) \tag{10}$$

4.3.2 Surrogate Model considering Uncertainties

The stochastic Kriging model uses a nugget effect to approximate both input uncertainties and output uncertainties. Yue et al. proposed a surrogate model considering part uncertainty, actuator uncertainty, and model uncertainty, which is a Gaussian process model with consideration of uncertainties in detail [18]. A surrogate model considering uncertainties was proposed as

$$\boldsymbol{Y_{ij}}(\boldsymbol{F_t}) = \boldsymbol{F_t S_j} + \boldsymbol{F_t}\tilde{\boldsymbol{S}}_{\boldsymbol{j}} + \widetilde{\boldsymbol{F}}_{\boldsymbol{t}}\boldsymbol{S_j} + \boldsymbol{z_j}(\boldsymbol{F_t}) + \boldsymbol{\varepsilon_{ij}}(\boldsymbol{F_t}), \tag{11}$$

where $i = 1,2, \ldots, n_t$; $j = 1,2, \ldots, p$; p is the number of output responses (key dimensional features). $\boldsymbol{F}_t$ is the target actuators' forces vector; $\widetilde{\boldsymbol{F}}_t$ is a vector of an additional random

deviation of actuators' forces that results from the actuators' uncertainty with distribution $\mathbb{N}(\mathbf{0},\ \boldsymbol{\Sigma_F})$. It can be obtained from the tolerance of actuators instruction; $\boldsymbol{F}_t + \widetilde{\boldsymbol{F}}_{\boldsymbol{t}}$ represents the true actuators' force vector. $\boldsymbol{S}_j$ is an ideal sensitivity vector (column vector) and $\tilde{\boldsymbol{S}}_j$ represents the random sensitivity vector variability from the part uncertainty, which is assumed to follow $\mathbb{N}(\mathbf{0},\ \boldsymbol{\Sigma_S})$. Both $\boldsymbol{S}_j$ and $\boldsymbol{\Sigma_S}$ are unknown. $\boldsymbol{z}_j(\boldsymbol{F}_t)$ is assumed to be a stationary Gaussian process $z_j \sim \boldsymbol{GP}(\mathbf{0},\ \boldsymbol{\Sigma}_{zj})$. $\varepsilon_{ij}(\boldsymbol{F}_t)$ is assumed to follow an independent normal distribution $\varepsilon_{ij}(\boldsymbol{F}_t) \sim \mathbb{N}(0,\ \sigma^2_{\varepsilon j}(\boldsymbol{F}_t))$, which represents the inherent simulation variability in a stochastic simulation, or measurement errors in a physical experiment. ε_{ij}, $\widetilde{\boldsymbol{F}}_t$, $\tilde{\boldsymbol{S}}_j$, and z_j are assumed to be mutually independent, and their higher order interaction term $\widetilde{\boldsymbol{F}}_{\boldsymbol{t}} \cdot \tilde{\boldsymbol{S}}_j$ is assumed to be zero. The model can be interpreted as a decomposition of the response $Y_{ij}(\boldsymbol{F}_t)$ into three parts: a regression term $\boldsymbol{F}_t\boldsymbol{S}_j + \boldsymbol{F}_t\tilde{\boldsymbol{S}}_j + \widetilde{\boldsymbol{F}}_t\boldsymbol{S}_j$, a Gaussian process term $z_j(\boldsymbol{F}_t)$, and a noise term $\varepsilon_{ij}(\boldsymbol{F}_t)$.

Assume that $\boldsymbol{S}_j$, $\boldsymbol{\Sigma}_{zj}$, $\boldsymbol{\Sigma_F}$, $\boldsymbol{\Sigma}_\varepsilon$, and $\boldsymbol{\Sigma_S}$ are known, the best MSPE (mean square prediction error) linear unbiased predictor can be derived as

$$\widehat{\boldsymbol{Y}}_{\boldsymbol{j}}(\boldsymbol{F_0} \mid \boldsymbol{\mathcal{D}}) = \boldsymbol{F_0 S_j} + \boldsymbol{R_j^T}(\boldsymbol{F_0},\cdot)\boldsymbol{R_j^{-1}}(\overline{\boldsymbol{Y}}_{\boldsymbol{j}} - \boldsymbol{F_{DOE}S_j}), \tag{12}$$

where $\boldsymbol{R}_j = \boldsymbol{F}_{DOE}\boldsymbol{\Sigma_S}\boldsymbol{F}_{DOE}^T + \boldsymbol{\Sigma}_{zj} + \boldsymbol{S}_j^T\boldsymbol{\Sigma_F}\boldsymbol{S}_j \cdot \boldsymbol{I} + \boldsymbol{\Sigma}_{\varepsilon j}$, and $\boldsymbol{R}_j(\boldsymbol{F}_0,\cdot) = \Big(\boldsymbol{F}_0\boldsymbol{\Sigma_S}\boldsymbol{F}_1^T + \tau_j^2 R_{zj}(\boldsymbol{\theta}, \boldsymbol{F}_0 - \boldsymbol{F}_1);\ \ldots;\ \boldsymbol{F}_0\boldsymbol{\Sigma_S}\boldsymbol{F}_k^T + \tau_j^2 R_{zj}(\boldsymbol{\theta}, \boldsymbol{F}_0 - \boldsymbol{F}_k)\Big)$. The best MSPE linear unbiased predictor is also simply called a best linear unbiased predictor (BLUP).

The surrogate model considering uncertainties in Equation (12) analyzes the different sources of uncertainties in the composite fuselage shape control system, while the

stochastic Kriging predictor in Equation (10) approximates all the uncertainties by introducing a nugget effect. Wang et al. proved that the stochastic Kriging and Gaussian process with input location errors asymptotically converge to the same limit [49]. In our active learning strategy design, we will analyze both cases.

4.3.3 Information Measure

Active learning is an iterative data selection algorithm for maximizing information acquisition and improving model performance with limited training samples. Firstly, we need to propose the information measure for Gaussian process considering uncertainties.

Suppose $\mathfrak{R}_j(\boldsymbol{F}_0,\cdot) = \left(\boldsymbol{F}_0\boldsymbol{\Sigma}_{\boldsymbol{S}}\boldsymbol{F}_1^T + \tau_j^2 R_{zj}(\boldsymbol{\theta}, \boldsymbol{F}_0 - \boldsymbol{F}_1);\ \ldots; \boldsymbol{F}_0\boldsymbol{\Sigma}_{\boldsymbol{S}}\boldsymbol{F}_k^T + \tau_j^2 R_{zj}(\boldsymbol{\theta}, \boldsymbol{F}_0 - \boldsymbol{F}_k)\right)$, $\mathfrak{R}_j = \boldsymbol{F}_{DOE}\boldsymbol{\Sigma}_{\boldsymbol{S}}\boldsymbol{F}_{DOE}^T + \boldsymbol{\Sigma}_{zj} + \boldsymbol{S}_j^T\boldsymbol{\Sigma}_{\boldsymbol{F}}\boldsymbol{S}_j \cdot \boldsymbol{I} + \boldsymbol{\Sigma}_{\varepsilon j}$ when the model is the surrogate model considering uncertainties, and $\mathfrak{R}_j(\boldsymbol{F}_0,\cdot) = \left(\tau_j^2 R_{zj}(\boldsymbol{\theta}, \boldsymbol{F}_0 - \boldsymbol{F}_1);\ \ldots; \tau_j^2 R_{zj}(\boldsymbol{\theta}, \boldsymbol{F}_0 - \boldsymbol{F}_k)\right)$, $\mathfrak{R}_j = \boldsymbol{\Sigma}_{zj} + \boldsymbol{\Sigma}_{\varepsilon j}$ when the model is the stochastic Kriging model. Suppose $\boldsymbol{\Sigma}_{\varepsilon j} = \sigma_j^2\boldsymbol{I}$, $\boldsymbol{\Sigma}_{\boldsymbol{S}} = \varphi_j^2\boldsymbol{I}$. Let Θ represent the key parameter set, for example in the stochastic Kriging model, $\Theta = \{\tau_j^2, \boldsymbol{\theta}_j, \sigma_j^2\}$, while in the surrogate model considering uncertainties, $\Theta = \{\tau_j^2, \boldsymbol{\theta}_j, \sigma_j^2, \varphi_j^2\}$.

Under the multivariate normal distribution, the log-likelihood function of $(\boldsymbol{S}_j, \tau_j^2, \boldsymbol{\theta}, \boldsymbol{\Sigma}_{\boldsymbol{S}})$ is

$$\mathcal{L}\left(\boldsymbol{S}_j, \Theta \mid \boldsymbol{\mathcal{D}}\right) = -\frac{1}{2}\ln[(2\pi)^k] - \frac{1}{2}\ln\left[\det\left(\mathfrak{R}_j\right)\right] - \frac{1}{2}(\overline{\boldsymbol{Y}}_j - \boldsymbol{F}_{DOE}\boldsymbol{S}_j)^T\mathfrak{R}_j^{-1}(\overline{\boldsymbol{Y}}_j - \boldsymbol{F}_{DOE}\boldsymbol{S}_j) \tag{13}$$

We can derive the estimated parameter $\widehat{\boldsymbol{S}}_j$ by making the first derivative of $\mathcal{L}\left(\boldsymbol{S}_j, \tau_j^2, \boldsymbol{\theta}_j, \boldsymbol{\Sigma}_{\boldsymbol{S}}\right)$ to $\boldsymbol{S}_j$ be equal to zero. Then we can get the generalized least-square estimation of the parameter $\widehat{\boldsymbol{S}}_j$

$$\frac{\partial \mathcal{L}}{\partial \boldsymbol{S}_j} = (\overline{\boldsymbol{Y}}_j - \boldsymbol{F}_{DOE}\boldsymbol{S}_j)^T \mathfrak{R}_j^{-1} \boldsymbol{F}_{DOE} = \boldsymbol{0}$$
$$\widehat{\boldsymbol{S}}_j(\Theta) = (\boldsymbol{F}_{DOE}^T \mathfrak{R}_j^{-1} \boldsymbol{F}_{DOE})^{-1} \boldsymbol{F}_{DOE}^T \mathfrak{R}_j^{-1} \boldsymbol{F}_{DOE} \overline{\boldsymbol{Y}}_j \tag{14}$$

One straightforward and widely used measure is variance. The variance of the predictor $\widehat{\boldsymbol{Y}}_j(\boldsymbol{F}_0 | \boldsymbol{\mathcal{D}})$ is $\mathrm{Var}_j(\boldsymbol{F}_0 \mid \boldsymbol{\mathcal{D}}) = \tau_j^2 - \mathfrak{R}_j^T(\boldsymbol{F}_0, \cdot)\mathfrak{R}_j^{-1}\mathfrak{R}_j(\boldsymbol{F}_0, \cdot)$.

The other information measure is the Fisher information matrix $I(\Theta) \in \mathbb{R}^{(m+2)\times(m+2)}$, which is calculated by

$$I_{ab}(\Theta | \boldsymbol{\mathcal{D}}) = -\mathbb{E}\left[\frac{\partial^2}{\partial \Theta_a \partial \Theta_b} \mathcal{L}(\Theta) | \Theta\right] \tag{15}$$

where $a, b = 1, \cdots, m+2$.

Based on Equation (6) and Equation (7), the Fisher information matrix of $\widehat{\Theta}$ is

$$I_{ab}\left(\widehat{\Theta} \mid \boldsymbol{\mathcal{D}}\right) = \left[\frac{\partial \boldsymbol{S}_j}{\partial \Theta_a}\right]^T \boldsymbol{F}_{DOE}^T \mathfrak{R}_j^{-1} \boldsymbol{F}_{DOE} \left[\frac{\partial \boldsymbol{S}_j}{\partial \Theta_b}\right] + \frac{1}{2} Tr\left[\mathfrak{R}_j^{-1} \frac{\partial \mathfrak{R}_j}{\partial \Theta_a} \mathfrak{R}_j^{-1} \frac{\partial \mathfrak{R}_j}{\partial \Theta_b}\right] \tag{16}$$

where $\mathfrak{R}_j$ is the covariance matrix of the Gaussian process; and the first-order derivative of the coefficients $\boldsymbol{S}_j$ with respect to each entry in the parameter vector can be represented as

$$\frac{\partial \boldsymbol{S}_j}{\partial \Theta_a}\left(\widehat{\Theta}\right) = -\left(\boldsymbol{F}_{DOE}^T \mathfrak{R}_j^{-1} \boldsymbol{F}_{DOE}\right)^{-1} \left[\boldsymbol{F}_{DOE}^T \mathfrak{R}_j^{-1} \frac{\partial \mathfrak{R}_j}{\partial \Theta_a} \mathfrak{R}_j^{-1} \left(\overline{\boldsymbol{Y}}_j - \boldsymbol{F}_{DOE}\boldsymbol{S}_j\right)\right] \tag{17}$$

According to Cramer-Rao inequality explanation for fisher information matrix [30], the inverse of Fisher information sets a lower bound on the variance of the model's parameter estimates. Maximizing the Fisher information is equivalent to minimizing the lower bound on the variance of parameter estimations. When the Fisher information is a matrix, we minimize the determinant of the inverse information matrix. This is called D-optimality in the optimal experimental design.

4.3.4 Active Learning

In this section, we propose algorithms to select the next sample sequentially, which is the main implementation of active learning. Suppose the next samples can be selected from a pool of candidates. We denote these candidate samples by $\mathcal{F} = \{\widetilde{\boldsymbol{F}}_1, \widetilde{\boldsymbol{F}}_2, \cdots, \widetilde{\boldsymbol{F}}_N\}$. N denotes the size of the pool $\mathcal{F}$. It is worth mentioning that the choice of candidate pool $\mathcal{F}$ is very important. The best active learning strategy should perform a trade-off between exploitation and exploration, where the exploitation suggests selecting samples in regions which were previously identified to be interesting. On the other hand, the exploration involves selecting samples in unrepresented regions of the design space. In our active learning strategy, the exploitation is relevant to algorithms of selecting next samples from the candidate pool, while the candidate pool determines the exploration. In our algorithms, the maximin Latin Hypercube Design [74], which demonstrates good space-filling properties and first-dimension projection properties, is implemented to obtain the samples in the candidate pool.

There are two information measures according to Section 4.3.C, the output variance of its prediction, and the Fisher information matrix. Firstly, we develop a variance-based weighted active learning (VWAL) algorithm for Gaussian process considering uncertainties. That means the next sample is selected based on

$$\begin{aligned} F_{new} &= \underset{F\in\{\tilde{F}_1,\tilde{F}_2,\cdots,\tilde{F}_N\}}{\arg\max} \sum_{j=1}^{p} W_j \cdot \mathrm{Var}_j(F \mid \boldsymbol{\mathcal{D}}) \\ &= \underset{F\in\{\tilde{F}_1,\tilde{F}_2,\cdots,\tilde{F}_N\}}{\arg\max} \sum_{j=1}^{p} \tau_j^2 - \boldsymbol{\Re}_j^T(\boldsymbol{F}_0,\cdot)\boldsymbol{\Re}_j^{-1}\boldsymbol{\Re}_j(\boldsymbol{F}_0,\cdot) \end{aligned} \tag{18}$$

where F_{new} is the next sample to be queried, $\mathrm{Var}_j(F \mid \boldsymbol{\mathcal{D}})$ is the variance of the predictor $\widehat{\boldsymbol{Y}}_j(\boldsymbol{F}_0 \mid \boldsymbol{\mathcal{D}})$ at the j^{th} critical dimension of the composite fuselage, and W_j is weight coefficient for the j^{th} critical dimension and we suppose $\sum_j W_j = 1$. The W_j $(j = 1,2,\dots,p)$ is determined by the engineering-domain knowledge. Under Gaussian assumption, the entropy of a random variable is a monotonic function of its variance. Hence the variance-based weighted active learning algorithm is equivalent to the entropy-based methods [46,47].

For the implementation of the active learning algorithm, firstly, we estimate model parameters for the Gaussian process model considering uncertainties by minimizing the log-likelihood function (13). Then we calculate the variance of predictors for each sample in the candidate pool. Next, the new sample point F_{new} can be selected based on solving Equation (18). The experiment will be conducted to collect the oracle response $\boldsymbol{Y}(F_{new})$**.** The existing sample set $\boldsymbol{\mathcal{D}}$ will be updated by adding the new sample point and corresponding response. The parameters will be iteratively updated, and the new samples

will be selected actively until the iteration number reaches the maximum iteration N_{iter} or the error of the model E_{GP} is smaller than a specific threshold. The pseudo code of this active learning algorithm is summarized in Algorithm 1.

Algorithm 1: Variance-based Weighted Active Learning (VWAL) for Gaussian Process Considering Uncertainties

---

Require: $\boldsymbol{\mathcal{D}}$, W_j

1: $i = 1$

2: Estimate parameters by minimizing log-likelihood function (13) on $\boldsymbol{\mathcal{D}}$

3: Calculate the variance of the predictor $\widehat{\boldsymbol{Y}}_j(\boldsymbol{F}_0|\,\boldsymbol{\mathcal{D}}), (j = 1,2,\dots,p)$ for each sample

4: **while** ($i \leq N_{iter}$) && (E_{GP} > threshold) **do**

5: get F_{new} from solving Equation (18)

6: Implement experiment for F_{new} and obtain $\boldsymbol{Y}(F_{new})$

7: $\boldsymbol{\mathcal{D}} \leftarrow \{\boldsymbol{\mathcal{D}} \cup (F_{new}, \boldsymbol{Y}(F_{new}))\}$

8: Estimate parameters by minimizing log-likelihood function (13) on $\boldsymbol{\mathcal{D}}$

9: Calculate the variance of the predictor $\widehat{\boldsymbol{Y}}_j(\boldsymbol{F}_0|\,\boldsymbol{\mathcal{D}}), (j = 1,2,\dots,p)$ for each sample

10: $i = i + 1$

11: **end while**

Based on another information measure, the Fisher information matrix, we also develop a D-optimal weighted active learning (DOWAL) algorithm for Gaussian process considering uncertainties. That means the next sample is selected based on

$$F_{new} = \underset{F\in\{\tilde{F}_1,\tilde{F}_2,\cdots,\tilde{F}_N\}}{\arg\min} \sum_{j=1}^{p} W_j \cdot \det\left(\left[I_{ab}\left(\widehat{\Theta} \mid \boldsymbol{\mathcal{D}}, \boldsymbol{F}\right)\right]^{-1}\right) \tag{19}$$

The inverse of Fisher information sets a lower bound on the variance of the model's parameter estimates, which is known as the Cramér-Rao inequality. By minimizing the determinant of the inverse Fisher information matrix (D-optimality), we can maximize the information acquisition in each step of active learning process. Furthermore, the D-optimality is relevant to minimizing the differential posterior entropy of the parameter estimation [75].

Similarly, we can summarize the pseudo code of this D-optimal weighted active learning algorithm for Gaussian process model considering uncertainties in Algorithm 2.

Algorithm 2: D-Optimal Weighted Active Learning (DOWAL) for Gaussian Process Considering Uncertainties

---

Require: $\boldsymbol{\mathcal{D}}$, W_j

1: $i = 1$

2: Estimate parameters by minimizing log-likelihood function (13) on $\boldsymbol{\mathcal{D}}$

3: Calculate the Fisher information matrix by solving Equations (16) and (17)

4: **while** ($i \leq N_{iter}$) && (E_{GP} > threshold) **do**

5: get F_{new} from solving Equation (19)

6: Implement experiment for F_{new} and obtain $\boldsymbol{Y}(F_{new})$

7: $\boldsymbol{\mathcal{D}} \leftarrow \{\boldsymbol{\mathcal{D}} \cup (F_{new}, \boldsymbol{Y}(F_{new}))\}$

8: Estimate parameters by minimizing log-likelihood function (13) on $\boldsymbol{\mathcal{D}}$

9: Calculate the Fisher information matrix by solving Equations (16) and (17)

10: $i = i + 1$

11: **end while**

In this section, we proposed two active learning algorithms for Gaussian process model considering uncertainties. In next subsections, we will explore the initial design, evaluation criteria, and stopping criteria for these active learning algorithms.

4.3.5 Initial Design

The initial design defines the preliminary parameter estimation and has a significant effect on efficiency and accuracy of the model. It is critical to determine initial samples with a suitable size. The initial sample points should explore the entire space with very good space filling property. Maximin distance criterion can be used to choose a good design with space filling property. In addition, the initial samples need to provide as much information as possible. So the Latin hypercube design with good projection property is helpful. We choose the maximin Latin hypercube design to ensure the good exploration and exploitation performance for the initial samples. In addition, the size of the initial samples is very important. Under-selection of initial samples may result in insufficient

parameter estimation for the proposed model, while over-selection of initial samples may reduce the efficiency and significance of the active learning algorithms. We choose the initial design by the rule of thumb of predictive modeling in composite fuselage shape control.

4.3.6 Stopping Criterion

A potentially important element of interactive learning applications in general is to determine when to stop learning [46]. We take modeling for composite fuselage shape control as an example. We hope to use minimum number of training samples to get a model with satisfied prediction accuracy. It is quite complex and time-consuming to collect experimental samples in the assembly process. Therefore, it is important to know that how to recognize when the accuracy of the model can satisfy the prediction requirement, and acquiring more samples is likely increasing the flow time without much improvement on the model. Active learning provides us with the capability to accurately balance model accuracy and reducing the cost of obtaining samples.

There are several stopping criteria for active learning, such as stopping based on an intrinsic measure of stability or self-confidence within the learner [76]. In our algorithms, we check the model prediction error is consistently smaller than the engineering specifications for several continuous steps. Additionally, we check that the total iteration number is smaller than a specific threshold to prevent an infinite iteration loop due to algorithm errors.

4.4 Case Study

We conducted a case study to demonstrate the effectiveness of the proposed active learning algorithms. Firstly, we introduced the automatic shape control of composite fuselage. Next, we discussed the parameter estimation algorithms for the predictive modeling. Three evaluation criteria have been used to evaluate the performance of active learning methods. By comparing our proposed methods with benchmark methods, we conclude that the proposed active learning methods can obtain better performance for predictive modeling. In addition, the proposed methods provide us with a decision point for stopping the collection of experimental samples.

4.4.1 Automatic Shape Control of Composite Fuselage

In current practice, experienced engineers adjust the shape of composite fuselage multiple times by trial-and-error, until the deviations between the real shape and the target shape are smaller than a specific engineering specification. This approach brings large uncertainties for the fuselage assembly process, and it may only reach an acceptable shape but not the optimal one. For the automatic shape control, the system is able to measure the real dimensional shape of the fuselage by a laser metrology system, then compute the optimal actuators' forces to minimize the dimensional deviations of current composite fuselage to the target one, and finally implement the shape adjustment. As shown in Fig. 25(a), ten actuators are installed at the edge of the composite fuselage. These actuators can push or pull the fuselage to adjust its shape to the target shape. One of the most challenging tasks for automatic shape control system is to develop a predictive model with limited

experimental samples. Thus, we proposed active learning strategies to maximize the information acquisition for predictive modeling and provide a stopping criterion for experiments.

In order to validate our proposed methodology economically, we developed a finite element model of the composite fuselage, with software ANSYS Composite PrepPost [50]. The finite element model, shown in Fig. 25(b), exactly mimics the fabrication process of composite fuselages, including material (carbon fiber and epoxy resin) introduction, stack-up/sub-laminates design, material orientation, geometrical setting, fixture set-up etc. Physical experiments with a fuselage from the sponsor company were conducted to calibrate and validate the accuracy of the developed computer simulation model. We applied an effective model calibration approach via sensible variable identification and adjustment [25]. After calibration, the Finite element analysis (FEA) simulation results and the physical experimental outputs are quite consistent [50, 25]. One simulation result of the total deformation is shown in Fig. 1(c).

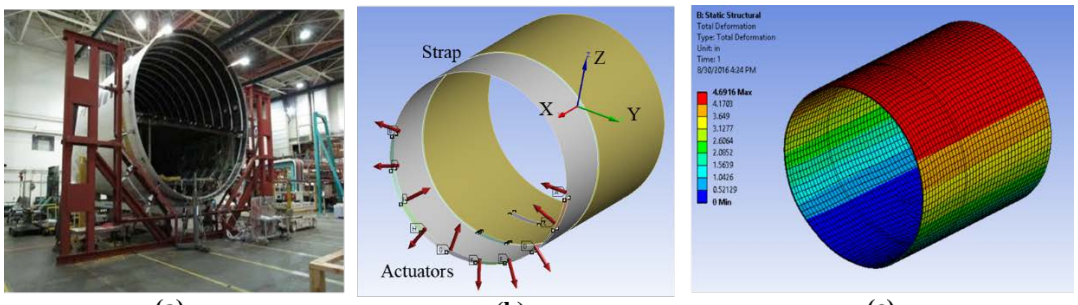

(a) Fuselage shape control, (b) Finite element model of shape control, (c) One simulation result

Fig. 25 Shape control of composite fuselage

After we obtain an accurate finite element model. We generate the training and testing datasets by computer experiments. Then Gaussian process models considering uncertainties are trained to predict dimensional deviations under specific actuators' forces. The performance of the Gaussian process models considering uncertainties can be found [7].

4.4.2 Validation Procedure of Active Learning Algorithms

To validate the performance of active learning algorithms, we use a Gaussian process model trained by the finite element simulation datasets as an oracle model. The oracle model is to imitate the real engineering system. We generate the initial design of input by maximin Latin hypercube design. Outputs of experimental samples are generated by the oracle model with input uncertainties. For each step of active learning algorithms, we conduct parameter estimation for Gaussian process considering uncertainties by minimizing the log-likelihood function in Equation (13). The detailed procedures of active learning algorithms are shown in Algorithm 1 and Algorithm 2. In the active learning algorithms, the candidate pool is generated by maximin Latin hypercube design with input bounds [-450 lbf, 450 lbf]. The size of the candidate pool is 200.

4.4.3 Evaluation Criteria

To evaluate the performance of active learning algorithms, we introduce three evaluation scores: mean of mean absolute deviations (mean MAD), maximum of mean absolute deviations (max MAD), and mean square error of cross-validation (cross-

validation MSE). All these three evaluation scores are calculated based on the evaluation pool, which includes 200 samples explored in the whole input space. The outputs are generated by the oracle model.

The mean of mean absolute deviations (mean MAD) for each iteration can be calculated by Equation (20)

$$MAD_{mean} = \underset{j}{\text{mean}} \left\{ \frac{1}{N_{eva}} \sum_{i=1}^{N_{eva}} \left| \widehat{\boldsymbol{Y}}_{\boldsymbol{j}}(\boldsymbol{F_i}) - \boldsymbol{Y}_{\boldsymbol{j}}^{*}(\boldsymbol{F_i}) \right| \right\} \tag{20}$$

where N_{eva} is the size of evaluation samples. $\widehat{\boldsymbol{Y}}_{\boldsymbol{j}}(\boldsymbol{F_i})$ is the predictive response of the j^{th} critical dimension at $\boldsymbol{F_i}$ for each iteration. It is worth mentioning that the predictive model is developed based on all samples at each iteration. $\boldsymbol{Y}_{\boldsymbol{j}}^{*}(\boldsymbol{F_i})$ is the oracle output of the j^{th} critical dimension at $\boldsymbol{F_i}$.

Similarly, the max of mean absolute deviations (max MAD) can be calculated by Equation (21)

$$MAD_{max} = \underset{j}{\max} \left\{ \frac{1}{N_{eva}} \sum_{i=1}^{N_{eva}} \left| \widehat{\boldsymbol{Y}}_{\boldsymbol{j}}(\boldsymbol{F_i}) - \boldsymbol{Y}_{\boldsymbol{j}}^{*}(\boldsymbol{F_i}) \right| \right\} \tag{21}$$

The two evaluation scores above are based on the mean absolute deviations (MAD). MAD is an important index to check the model performance in composite fuselage shape control. We also introduce the cross-validation of mean square errors (MSE). We use leave-one-out cross-validation in which the accuracy measures are obtained by using Equation (22).

$$MSE_{cv} = \frac{1}{N_{eva}} \sum_{i=1}^{N_{eva}} \underset{j}{\text{mean}} \left\{ \left\| \widehat{\boldsymbol{Y}}_{\boldsymbol{j}}^{[i]}(\boldsymbol{F_i}) - \boldsymbol{Y_j^*}(\boldsymbol{F_i}) \right\|^2 \right\} \tag{22}$$

where $\widehat{\boldsymbol{Y}}_{\boldsymbol{j}}^{[i]}(\boldsymbol{F_i})$ denotes the predicted response of the j^{th} critical dimension at $\boldsymbol{F_i}$, whose preditive model is trained by all the residual samples except the i^{th} one.

Cross-validation is primarily a way of measuring the predictive performance of a statistical model. The procedure of calculating cross-validation MSE at each iteration includes (i) letting sample $\boldsymbol{i}$ form the testing data, and $\boldsymbol{Y_j^*}(\boldsymbol{F_i})$ is the oracle output of this testing sample; (ii) training the predictive model by all the residual samples except the i^{th} one at this iteration, then predict the response at $\boldsymbol{F_i}$, and next calculate the mean square error; (iii) repeat step (i) and (ii) for all samples at this iteration, and get the mean of obtained MSEs from step (ii). This mean is cross-validation MSE.

4.4.4 Comparison with Benchmark Methods

In this subsection, we compare the performance of our proposed active learning algorithms with several benchmark methods. The first benchmark method is to obtain design samples by running design of experiment for each sample size. In this method, we do not use active learning strategy. The second benchmark method is random selection from the candidate pool, which is the most basic pool-based sampling strategy. The third benchmark method is to select the next sample which has the largest maximin distance from the current samples. This method makes full use of the space filling information in the current input variables, but not utilize the information in the response. The fourth method is expected improvement (EI) approach. The EI algorithm identifies the nature of

input-output relationships, and then subsequently choose design point one at a time to maximize the expected improvement on the objective. It is widely used in sequential design, especially for computer experiments.

The evaluation criteria for these active learning methods are introduced in Section 4.4. C. Three evaluation scores, mean MAD, max MAD, and cross-validation MSE, are calculated as the increase of sample size. These Active learning curves are shown in Fig. 26-28. In the figures, the four benchmark methods are represented by a black dashed line (no active learning), a blue dash-dot line (random selection), a green solid line (selection based on maximin distance), and a magenta dotted line (EI algorithm). The proposed active learning algorithms are represented by a red solid line with asterisk marker (the proposed variance-based weighted active learning, VWAL algorithm) and a black solid line with plus-sign marker (the proposed D-optimal weighted active learning, DOWAL algorithm).

In Fig. 26-28, we can find that as the number of samples increases, the mean MAD becomes small for most of these methods. It makes sense because more samples tend to provide more information for training of predictive models. Without active learning, the learning curve have pretty large fluctuations. In Fig. 26 and Fig. 27, among all these active learning methods, the proposed VWAL algorithm realizes the best performance and it has the smallest mean MAD and max MAD when the number of samples becomes larger than 17. But the proposed DOWAL algorithm does not have a superior performance. It shows the variance-based weighted active learning algorithm is the best choice if the main objective is to realize the smallest mean or max MAD.

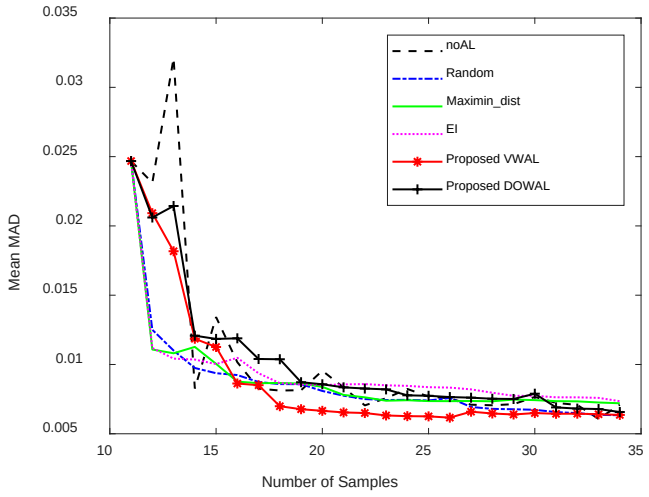

Fig. 26. Active learning curves for the mean of mean absolute deviations (MAD) of different methods

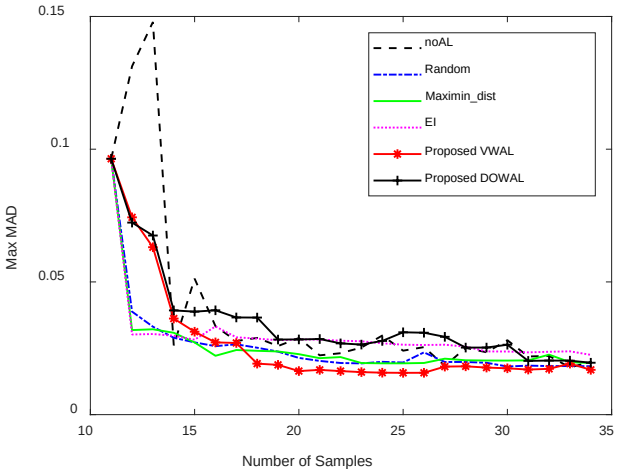

Fig. 27. Active learning curves for the maximum of mean absolute deviations (MAD) of different methods

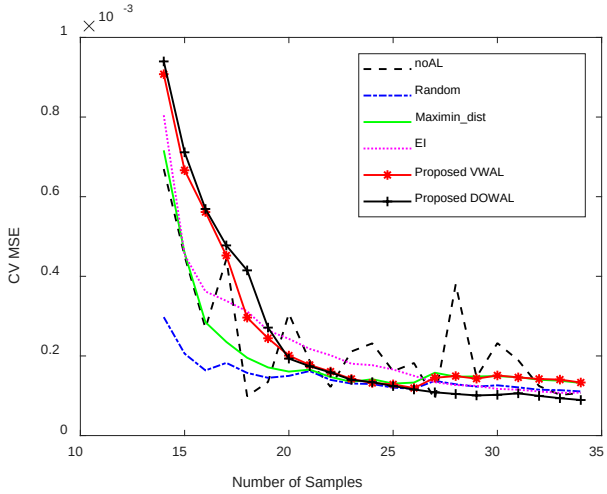

Fig. 28. Active learning curves for the cross-validation mean square errors (MSE) of different methods

If we take cross-validation MSE as the evaluation criterion, the proposed DOWAL algorithm realizes the best performance and has the smallest cross-validation MSE, as shown in Fig. 28. From Fig. 26 to 28, we can find the benchmark methods (e.g. random selection, selection based on maximin distance, and EI algorithm) can also realize good performance. The main reason is that the candidate pool is well chosen according to maximin Latin hypercube design, and the Gaussian process model considering uncertainties can capture the main information structure and response surface within the datasets.

As shown in Section 4.4.3. F, another important element of active learning application is knowing when to stop collecting new experimental samples. For specific threshold from the engineering domain knowledge, e.g., mean MAD is smaller than 0.007 inches, we know if we collect 20 experimental samples, we can train a predictive model

which has enough accuracy. This shows that active learning algorithms can not only improve the accuracy of predictive modeling, but also reduce the flow time for experimental sampling.

4.5 Summary

To realize automatic shape control of composite fuselage, it is critical to develop an accurate predictive model. However, getting an accurate model requires many experiments by obtaining dimensional shape under different actuators' forces which are expensive and time-consuming. Thus, there is an urgent need for active learning in this application to maximize information extraction with limited experimental samples. In practice, an industrial system inevitably has numerous uncertainties, such as input uncertainties, measurement errors, modeling uncertainties, uncertainties from system parameters. Current active learning approaches mainly target for classification problems or regression models without considering uncertainties. Therefore, there is a gap between existing active learning methods and the need in this kind of applications.

The main contribution of this paper is to propose two active learning algorithms for Gaussian process model considering uncertainties. The proposed algorithms investigate two predictive models with uncertainties: stochastic Kriging model and surrogate model considering uncertainty. We take two kinds of information measure, variance-based information and Fisher information, into consideration. Two active learning algorithms are proposed to obtain most informative samples for Gaussian process modeling considering uncertainties. We also explored the initial design, stopping criteria for active learning

algorithms. To validate the performance of the proposed algorithms, we introduced three evaluation criteria, including mean of mean absolute deviations (MAD), maximum of MAD, and cross-validation mean square errors. The proposed approaches are compared with four benchmark methods in the case study. It shows that the proposed variance-based weighted active learning algorithm can realize the best MAD performance, and the proposed D-optimal weighted active learning algorithm can realize the best cross-validation MSE performance. The proposed active learning algorithms can also be used to trigger the stopping point of experimental sampling. These strategies can be extended to other regression models with uncertainties.

CHAPTER 5. VIRTUAL ASSEMBLY AND RESIDUAL STRESS ANALYSIS FOR COMPOSITE FUSELAGE ASSEMBLY PROCESS

Composite parts have been widely used in the aircraft industry due to the advantages of high stiffness and high strength with light weight. Due to the difference of manufacturing suppliers and the complexity of fabrication processes, there are inevitable dimensional variabilities in composite fuselages. To improve the dimensional quality and increase the fuselage assembly productivity, a new shape control system has been developed to conduct dimensional shape adjustment before the fuselage assembly. Since actuators' forces are applied to each fuselage during the assembly, residual stresses may remain after the release of actuators. The residual stresses could lead to severe mechanical problems for the fuselage. Therefore, we propose a new finite element simulation and analysis method for evaluating the assembly process of two composite fuselages. Our method simulates the release of actuators directly instead of applying reverse forces, which mimics the assembly process and increases the simulation accuracy. The dimensional change and residual stresses during and after the assembly process are evaluated. The results show that the assembly process with new shape control system is feasible since the residual stresses resulting from the control system are smaller than the failure threshold.

5.1 Introduction

Composite parts have been increasingly used in the aircraft industry due to their advantages such as high durability, strength-to-weight ratio, and stiffness-to-weight ratio [14]. A new commercial aircraft has major structural parts made from composite materials, which consists of more than 50% by weight [16]. Since the global suppliers have a diversity of manufacturing and fabrication process, dimensional variability of composite fuselages inevitably exists. According to a report [17], there was a gap of 0.3 inches when two fuselage bodies were lined up in a major aircraft assembly process.

To reduce the dimensional variability and residual stress of the composite fuselage assembly, a new shape control system with multiple actuators has been proposed to adjust the dimension of the composite fuselage before assembly [18, 50]. As shown in Fig. 29 (a) and (b), ten actuators are located uniformly at the lower semi-circle of the fuselage. These ten actuators, which are hydraulic systems, can provide push or pull forces to change the shape of the fuselage. The new shape control system is capable of (i) computing the optimal actuators' forces to minimize the dimensional deviations of current composite parts to the ideal shape; (ii) implementing the shape adjustment automatically; and (iii) reducing the large uncertainty and inconsistency from manual operations.

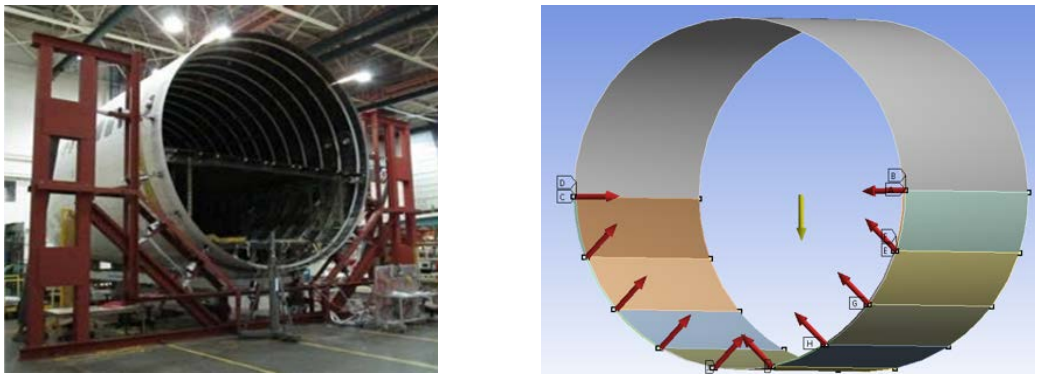

(a) The shape control system in the facility [50] (b) Schematic diagram of the shape control system

Fig. 29. Illustration of fuselage and actuator positions

During the fuselages assembly, two fuselages will be adjusted individually to the ideal shape by the shape control system. Fig. 30 shows the schematic diagram of the two fuselages that are adjusted separately by the ten actuators. After the two fuselages are aligned to the ideal shape, they are assembled by the riveting process. Next, the actuators applied on the two fuselages will be released, which will cause the springback of the fuselages and the occurrence of residual stress. Large residual stress may hurt the part as well as generate other severe side effects (e.g., fatigue, stress corrosion cracking and structural instability). Therefore, it is important to develop an effective platform and associated methods to evaluate the residual stress during and after the assembly process when the shape control system is implemented.

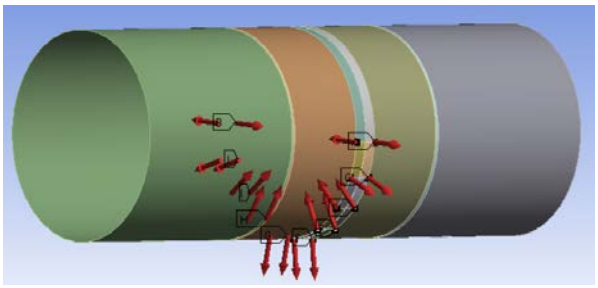

Fig. 30 Schematic diagram of the fuselages' adjustments before assembly

In the literature, Stewart [77] used piecewise-linear elastic analysis to evaluate the residual stress in assembly fixtures. Abdelal [78] developed a nonlinear explicit finite element model to simulate the riveting process of a small panel and evaluate the deformation as well as the residual stress. These papers focused on the assembly of isotropic metal parts, which could not be directly applied to the composite parts assembly due to their anisotropic properties. For the assembly process of composite parts, Dong and Kang [1] proposed a response surface model and analyzed the relationship between part variation and assembly stress by using a finite element model. Zhang and Shi built a stream of variation model for prediction and control of dimensional variations of composite part assembly in single-station [2] and multi-station processes [3]. In their model, different sources of variabilities such as composite part manufacturing errors, fixture position errors, and relocation-induced errors were considered for analyzing dimensional variation and its propagation. Gómez et al. proposed a supporting model and ad-hoc software for the decision-making process during the conceptual design of aircraft final assembly lines [4]. The literature gave a general framework of dimensional variation modeling of the composite parts assembly process and conceptual design of aircraft assembly line.

However, these methods cannot be applied to our proposed shape control system due to the complexity of the fuselage structure, actuator design, as well as support structure placement.

Residual stress test based on physical experiments is not practical for the preliminary step of new technology development due to the high cost and time. Thus, we develop a finite element model to mimic the assembly process of two composite fuselages. In order to realize the dimensional uncertainties, fuselages with different initial shapes are simulated. After that, the stresses during and after the adjustment process are evaluated, and failure tests are conducted via simulation.

The remainder of this paper is organized as follows. Section 5.2 introduces the detailed procedure of the finite element modeling of the composite fuselage assembly process, which includes generation of initial deformed fuselages, automatic shape adjustment, joining process, and release of the actuators. Section 5.3 shows the dimensional deformation analysis and residual stress analysis for the composite fuselage assembly process. Section 5.4 provides a summary of the work.

5.2 Composite Fuselage Assembly Simulation via Finite Element Analysis

This section provides a detailed finite element modeling procedure for the composite fuselage assembly process. The finite element analysis (FEA) model is developed by using the Ansys composite PrepPost workbench [45]. Figure 31 shows the flowchart of the assembly process, which has five major steps: (i) generate two fuselages with the design

shape (ideal shape); (ii) introduce the manufacturing deviations to the design shape and use the new shapes as their initial shapes; (iii) calculate and apply the actuators' forces needed to adjust the two fuselages to the target shape by using the Automatic Optimal Shape Control (AOSC) system [18]; (iv) add contact structure to bond the edge of the two fuselages; and (v) release the actuators' forces and the two fuselages will spring back to the final shape simultaneously.

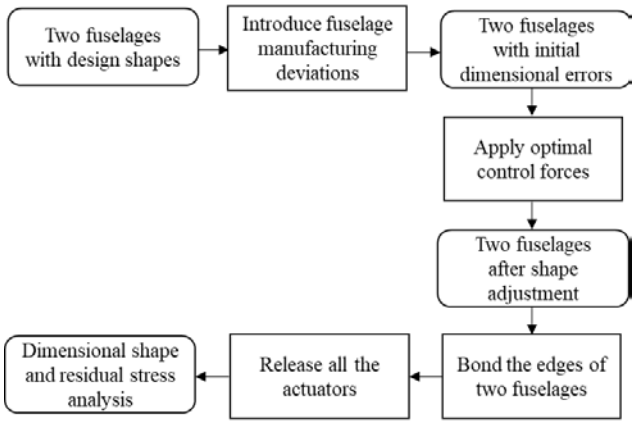

Fig. 31. The flowchart for the fuselage assembly process

5.2.1 Generation of Initial Deformation of Fuselages

Before conducting the shape control and fuselage assembly, the incoming fuselages should have some inherent dimensional deviations, or initial deformations. Thus, we need to use simulation tools to generate initial shapes of the fuselages, which realize the fuselage deformations that are close to the real fuselage in the plant. Because a fuselage has its inherent design structure and stress, it is not reasonable to randomly generate the shape of the fuselage. In our simulation, we use the actuators to push and pull an ideal shape of the

fuselage to get different dimensions of fuselages. The magnitude and direction of the actuators' forces are assigned accord to engineering knowledge. As shown in Fig. 32, eighteen forces are applied to the edge of each fuselage to generate deformed fuselages that are close to the real fuselages.

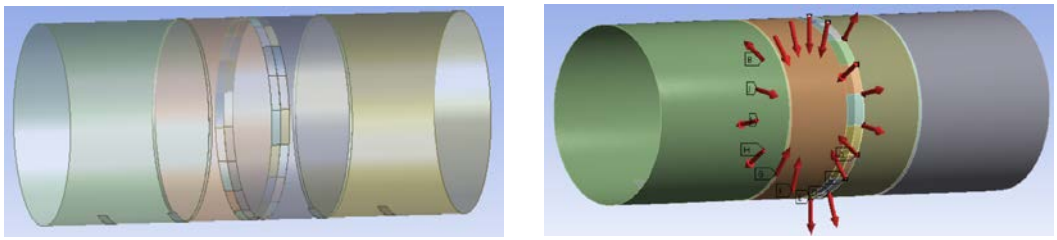

(a) The geometry of fuselage assembly (b) Force allocation for initial deformation generation

Fig. 32 Eighteen actuators and their locations for initial deformation generation

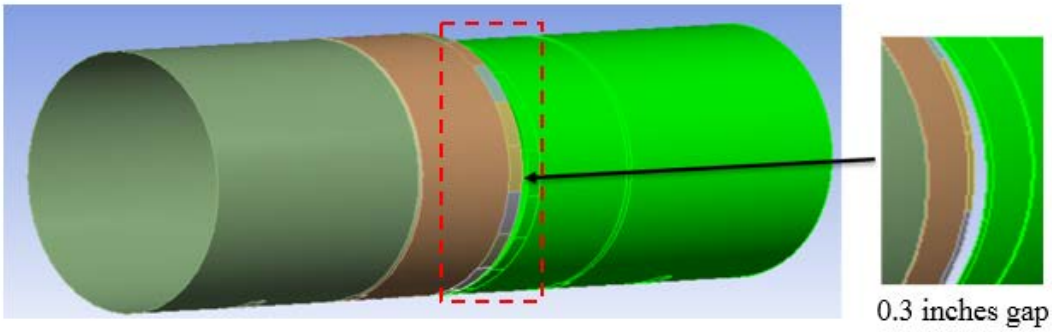

Fig. 33. Fuselage with different initial shapes

After obtaining two fuselages with different initial dimensions, they will be used in the shape control during the fuselage assembly process. The largest gap between two fuselages ranges from 0.1 inches to 1 inch depending on how large the actuators' forces are, which

covers the 0.3 inches gap reported from literature [17]. The generation of initial deformation of the fuselages is illustrated in Fig. 33.

5.2.2 Adjustment of Fuselages to Target Shape via AOSC System

In an AOSC system, a set of actuators are uniformly located at the bottom half of the fuselage. The optimal forces for the actuators are calculated to change the two fuselages shapes to the target nominal shape. A surrogate model is developed with the consideration of uncertainties [5], which has the format as

$$Y_{ij}(\boldsymbol{F}_t) = \boldsymbol{F}_t\boldsymbol{S}_j + \boldsymbol{F}_t\tilde{\boldsymbol{S}}_j + \widetilde{\boldsymbol{F}}_t\boldsymbol{S}_j + z_j(\boldsymbol{F}_t) + \varepsilon_{ij}(\boldsymbol{F}_t), \tag{23}$$

where $i = 1,2,\dots,n_t$; $j = 1,2,\dots,p$; n_t is the number of simulation replications; p is the number of nodes at the edge of fuselage. $\boldsymbol{F}_t$ is the actuators' forces; $\widetilde{\boldsymbol{F}}_t$ is the additional random deviation vector of actuators' forces, that is relevant to the tolerance of the actuator; $\boldsymbol{S}_j$ is the sensitivity matrix and $\tilde{\boldsymbol{S}}_j$ represents the sensitivity variability from the part uncertainty. $\boldsymbol{z}_j(\boldsymbol{F}_t)$ is a zero mean Gaussian process and $\varepsilon_{ij}(\boldsymbol{F}_t)$ is assumed to follow an independent normal distribution $\varepsilon_{ij}(\boldsymbol{F}_t) \sim \mathbb{N}(0,\ \sigma^2_{\varepsilon j}(\boldsymbol{F}_t))$.

The training datasets and testing datasets are generated according to the same material property, dimensions of the fuselage and support structures used in the real assembly process; we use the obtained surrogate model in [5] with the feed-forward control algorithm. The objective function of the feed-forward control is

$$\min_{\boldsymbol{F}} \boldsymbol{J} = (\boldsymbol{Y_c} + \widehat{\boldsymbol{Y}}(\boldsymbol{F}) - \boldsymbol{Y}^*)^{\boldsymbol{T}}\boldsymbol{W}(\boldsymbol{Y_c} + \widehat{\boldsymbol{Y}}(\boldsymbol{F}) - \boldsymbol{Y}^*) \tag{24}$$

$$s.t. \qquad \boldsymbol{F_L} \preccurlyeq \boldsymbol{F} \preccurlyeq \boldsymbol{F_U}$$

where $\boldsymbol{Y_c}$ is a dimensional vector of the current fuselage; $\widehat{\boldsymbol{Y}}(\boldsymbol{F})$ is the predicted dimensional deviation vector; $\boldsymbol{Y}^*$ is the designed target dimensional vector; $\boldsymbol{W}$ is the weighting coefficients; $\boldsymbol{F_L}$ and $\boldsymbol{F_U}$ are the lower and upper bound of actuators' force. The optimized actuators' forces $\boldsymbol{F}$ will be used to adjust the fuselage to the nominal shape.

5.2.3 Joining of Two Fuselages

After the adjustment step, the two fuselages will have the same shape at the edge with different actuator forces applied. The next step is to assemble the two fuselages via riveting joins. Riveting is a forging process that can be applied to assemble different parts together by a metal part named rivet. The rivet is able to join the two parts through adjacent surfaces. In order to mimic the riveting joining process with two composite fuselages, we used bonded structures from Ansys composite workbench to limit the deformation of the edges of two fuselages, which is shown in Fig .34. Since the fuselage is virtually divided into several segments at the edge, we bonded each pair of edges for both fuselages, as shown in Fig. 34. The bonded structures restrict the two fuselages to deform simultaneously on the edge after we release the applied actuator forces.

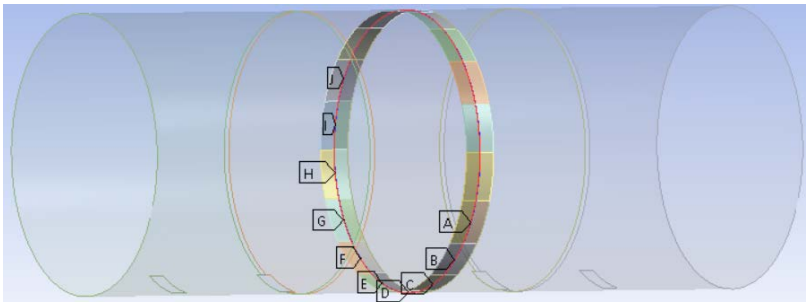

Fig. 34 Bonded structure of the riveting joins

5.2.4 Release of the Actuators

When the two fuselages are joined, the actuators' forces applied on the two fuselages still remain. Hence the last step of the simulation is to release the actuators, which means that the actuators' forces are reduced from the target values to zero during this period. In literature, the common method to simulate the release of the actuators is to apply the reverse force at the positions where the actuators are applied [2, 79]. In this paper, a new method is proposed to simulate the application and release of fuselage actuator forces by using dynamic force curve.

In literature [2, 79], a three-step method is used to simulate the assembly process. The first step is to apply the static actuator forces to adjust the two parts to achieve the same shape; the second step is to join these parts via riveting process; and the last step is to apply the reverse forces in step one, which is considered as the releasing forces of the springback effect. An example to illustrate the reverse force method is shown in Fig. 35. In Fig. 35(a), one actuator is used to pull the right fuselage at +500 pounds. Then a -500 pound force is applied to push the right fuselage back to nominal. Next, the two fuselages are bonded and +500 pound force is applied as reverse force, which results in the spring back of two fuselages. The residual stresses after the spring back are shown in Fig. 35(b). The maximum stress is near the actuator location, and the residual stresses around the actuator are very large, which is shown in Fig. 35(c). The results show that the residual stresses are mainly caused by the reverse force, which does not make sense. the residual

stresses should result from the mixed effects of the releasing forces, bonded structures as well as support structures.

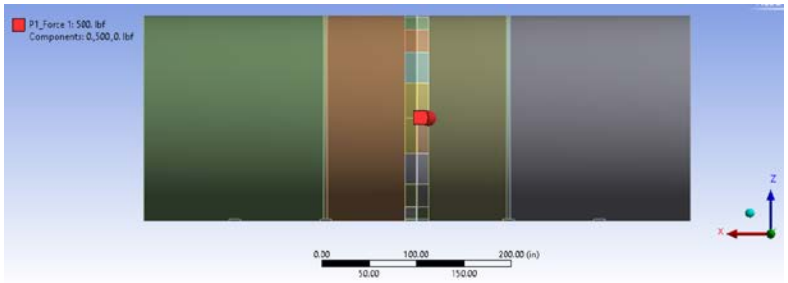

(a) One actuator is used to pull the right fuselage at 500 pounds

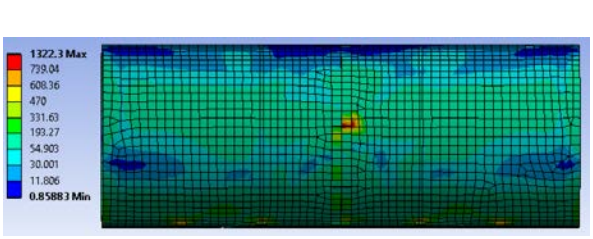

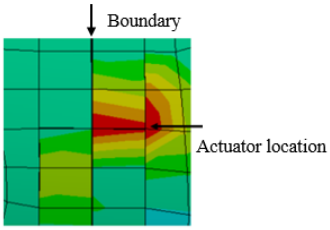

(b) -500 pound force is applied to push the right fuselage back (c) Residual stress near the actuator

Fig. 35 Simulation of the assembly process via the three-step method

To improve the simulation accuracy, we propose an improved approach which is named after dynamic force curve method. In Ansys, the force can be constant, tabular, or functional. Hence the application of actuator's force is equivalent to the increase of force from zero to target value. The release of actuator's forces can be considered as the decrease of force from the target value to zero. As shown in Fig. 36 (a), the x-axis is the time stamp,

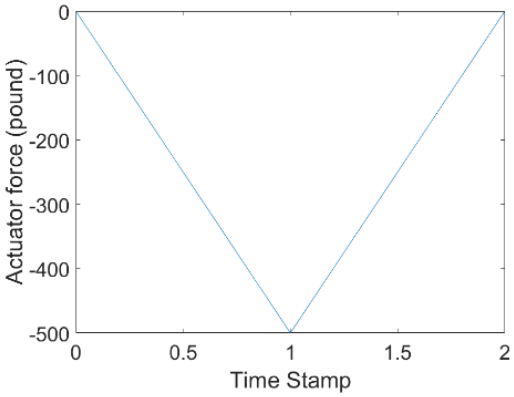

(a) Dynamic force curve for the actuator

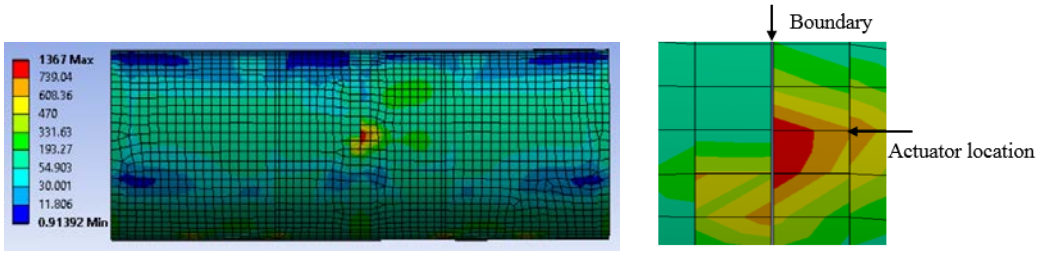

(b) Residual stress after the joining process (c) Residual stress near the actuator location

Fig. 36 Simulation of the assembly process via the dynamic force curve method

and the y-axis is the force in pound. From time stamp 0 to 1, the actuators' force decreases from zero to -500 pounds, which is the adjustment step discussed in subsection 5.2.2. At time stamp 1, the bond structures are added, which is the joining step discussed in subsection 5.2.3. From time stamp 1 to 2, the actuator force increases from -500 pounds to zero, which is the release step discussed in subsection 5.2.4. The use of dynamic force curve integrates the three steps into one simulation via element birth and death for contact elements. The residual stress by using the dynamic force curve method is shown in Fig. 36 (b) and (c). The major difference between Fig. 35 (c) and Fig. 36 (c) is the location of high

stresses. In Fig. 35 (c), the high residual stresses can be found around the actuator location. In Fig. 36 (c), however, the high residual stresses occur around the boundary of two fuselages. The dynamic force curve method is more accurate because the right fuselage will spring back after the actuator is released in reality. However, the left fuselage is bonded with the right fuselage, and as a result, residual stresses occur at the boundary area of both fuselages in really.

5.3 Dimensional Deformation and Residual Stress Analysis

5.3.1 Simulation Configurations

In this simulation study, two composite fuselages are assembled with actuator forces applied, which is illustrated in Fig. 30. Each fuselage has a length of 24 feet and a diameter of 18 feet. The thickness of each fuselage is 0.295 inch. The ply design follows the fabrication of composite fuselage, and the detailed information about the material properties can be found in [50]. The initial gap between two fuselages is about 0.3 inches. We use Latin Hypercube design to create 20 different initial shapes for individual fuselages. The maximum force in the design is 500 pounds. For example, by using the actuators' forces shown in Fig. 32 (b), the initial total deformation for the two fuselages is shown in Fig. 37 (a) and the deformation at the edge is shown in Fig. 37 (b) and (c) for those two fuselages respectively. The deformation at the edge in Fig. 37 (b) and (c) is viewed from negative X direction. At the right top corner of each fuselage, the left fuselage deforms toward left about 0.2 inches while the right one deforms toward right about 1 inch, which introduces a gap of more than 1 inch. The goal is to use the finite element model

developed in section 5.2 to simulate the assembly process of those two fuselages and estimate the deformation and stress during the process. For illustration purpose, the following figures show the simulation results based on the initial shape design in Fig. 32 (b).

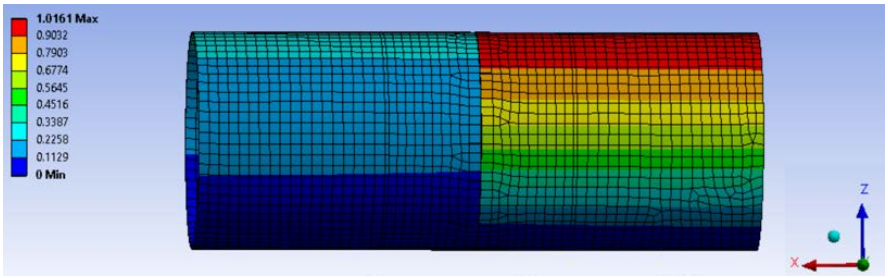

(a) Two fuselages to be assembled

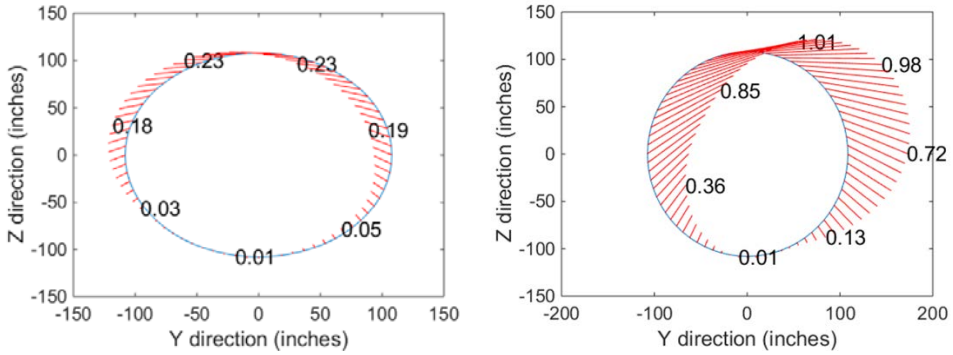

(b) Dimensional deviation of the left fuselage (c) Dimensional deviation of the right fuselage

Fig. 37 Initial deformations of both fuselages

5.3.2 Simulation Result

5.3.2.1 Dimensional Variation between Adjusted Shape and Target Shape

During the shape control of fuselages, the ten actuators' forces at each fuselage are calculated using the model provided in section 5.2.2. Fig. 38 shows the deformation of two fuselages after the actuators' forces are applied. The total deformation during shape adjustment in Fig. 38 (a) is similar to the initial total deformation in Fig. 37 (a), but in a negative direction. Fig. 38 (b) shows the deformation at the edge of left fuselage after the actuators' forces are applied. At each node, the deformation ought to have a similar number but in the opposite direction to the node in Fig. 9 (b). Fig. 38 (c) shows the control error of the left fuselage. The average error is 0.0056 inches. Fig. 38 (d) and (e) illustrate the deformation and control error at the edge of the right fuselage. The average error is 0.0009 inches.

To ensure that the two fuselages are adjusted to the same target shape, the control errors between the 40 adjusted shapes and the target shape at each node are calculated. Fig. 39 (a) shows the box plot of the control error at each node. 91 nodes are collected at the edge of a fuselage. One node is selected for illustration from every four adjacent nodes. Thus, the control errors of the 40 adjusted shapes at 23 selected nodes are shown, and the locations of the nodes are shown in Fig. 39 (b). Nodes located at the bottom of the semi-

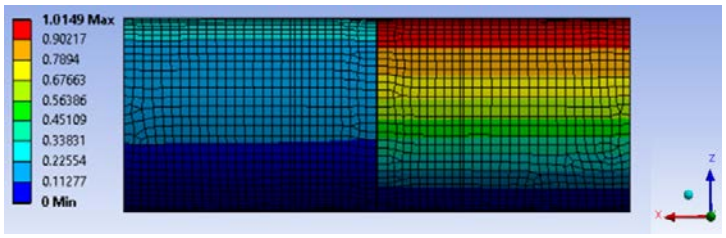

(a) Deformation after actuators' forces applied

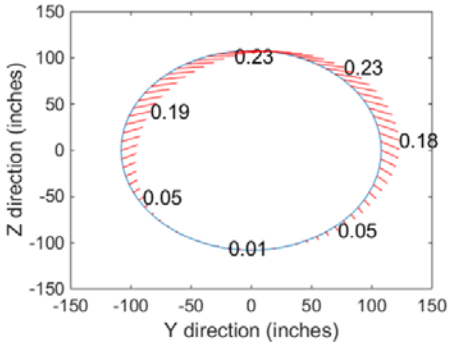

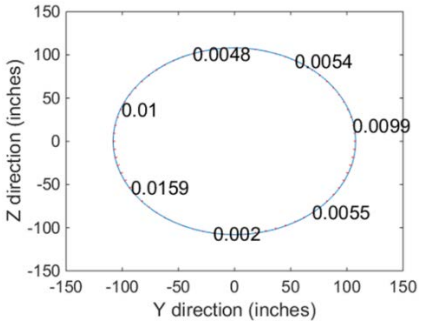

(b) Deformation at the edge of left fuselage (c) Control error at the edge of left fuselage

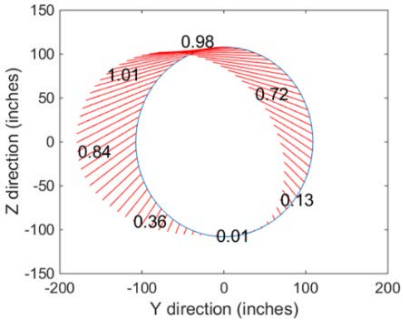

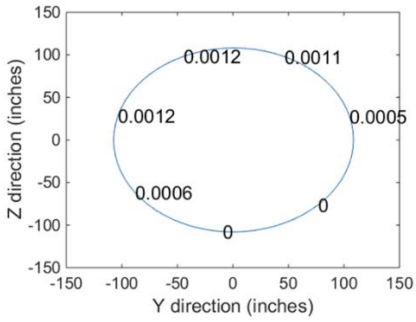

(d) Deformation at the edge of the right fuselage (e) Control error at the edge of the right fuselage

Fig. 38 Initial deformations and adjustment error after adjustments

fuselage have better control accuracy compared with the top ones, which makes sense because the actuators are installed in the lower semi-fuselage. The average control error is 0.002 inches, which is lower than the 1% of the 0.3 inches gap in average.

Therefore, the shape control system is adequate to change the initial shape of two fuselages to the target shape.

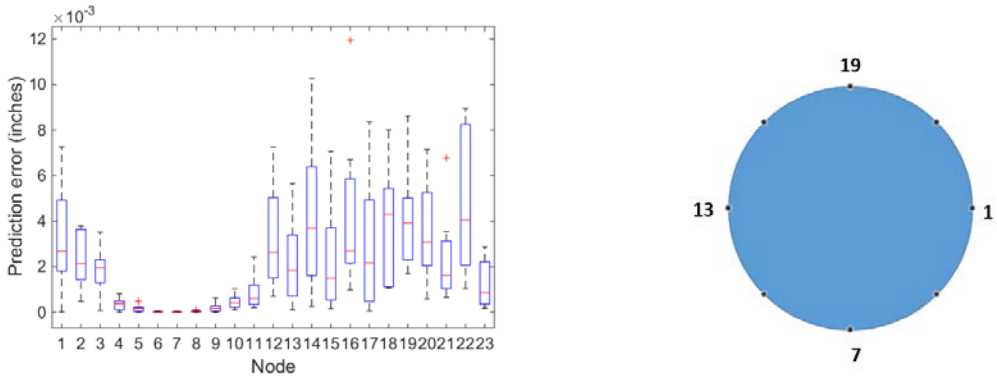

(a) Control errors box plot (b) Location of node

Fig. 39 Performance of the shape adjustments

5.3.2.2 Deformation During and After the Assembly Process

During the shape control of those two fuselages, the deformation after the actuators' forces applied is shown in Fig. 38 (a). The maximum deformation is 1.015 inches. Then the two fuselages will have the same target shape and be bonded together at the edge. After that, the actuators' forces will be released and the deformation after the springback of two fuselages is shown in Fig. 40. Although the two fuselages have similar deformation in magnitude at adjacent locations, the directions of the deformation are not the same. As shown in Fig. 40 (b), the left fuselage deforms towards –z direction in the middle while the right fuselage deforms towards +z direction. The maximum deformation after the two fuselages spring back is 0.625 inches, which is lower than the maximum deformation after the actuators' forces applied.

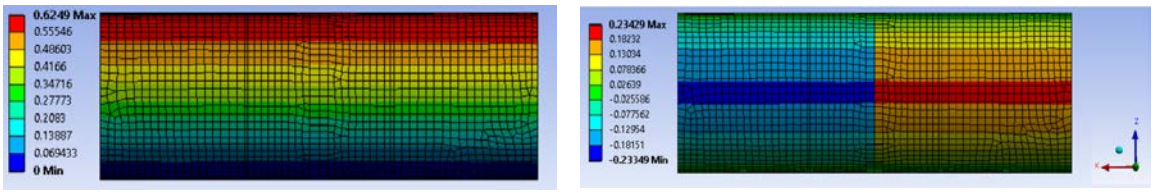

(a) Total deformation (b) Z directional deformation

Fig. 40 Deformation of both fuselages from initial the shapes to the shapes after springback

5.3.2.3 Stress During and After the Assembly Process

The stress during and after assembly is the key metric that engineers attach importance to since it reflects whether the composite fuselage will be hurt during the assembly process. For the shape control step, the stresses caused by actuators are shown in Fig. 41 (a). The maximum stress is 1192.4 psi, which is located at the bottom support structure of the right fuselage. After the joining process, the two fuselages cannot spring back to their original shapes. Hence the residual stresses remain after the release of actuators, which is shown in Fig 41 (b). The maximum residual stress is 739.04 inches, and it is also located at the bottom support structure of the right fuselage.

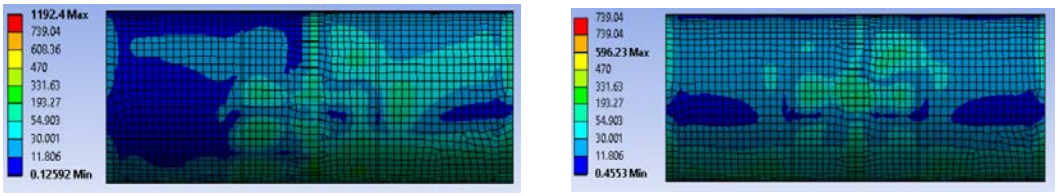

(a) Stresses after the actuators' forces applied (b) Stress after the release of actuators

Fig. 41 Stresses distribution of both fuselages

5.3.2.4 Stress Analysis and Failure Test

One practical concern is whether the implementation of the shape control system in the assembly process will introduce very large stress that damages the fuselage. Through the simulation of 20 pairs of fuselages assembly, the maximum stress during and after the assembly is less than 3000 psi; and the maximum stress mostly occurs in the support area of fixtures. The residual stress at the assembly edge is even smaller. The maximum residual stress from shape control and assembly process is much smaller than the failure threshold. Stress test under Tsai–Wu failure criteria is also conducted [14]. Among all the experiments, the largest inverse reserve factor, which calculates the inverse margin to failure, is 0.19. It is much lower than the threshold at 1.00. Therefore, it is safe to conduct the automatic shape control and assembly for the composite fuselages.

5.3.3 Discussion

5.3.3.1 Location of Maximum Stress

Among the 20 pairs of fuselages assembly simulations, 7 cases have the maximum stress located at the node where an actuator force is applied. The rest 13 have the maximum stress located at the support structure area. Residual stress for one pair of fuselages assembly is shown in Fig. 42. The fuselages are viewed from the bottom in the figure. Therefore, stress test in the factory should have higher priority at the edge of the fuselage where actuators are applied, as well as the support structure area during the assembly.

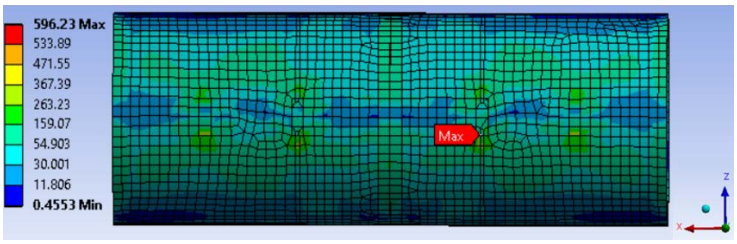

Fig. 42 Location of maximum stress after assembly

5.3.3.2 Relation between Maximum Deformation and Maximum Stress

Through the experiments, the pair of fuselages with larger maximum deformation is not always generating larger maximum stress. The residual stress is affected by mixtures of factors, including the release of actuators' forces, the bonded structures, and the support structures. Those factors and their combined effects will generate different fuselage deformations and stress patterns. For example, the maximum residual stress in Fig. 41 is 739.04 psi while the one in Fig. 42 is 596.23 psi. However, the maximum deformation for the pair of fuselages in Fig. 41 is 0.625 inches while the one for the pair of fuselages in Fig. 42 is 0.701 inches.

5.4 Summary

Composite parts have been increasingly used in the aircraft industry due to their superior properties. Dimensional variability of fuselage is an important problem due to the diverse sources of manufacturing suppliers and the complex fabrication process. A new shape control system with actuators has been developed to adjust the shape of fuselage during the assembly. In such a system, residual stress exists in the fuselages after the release

of actuators during the assembly. Thus, modeling and analysis of the residual stress are very important to avoid severe mechanical problems for the fuselage assembly and usage. In this paper, a new finite element simulation is developed to realize the virtual assembly of two composite fuselages with actuators' forces applied. We utilize the AOSC system [18] to conduct the shape adjustment. For the assembly process, a new dynamic force curve approach is proposed to simulate the springback effect after the assembly. The actuator force during the assembly is dynamically applied, which means that it increases from zero to the target value during assembly and reduces from the target value to zero after the two fuselages are bonded. It is more accurate than the traditional three-step approach that is using reversed force to realize the springback. Our proposed simulation can estimate the deformations and stresses of the two fuselages during the entire assembly process, including the adjustments of two initial fuselages, the bond of the adjusted fuselages, and the release of actuators. The simulation result indicates that the new shape control system with actuators' forces is effective in the fuselage assembly, which achieves high assembly accuracy. Meanwhile, the residual stresses generated from the shape control and the assembly process is much smaller than the threshold.

CHAPTER 6. SUMMARY AND FUTURE WORK

6.1 Summary of Original Contributions

This thesis contributes to the area of System Informatics and Control by developing innovative and effective methodologies for engineering driven data analytics in advanced manufacturing. Specifically, this research has interdisciplinary nature that integrates techniques in advanced statistics, mechanical engineering and material science. The proposed methodologies mainly focus on developing FEA platforms, surrogate modeling, and predictive control for composite fuselage assembly. The original contributions of the dissertation include the following aspects:

1. *A novel finite element simulation platform was developed to mimic the fuselage shape control and to visualize the adjustment of composite fuselage assembly process*. The finite element simulation is built based on the Ansys PrePost Composite Workbench. It follows the process of composite part manufacturing and the parameters are tuned via calibrations. The FEA platform is validated with physical experiments with real fuselage conducted from the plant. The development of this FEA platform makes it feasible in simulation of fuselage shape control and assembly as well as performance evaluation of the assembly precision, deformation, and residual stresses.
2. *A surrogate model consider uncertainties is proposed and integrated into a feed-forward shape control system to realize automatic shape control of composite*

fuselage. Actuator uncertainty, part uncertainty, modeling uncertainty, and unquantified uncertainty are considered to link the relationship between actuators' forces (e.g. inputs of the system) and dimensional deviations (e.g. outputs of the system) of composite fuselages. A feed-forward control law is obtained by solving the optimization problem that minimizes the weighted sum of square of dimensional deviations between the real dimensional positions and the designed positions of the part. The AOSC system we developed achieves ultra-high precision in fuselage shape control to meet the dimensional error specification required in fuselage assembly.

3. *Two active learning algorithms are developed to realize better prediction performance of the stochastic model with uncertainties when the training samples are limited.* The existing active learning methods do not incorporate the uncertainties for Gaussian process. Therefore, we propose two new active learning algorithms for the Gaussian process with uncertainties, which are variance-based weighted active learning algorithm and D-optimal weighted active learning algorithm. Our algorithms have better predictive accuracy when compared with random selection, selection based on maximin distance, and EI algorithm. The algorithms help to reduce the number of experiments needed for training the surrogate model, which saves time and cost for the automatic shape control of composite fuselage and its assembly.
4. *An FEA platform of automatically fuselage virtual assembly via AOSC system is developed to visualize and evaluate the entire fuselage assembly process.* The

ultimate goal for the AOSC system is to assemble two fuselages together with a high dimensional precision and minimum residual stresses. Therefore, a framework of the assembly is proposed to virtually assemble the two fuselages with the AOSC system applied and provide real-time evaluations of part deformation and residual stresses. In addition, a novel FEA platform with the application of dynamic forces is developed to accurately simulate the springback of fuselages after releasing the actuators' forces.

6.2 Future Research

There are several important topics to be explored for further development of shape control and dimensional variation reduction in the composite fuselage industry.

With the successful development of single fuselage shape control, it is important and challenging to extend the shape control to multi-station fuselage assemblies. The previous assemblies may have impacts on the later assemblies through variation propagation. How to extend the stream of variation modeling and analysis theory for automotive manufacturing to the composite fuselage assembly is of great interest and need.

In chapter 2 and chapter 5, we have developed FEA platforms to simulate the residual stresses after the shape control and the assembly. The future research should focus on systematical method to predict residual stress without the need of simulation to realize in-situ stress prediction and feasibility analysis.

The third research potential is the residual stress optimization. Our previous models focus on dimensional error optimization. After achieving an ultra-high precision of the predictive model, it is also of high importance to minimize the residual stress after assembly to increase the product life and reduce life-cycle cost of the composite fuselage. We have shown that different locations of fixtures and support structures have large influence on the residual stress after assembly. An optimal fixture placement strategy needs further investigation.

REFERENCES

[1] Dong, C. and Kang, L., 2012, "Deformation and stress of a composite–metal assembly," *The International Journal of Advanced Manufacturing Technology*, 61(9), pp.1035-1042.

[2] Zhang, T., and Shi, J., 2016, "Stream of Variation Modeling and Analysis for Compliant Composite Part Assembly—Part I: Single-Station Processes," *ASME. J. Manuf. Sci. Eng.*, 138(12), pp. 121003-121003-15. doi:10.1115/1.4033231.

[3] Zhang, T., and Shi, J., 2016, "Stream of Variation Modeling and Analysis for Compliant Composite Part Assembly— Part II: Multistation Processes," *ASME. J. Manuf. Sci. Eng., 138(12)*, pp. 121004-121004-15. doi:10.1115/1.4033282.

[4] Gómez, A., Ríos, J., Mas, F. and Vizán, A., 2016, "Method and software application to assist in the conceptual design of aircraft final assembly lines," *Journal of Manufacturing Systems*, 40, pp.37-53.

[5] Djurdjanovic, D. and Ni, J., 2001, "Linear State Space Modeling of Dimensional Machining Errors," *NAMRI/SME Trans.*, Vol. 29, pp. 541-548.

[6] Djurdjanovic, D. and Ni, J, 2003, "Dimensional Errors of Fixtures, Locating and Measurement Datum Features in the Stream of Variation Modeling in Machining," *ASME. J. Manuf. Sci. Eng.*,Vol. 125, pp. 716-730.

[7] Camelio, J., Hu, S., and Ceglarek, D., 2004, "Modeling Variation Propagation of Multi-Station Assembly Systems With Compliant Parts," *ASME. J. Mech. Des.*, 125(4), pp. 673-681. doi:10.1115/1.1631574.

[8] Liu, S., and Hu, S., 1997, "Variation Simulation for Deformable Sheet Metal Assemblies Using Finite Element Methods," *ASME. J. Manuf. Sci. Eng.*, 119(3), pp. 368-374. doi:10.1115/1.2831115.

[9] Zhou, K., Doyle, J. C., and Glover, K., 1996, "Robust and optimal control," *New Jersey: Prentice hall*. ISBN: 0-13-456567-3.

[10] Hansen, L. P., and Sargent, T. J., 2001, “Robust control and model uncertainty,” *The American Economic Review*, 91(2), 60-66.

[11] Uusitalo, L., Lehikoinen, A., Helle, I., and Myrberg, K., 2015, “An overview of methods to evaluate uncertainty of deterministic models in decision support,” *Environmental Modelling and Software*, 63, 24-31.

[12] Draper, D., 1995, “Assessment and propagation of model uncertainty,” J. *of the Royal Stat. Society*, Series B, 45-97.

[13] Ayyub, B. M., and Klir, G. J., 2006, *Uncertainty modeling and analysis in engineering and the sciences*. CRC Press. ISBN: 1-58-488644-7.

[14] Jones, R. M., 1998, *Mechanics of Composite Materials*, CRC press, Boca Raton, USA, ISBN: 1-56032-712-X.

[15] United States Department of Transportation, 2012, *Administration Federal Aviation, Aviation Maintenance Technician Handbook* – Airframe, chapter 7, Advanced Composite Materials, pp 1-57.

[16] Chawla, K. K., 2012, *Composite Materials: Science and Engineering, Springer Science & Business Media*, New York, USA, Chap. 5, ISBN: 978-0-387-74364-6.

[17] Gates, D., 2007, "Boeing Finds 787 Pieces Aren’t Quite A Perfect Fit," *Seattle Times aerospace report*, Seattle Times.

[18] Yue, X., Wen, Y., Hunt, J. H., and Shi, J., 2018, "Surrogate Model-Based Control Considering Uncertainties for Composite Fuselage Assembly," *ASME Transactions, Journal of Manufacturing Science and Engineering*, vol. 140, No. 4: 041017.

[19] Pinkerton, J.L. and Moses, R.W., 1997, "A feasibility study to control airfoil shape using THUNDER," NASA Technical Report.

[20] Sofla, A.Y.N., Meguid, S.A., Tan, K.T. and Yeo, W.K., 2010, "Shape morphing of aircraft wing: status and challenges," *Materials & Design*, 31(3), pp. 1284-1292.

[21] Sodano, H.A., Park, G. and Inman, D.J., 2004, "An investigation into the performance of macro-fiber composites for sensing and structural vibration applications," *Mechanical systems and signal processing*, 18(3), pp.683-697.

[22] Barbero, E.J., 2013, *Finite element analysis of composite materials using ANSYS*. CRC press.

[23] ANSYS, 2013, "ANSYS Composite PrepPost User's Guide," https://support.ansys.com/staticassets/ANSYS/Conference/Irvine/downloads/.

[24] ANSYS, 2016, "ANSYS Engineering Data Sources," Composite Materials.

[25] Wang, Y., Yue, X., Tuo, R., Hunt, J. H., and Shi, J., 2018, "Effective Model Calibration via Sensible Variable Identification and Adjustment, with application to Composite Fuselage Simulation," Technical Report

[26] Jin, J., and Shi, J., 1999, "State Space Modeling of Sheet Metal Assembly for Dimensional Control," *ASME. J. Manuf. Sci. Eng.*, 121(4), pp. 756-762. doi:10.1115/1.2833137.

[27] Shi, J.,2006, *Stream Of Variation Modeling And Analysis For Multistage Manufacturing Processes*, CRC Press, Boca Raton, USA, ISBN: 0-8493-2151-4.

[28] Li Z, Zhou S., 2005, "Robust Method of Multiple Variation Sources Identification in Manufacturing Processes For Quality Improvement," *ASME. J. Manuf. Sci. Eng.*, 128(1):326-336. doi:10.1115/1.2117447.

[29] Zhang, B., Ni, J., 2003, "Adaptive Product Process and Tooling Design Strategy for Optimal Dimensional Quality of Automotive Body Assemblies," *ASME. J. Manuf. Sci. Eng*, 125(4):835-843. doi:10.1115/1.1616946.

[30] Abad, AG., Paynabar, K., Jin, J., 2011, "Modeling and Analysis of Operator Effects on Process Quality and Throughput in Mixed Model Assembly Systems," *ASME. J. Manuf. Sci. Eng.*, 133(2):021016-021016-9. doi:10.1115/1.4003793.

[31] Camelio, JA., Hu, S., Marin, SP., 2004, "Compliant Assembly Variation Analysis Using Component Geometric Covariance", *ASME. J. Manuf. Sci. Eng.*, 126(2):355-360. doi:10.1115/1.1644553.

[32] Zhong, J., Liu, J. A., and Shi, J. J., 2010, "Predictive Control Considering Model Uncertainty for Variation Reduction in Multistage Assembly Processes," *IEEE Trans. Autom. Sci. Eng.*, vol. 7, pp. 724-735.

[33] Djurdjanovic, D., and Ni, J., 2007, "Online stochastic control of dimensional quality in multistation manufacturing systems," *J. of Eng. Manuf.*, 221(5), pp. 865-880.

[34] Åström, K. J., and Wittenmark, B., 2013, *Adaptive control.* Prentice Hall, Upper Saddle River, NJ, ISBN: 978-0-20155-866-1.

[35] Basar T. and Bernhard P., 1995, H-*Infinity Optimal Control and Related Minimax Design Problems: A Dynamic Game Approach*, 2nd ed. Boston, MA: Birkhäuser. ISBN: 978-0-8176-4757-5.

[36] Tanaka K. and Sugeno M., 1992, “Stability analysis and design of fuzzy control systems,” *Fuzzy Sets and Systems*, vol. 45, no. 2, pp. 135–156.

[37] Jones, R. M., 1998, *Mechanics of Composite Materials*, CRC press, Boca Raton, USA, ISBN: 1-56032-712-X.

[38] Neter, J., Kutner, M. H., Nachtsheim, C. J., and Wasserman,W., 1996, *Applied Linear Statistical Models*, vol. 4, the McGraw-Hill Company, New York, USA, ISBN: 978-0-07301-344-2.

[39] Santner, T. J., Williams, B. J., and Notz, W. I., 2003, *The Design And Analysis of Computer Experiments*, Springer Science & Business Media, New York, USA, ISBN: 978-0-387-95420-2.

[40] Ankenman, B., Nelson, B. L., and Staum, J., 2010, "Stochastic Kriging For Simulation Metamodeling," *Operations research*, vol. 58, pp. 371-382.

[41] Stein, M. L., 1999, *Interpolation Of Spatial Data: Some Theory For Kriging*, Springer Science & Business Media, USA. ISBN 978-1-4612-1494-6.

[42] A. M. T. Handbook-Airframe, 2012, "United States Department of Transportation," *Federal Aviation Administration*, Oklahoma City, OK, pp. 13-22.

[43] Izquierdo, L. E., Shi, J., Hu, S. J., and Wampler, C. W., 2007, "Feedforward Control Of Multistage Assembly Processes Using Programmable Tooling," *Trans. NAMRI/SME*, vol. 35, pp. 295-302.

[44] Boyd, S., and Vandenberghe, L., 2004, *Convex Optimization*, Cambridge University Press, USA, ISBN: 9780521833783.

[45] ANSYS, 2015, "ANSYS Composite PrepPost User's Guide 17.0," https://support.ansys.com/staticassets/ANSYS/Conference/Irvine/downloads/.

[46] Settles, B., 2012, "Active learning," *Synthesis Lectures on Artificial Intelligence and Machine Learning*, vol. 6, no. 1, pp. 1-114.

[47] Lam. C. Q., 2008, "Sequential adaptive designs in computer experiments for response surface model fit," The Ohio State University.

[48] Cervone, D. and Pillai, N. S., 2015, "Gaussian process regression with location errors," *arXiv preprint arXiv*:1506.08256.

[49] Wang, W., Yue, X., Haaland, B., Hunt, J. H., Shi, J., and Wu, C. J., 2018, "Gaussian Process with Input Location Error and Applications to Composite Fuselage Shape Control," Technical Report.

[50] Wen, Y., Yue, X., Hunt, J. H., and Shi, J., 2018, "Feasibility analysis of composite fuselage shape control via finite element analysis," *Journal of manufacturing systems*, vol. 46, pp. 272-281.

[51] Olsson, F., 2009, "A literature survey of active machine learning in the context of natural language processing,".

[52] Lewis, D. D. and Catlett, J., 1994, "Heterogeneous uncertainty sampling for supervised learning," in *Machine Learning Proceedings 1994*: Elsevier, pp. 148-156.

[53] Cohn, D. A., Ghahramani, Z., and Jordan, M. I., 1996, "Active learning with statistical models," *Journal of artificial intelligence research*, vol. 4, pp. 129-145.

[54] Sugiyama, M., 2006, "Active learning in approximately linear regression based on conditional expectation of generalization error," *Journal of Machine Learning Research*, vol. 7, no. Jan, pp. 141-166.

[55] Burbidge, R., Rowland, J. J., and King, R. D., 2007, "Active learning for regression based on query by committee," in *International Conference on Intelligent Data Engineering and Automated Learning*, pp. 209-218: Springer.

[56] Sugiyama, M. and Rubens, N., 2008, "Active learning with model selection in linear regression," in *Proceedings of the 2008 SIAM International Conference on Data Mining*, pp. 518-529: SIAM.

[57] Pasolli, E. and Melgani, F., 2011, "Gaussian process regression within an active learning scheme," in Geoscience and Remote Sensing Symposium (IGARSS), *2011 IEEE International*, pp. 3574-3577: IEEE.

[58] Cai, W., Zhang, Y., and Zhou, J., 2013, "Maximizing expected model change for active learning in regression," in Data Mining (ICDM), *2013 IEEE 13th International Conference*, pp. 51-60: IEEE.

[59] Schreiter, J., Nguyen-Tuong, D., Eberts, Bischoff, M., B., Markert, H., and Toussaint, M., 2015, "Safe exploration for active learning with Gaussian processes," in Joint European Conference on Machine Learning and Knowledge Discovery in Databases, pp. 133-149: Springer.

[60] Santner, T. J., Williams, B. J., and Notz, W. I., 2013, *The design and analysis of computer experiments*. Springer Science & Business Media.

[61] Sacks, J., Welch, W. J., Mitchell, T. J., and Wynn, H. P., 1989, "Design and analysis of computer experiments," *Statistical science*, pp. 409-423.

[62] Currin, C., Mitchell, T., Morris, M., and Ylvisaker, D., 1991, "Bayesian prediction of deterministic functions, with applications to the design and analysis of computer experiments," *Journal of the American Statistical Association*, vol. 86, no. 416, pp. 953-963.

[63] Mockus, J., Tiesis, V., and Zilinskas, A., 1978, "Toward global optimization, volume 2, chapter bayesian methods for seeking the extremum..

[64] Jones, D. R., Schonlau, M., and Welch, W. J., 1998, "Efficient global optimization of expensive black-box functions," *Journal of Global optimization*, vol. 13, no. 4, pp. 455-492.

[65] Williams, B. J., Santner, T. J., and Notz, W. I., 2000, "Sequential design of computer experiments to minimize integrated response functions," *Statistica Sinica*, pp. 1133-1152.

[66] Williams, B. J., Santner, T. J., Notz, W. I., and Lehman, J. S., 2010, "Sequential design of computer experiments for constrained optimization,", *Statistical Modelling and Regression Structures: Springer*, pp. 449-472.

[67] Vazquez, E. and Bect, J., 2010, "Convergence properties of the expected improvement algorithm with fixed mean and covariance functions," *Journal of Statistical Planning and inference*, vol. 140, no. 11, pp. 3088-3095.

[68] Deng, X., Joseph, V. R., Sudjianto, A., and Wu, C. J., 2009, "Active learning through sequential design, with applications to detection of money laundering," *Journal of the American Statistical Association*, vol. 104, no. 487, pp. 969-981.

[69] Crombecq, K., Gorissen, D., Deschrijver, D., and Dhaene, T., 2011, "A novel hybrid sequential design strategy for global surrogate modeling of computer

experiments," *SIAM Journal on Scientific Computing*, vol. 33, no. 4, pp. 1948-1974.

[70] Jin, R., Chang, C.-J., and Shi, J., 2012, "Sequential measurement strategy for wafer geometric profile estimation," *IIE Transactions*, vol. 44, no. 1, pp. 1-12.

[71] Yan, H., 2017, "High dimensional data analysis for anomaly detection and quality improvement," Georgia Institute of Technology.

[72] Cressie, N., 1992, "Statistics for spatial data," *Terra Nova*, vol. 4, no. 5, pp. 613-617.

[73] Stein, M. L., 1999, *Interpolation of spatial data: some theory for kriging*. Springer Science & Business Media.

[74] Joseph, V. R. and Hung, Y., 2008, "Orthogonal-maximin Latin hypercube designs," *Statistica Sinica*, pp. 171-186.

[75] Chaloner, K. and Verdinelli, I., 1995, "Bayesian experimental design: A review," *Statistical Science*, pp. 273-304.

[76] Olsson, F. and Tomanek, K., 2009, "An intrinsic stopping criterion for committee-based active learning," in *Proceedings of the Thirteenth Conference on Computational Natural Language Learning*, pp. 138-146: Association for Computational Linguistics.

[77] Stewart M., Chase K., 2005, "Variation Simulation of Fixtured Assembly Processes for Compliant Structures Using Piecewise-Linear Analysis", *ASME proceedings, Manufacturing Engineering and Materials Handling*, Parts A and B ():591-600. DOI: 10.1115/IMECE2005-82371

[78] Abdelal, G., Georgiou, G., Cooper, J., Robotham, A., Levers, A., and Lunt, P., 2015, "Numerical and Experimental Investigation of Aircraft Panel Deformations During Riveting Process," *ASME Transactions, Journal of Manufacturing Science and Engineering*, 137(1), p. 011009.

[79] Liu, S. C., and Hu, S. J., 1995, “An Offset Element Model and Its Applications in Predicting Sheet Metal Assembly Variation,” *Int. J. Mach. Tools Manuf.*, 35(11), pp. 1545–1557.

[80] Wen, Y., Yue, X., Hunt, J.H., Shi, J., 2018, “Virtual Assembly and Residual Stress Analysis for Composite Fuselage Assembly Process”, *Journal of Manufacturing Systems*, Submitted

[81] Yue, X., Wen, Y., Hunt, J. H., Shi, J., 2018, “Active Learning for Gaussian Process Considering Uncertainties with Application to Shape Control of Composite Fuselage”, under the Boeing Company review